The role of oxygen on the interaction of *Candida albicans* with intestinal epithelial cells

Dissertation

To Fulfill the Requirements for the Degree of

“doctor rerum naturalium“ (Dr. rer. nat.)

FRIEDRICH-SCHILLER-
UNIVERSITÄT
JENA

submitted to the Council of the Faculty of Biological Sciences
of the Friedrich Schiller University Jena

by Master of Science (M.Sc.) Biochemistry

Nicole Engert-Ellenberger

born on 26.09.1989 in Erfurt

Examiner

Prof. Dr. Ilse D. Jacobsen

Research Group Microbial Immunology, Leibniz Institute for Natural Product Research and Infection Biology – Hans Knöll Institute, Jena

PD Dr. Alexander S. Mosig

Institute for Biochemistry II, Jena University Hospital, Jena; Research Group INSPIRE, Center for Sepsis Control and Care, Jena University Hospital, Jena

Prof. Dr. Salomé LeibundGut-Landmann

Section of Immunology, Institute of Virology, University of Zurich, Zurich

Day of defense

29.03.2019

This thesis was performed at the “Leibniz Institute for Natural Product Research and Infection Biology – Hans Knöll Institute” in the Research Group Microbial Immunology under the supervision of Prof. Ilse D. Jacobsen.

This work was financed by the Excellence Graduate School “Jena School for Microbial Communication” (JSMC) and the HKI. This thesis was supported by the Collaborative Research Center/Transregio 124 – FungiNet “Pathogenic fungi and their human host: Networks of interaction”.

Table of Contents

Summary

Candida albicans colonizes mucosal surfaces of humans as an opportunistic fungal pathogen. While being considered to be a harmless commensal in healthy individuals, it can cause life-threatening disseminated infections in hospitalized patients. These infections are thought to be caused predominantly by translocation of endogenous *C. albicans* through the intestinal epithelial barrier into the blood stream. Necessary prerequisites for translocation are immunosuppression and impairment of the gut epithelial barrier function. Such a barrier dysfunction can be caused by e.g. ischemia-reperfusion (IR) injury occurring during major surgeries or in traumatic shock situations. Several *in vivo* studies have shown that IR injury leads to bacterial and *C. albicans* translocation. The exact role of oxygen availability for IR-mediated fungal translocation has however not been addressed so far. Therefore, the aim of this study was to investigate *C. albicans*-enterocyte interactions in dependence of oxygen availability, including constant oxygen supply within the physiological range, and hypoxic shock and reoxygenation as changes occurring during ischemia and reperfusion, respectively. To allow experimentation under controlled oxygen supply, an *in vitro* enterocyte model was used in this study. Enterocytes were able to maintain barrier function across a range of oxygen concentrations and in conditions mimicking hypoxic shock and reperfusion. Their susceptibility to *C. albicans* infection was however significantly influenced by oxygen: The shift from low to high oxygen enhanced susceptibility to infection, likely mediated by increased intracellular oxidative stress and alterations of tight junctions facilitating increased invasion of the fungus. In contrast, low oxygen concentrations and especially hypoxic shock were associated with less damage and partially retained barrier function. Additionally, fungal translocation was reduced after hypoxic shock. HIF-1α contributed to the protective effect, independent of the antimicrobial cathelicidin LL-37. Furthermore, peracute hypoxic preconditioning, compared to enterocytes constantly cultured at low oxygen, led to enhanced adhesion but reduced invasion and reduced hyphal growth of *C. albicans*, suggesting that oxygen-mediated changes of enterocytes also directly influence the fungus. Fungal adaptation to oxygen availability contributes to these interactions, as a *C. albicans TYE7* deletion mutant showed oxygen-dependent alterations in virulence. Finally, this study provides evidence that the early stages of the infection process determine the fate of enterocytes during their interaction with *C. albicans* in an oxygen-dependent manner. In summary, this study demonstrates that oxygen availability significantly influences the interaction between *C. albicans* and the intestinal barrier by affecting both host cells and pathogen.

Zusammenfassung

Candida albicans besiedelt menschliche Schleimhäute als opportunistischer Krankheitserreger. Während er in gesunden Menschen als harmloser Kommensale betrachtet wird, kann dieser Pilz lebensbedrohliche, disseminierte Infektionen in hospitalisierten Patienten hervorrufen. Es wird angenommen, dass diese Infektionen hauptsächlich durch die Translokation der endogenen *C. albicans*-Population durch die intestinale Epithelbarriere in den Blutstrom verursacht werden. Notwendige Voraussetzungen für eine Translokation und disseminierte Infektion sind Immunsupprimierung und Beeinträchtigung der Barrierefunktion des Darmepithels. Barrierestörungen können bspw. durch Ischämie-Reperfusion (IR) hervorgerufen werden, die während aufwendiger Operationen oder in traumatischen Schocksituationen auftritt. Mehrere *in vivo*-Studien haben gezeigt, dass IR-Schädigung zu bakterieller und *C. albicans*-Translokation führt. Die genaue Bedeutung der Sauerstoff-Verfügbarkeit für die IR-vermittelte Translokation des Pilzes wurde jedoch bisher nicht adressiert. Daher war das Ziel dieser Arbeit, die *C. albicans*-Enterozyten-Interaktion in Abhängigkeit der Sauerstoff-Verfügbarkeit zu untersuchen, sowohl unter konstanter Sauerstoff-Versorgung innerhalb des physiologischen Bereichs, als auch bei Schwankungen wie sie im hypoxischen Schock und bei der Reperfusion auftreten. Um eine Versuchsdurchführung unter kontrollierter Sauerstoff-Versorgung zu gewährleisten, wurde ein *in vitro*-Enterozyten-Modell verwendet. Die Barrierefunktion der Enterozyten wurde bei konstanter Verfügbarkeit von 1 % - 21 % Sauerstoff und auch bei plötzlichen Schwankungen in diesem Bereich aufrechterhalten. Die Anfälligkeit der Enterozyten gegenüber der Infektion mit *C. albicans* wurde jedoch erheblich durch Sauerstoff beeinflusst: Der Wechsel von wenig zu viel Sauerstoff erhöhte die Empfindlichkeit gegenüber der Infektion, vermutlich aufgrund der intrazellulären Akkumulation von Sauerstoffradikalen und einer erhöhten Invasionsrate des Pilzes. Im Unterschied dazu waren niedrige Sauerstoff-Konzentrationen, insbesondere hypoxischer Schock, mit geringer Schädigung und partiell erhaltener Barrierefunktion assoziiert. Zusätzlich war die Translokation des Pilzes nach hypoxischem Schock reduziert. HIF-1α trug unabhängig vom antimikrobiellen Cathelicidin LL-37 zu diesem protektiven Effekt bei. Im Vergleich zu Enterozyten, die konstant bei niedrigem Sauerstoff kultiviert wurden, führte die perakute hypoxische Vorbehandlung des Weiteren zu erhöhter Adhäsion aber verminderter Invasion und reduziertem Hyphenwachstum von *C. albicans*. Dies deutet darauf hin, dass Sauerstoff-vermittelte Veränderungen der Enterozyten auch direkt den Pilz beeinflussen. Die Anpassung des Pilzes an die Sauerstoff-Verfügbarkeit trägt zu diesen Interaktionen insofern bei, als dass eine *C. albicans TYE7* Deletionsmutante

Sauerstoff-abhängige Virulenz-Veränderungen aufwies. Schließlich liefert diese Studie auch Anhaltspunkte dafür, dass frühe Phasen des Infektionsverlaufes das Schicksal der Enterozyten während ihrer Interaktion mit *C. albicans* in Sauerstoff-abhängiger Art und Weise bestimmen. Zusammenfassen betrachtet, zeigt diese Studie, dass die Sauerstoff-Verfügbarkeit über Effekte sowohl auf die Wirtzellen als auch auf das Pathogen die Interaktion zwischen *C. albicans* und der intestinalen Barriere maßgeblich beeinflusst.

1. Introduction

Members of the microbial community inhabiting humans have to adapt to the environmental conditions in the respective body niche to establish themselves as stable members of the microbiota. Depending on the host site microbes need to adapt to e.g. pH, nutrient availability and oxygen availability [1]. The highest oxygen concentrations are found on the skin, in the airways and the oral cavity, but the majority of the microbiota in the human body has to cope with strongly reduced oxygen levels compared to breathable air (~21 % O_2) [2,3]. Almost anoxic conditions are found in the lumen of the gastrointestinal tract (GIT) where in healthy individuals a diverse microbial community mediates protection against enteropathogens, contributes to the utilization of nutrients and immune homeostasis [4-6]. The majority of the microbiota in the GIT are bacteria with Bacteroidetes and Firmicutes as the dominating phyla [5,7]. Besides bacteria, the gut microbiota consists of viruses, archaea and eukaryotes (mainly fungi, but also protozoa) [4,5,7-10]. Among the non-bacterial microbes within the GIT microbiota, fungi are the best studied but have still received little attention compared to bacteria [11]. The most common fungal species found in the GIT belong to the genera *Candida*, *Cladosporium* and *Saccharomyces* [7,8,11] with *Candida albicans* being the most frequently found fungus [11,12].

1.1. *C. albicans* as a human pathogen

Among more than 150 described *Candida* species, only 10 % are known to be responsible for human infections [13-15]. The two main types of these infections are superficial and disseminated or deep-seated candidiasis [16,17]. Superficial mucosal *Candida* infections, like vulvovaginal candidiasis (VVC) or oral thrush, frequently occur in immunocompromised patients, like HIV-infected individuals, and are easy to handle [13,16,18]. But also immunocompetent people commonly suffer from superficial *Candida* infections [13]. VVC affects approx. 50 % - 75 % of women in their reproductive years [18,19]. Oral *Candida* infections are common in babies and in the elderly, especially in those wearing dentures [18,20]. In contrast, disseminated candidiasis is a severe and life-threatening infection occurring in critically ill and hospitalized patients, often associated with the application of broad-spectrum antibiotics, catheters, and gastrointestinal trauma or surgery [17,18,21]. Further risk factors for the development of candidiasis are neutropenia, organ transplantation, cancer chemotherapy, surgical procedures of the abdomen and extended stays in intensive care units [13,16,18]. After *Candida* enters the bloodstream, infection can involve nearly all inner organs of the human body [16]. These systemic

infections are associated with high mortality rates of up to 50 % [13,14,16,18,22]. Thus, there is a great need for more sensitive and specific diagnostic tools and for more effective antifungal therapies although many antifungal agents are available. Within disseminated candidiasis, candidaemia (*Candida* isolation from the blood stream) and isolated infections of one or several organs can be distinguished [13,23]. With medical advances and an increasing population of patients at risk, *Candida* species are nowadays the fourth most common cause of nosocomial bloodstream infections [14,16,18,24] with *C. albicans* being the most common cause of candidiasis and the most frequently found *Candida* species from deeper tissue, blood and organs [14,16].

C. albicans is an opportunistic fungal pathogen that colonizes human mucosal surfaces in healthy individuals as part of the normal microbiota in the oral cavity, vagina, and GIT [17,25-27] in 30 % - 75 % of healthy people [13,19,20]. The GIT is thought to be the main source of disseminated *C. albicans* infections [12,28-30]. An imbalance of the microbiota due to antibiotic treatment in combination with immunosuppression, enhancing colonization, and impairment of gut epithelial barrier function are prerequisites for the translocation of *C. albicans* from the GIT into the blood stream and internal organs leading to severe disseminated infections [13,16-18,21,31,32]. But so far, little is known about the process of translocation through the gut epithelium and the subsequent dissemination of *C. albicans*.

1.1.1. Virulence attributes

C. albicans is a polymorphic fungus and can grow as classical spherical yeast (“white form”), filamentous pseudohyphae, true hyphae, chlamydospores and various yeast-like morphologies like opaque, GUT and gray cells [33-37]. Whereas the opaque morphology is linked to mating and biofilm formation [15,34], both the yeast and hyphal growth form contribute to fungal virulence [38]. Yeast cells are proposed to be crucial for the dissemination of *C. albicans via* the bloodstream while fungal hyphae are essential for the penetration and invasion into epithelial cells and host tissues [15,36,38]. Furthermore, hypha formation is associated with the expression of virulence factors [14,36] which are important for the shift from the commensal to the pathogenic life style by mediating colonization, adherence and invasion to host surfaces and tissue damage [15,16]. These hypha-associated factors include adhesins, like the agglutinin-like sequence 3 (Als3) protein and the hyphal wall protein 1 (Hwp1), secreted hydrolases, like the secreted aspartyl proteinases (Saps) Sap4 – 6, and candidalysin, the first identified fungal peptide toxin which directly damages epithelial membranes [15,38-40]. Further virulence factors of *C. albicans* are mannosyltranferases, which modify the fungal cell wall necessary for

adherence, invasins like the heat shock protein 70 (Hsp70) family member Ssa1, as well as secreted hydrolytic enzymes like lipases and phospholipases [16,41-44]. Biofilm formation and the response to environmental stressors like reactive oxygen species (ROS) *via* superoxide dismutases (Sods) are also important virulence attributes of *C. albicans* [13,15,16,38]. Metal acquisition, especially of zinc, iron, copper and manganese, pH sensing and metabolic adaptation are furthermore essential for the adaptation to different host niches and, therefore, are crucial for survival and avoiding host immune response [14-16,38,45].

1.2. Adaptation of *C. albicans* to hypoxia

During commensal growth at mucosal surfaces in the urogenital tract and in the GIT as well as during invasive growth into deeper tissues and organs in the context of systemic infections, *C. albicans* has to withstand and to adapt to different oxygen availabilities especially hypoxia and almost anoxic conditions in the gut lumen. Hypoxic conditions enhance filamentous growth, especially in the presence of high CO_2 levels, induce ethanol production *via* fermentation of glucose and promote further metabolic changes towards glycolysis and fatty acid production [46-48]. Furthermore, hypoxia increases the ergosterol biosynthesis and thus leads to alterations in cell wall and membrane structure [47,48]. The transcriptional response to hypoxia occurs within the first 30 min [48] showing that *C. albicans* is able to rapidly adapt to oxygen changes.

1.2.1. Crucial factors for hypoxic adaptation of *C. albicans*

Transcriptional analysis of *C. albicans* during hypoxia revealed several factors involved in the adaptation to hypoxic conditions [47]. The most important factors for hypoxic adaptation are Efg1, Ace2, Tye7 and Upc2 [48-50].

Efg1, the essential positive regulator of *C. albicans* morphogenesis at ambient (~ 21 % O_2) conditions [51], is also required for biofilm formation [52]. Its role in filamentation at hypoxia is temperature-dependent: Efg1 acts as an inducer of hyphal morphogenesis at 37 °C but represses filamentation at temperatures below 37 °C [53]. The respective counterpart for hyphal morphogenesis during hypoxia at lower temperatures (25 °C, 30 °C) is Ace2 which forms a regulatory hub with Efg1 to control *C. albicans* morphogenesis at these conditions [54]. But Ace2 is also required for the filamentation during hypoxia at 37 °C [54,55].

The depletion of ergosterol levels from fungal membranes during hypoxia, which is due to the reduced ergosterol biosynthesis because of the reduced oxygen availability, is

sensed by membrane-bound sterol regulatory element-binding proteins (SREBPs) [47]. In the human fungal pathogens *Cryptococcus neoformans* and *Aspergillus fumigatus* as well as in the fission yeast *Schizosaccharomyces pombe*, SREBPs regulate the expression of genes involved in ergosterol biosynthesis after their proteolytic activation [47,50]. A direct SREBP homolog in *C. albicans* has not been identified yet, but Upc2 shares functional similarities with these transcriptional regulators [49,50]. The C-terminus of Upc2 binds ergosterol which represses its transcriptional activity [56]. Thereby, ergosterol depletion during hypoxia leads to de-repression and activation of this zinc finger transcription factor [47,50,56]. The dissociation of ergosterol at hypoxic conditions leads to the relocalization of Upc2 from the cytosol to the nucleus and induces the expression of genes involved in the oxygen-dependent part of the ergosterol biosynthesis [56,57]. Additionally, the expression of *UPC2* is upregulated in response to hypoxia mediated by Tye7 [48]. This transcription factor is involved in the complete activation of the glycolytic genes at hypoxic conditions which occurs initially during hypoxia [48,58,59]. This allows a rapid adaptation to low-oxygen conditions and facilitates the maintenance of ATP production [58]. Furthermore, Tye7 is involved in the activation of fermentation and is required for efficient biofilm formation by upregulating glycolytic gene expression and preventing uncontrolled hyphal formation [58,59]. Thus, Tye7 is a central transcriptional regulator of the carbohydrate metabolism [59]. It is also important for GIT colonization and proliferation of *C. albicans* in a murine GIT colonization model [48,59,60].

1.3. The gastrointestinal tract

With an area of approx. 250 – 400 m^2 the GIT is one of the major interfaces between the host, the environment and antigens in the human body [61,62]. Furthermore, the GIT harbors a huge abundance of microorganisms which aids the host by providing nutrients, and thus energy, protecting against pathogens, and developing and regulating host immunity [61-63].

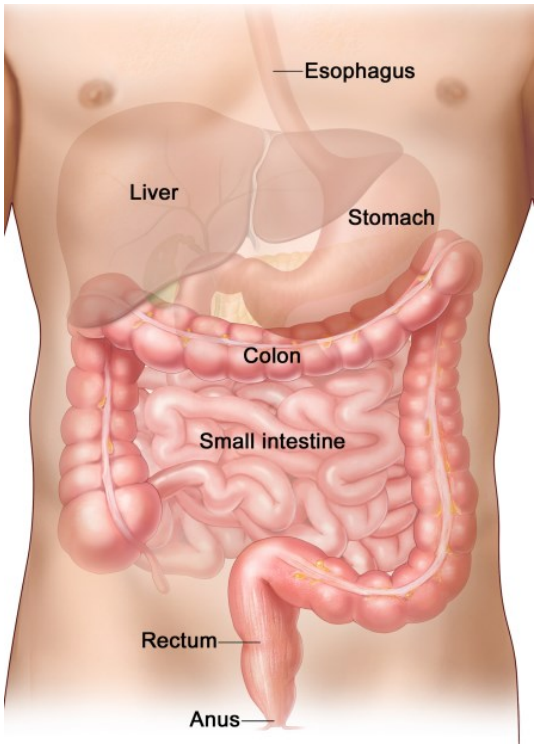

Figure 1: Schematic structure of the human GIT. The segments representing the GIT are the esophagus, the stomach, the small intestine and the large intestine or colon. Adapted from PubMed Health (www.ncbi.nlm.nih.gov/pubmedhealth/PMHT0022856/) [64].

The GIT consists of the esophagus, the stomach, the small intestine and the large intestine, also named colon [65-67] (Figure 1). As the foremost part, the esophagus transports the food from the mouth to the stomach where the solid food is stored, predigested, and fragmented and homogenized *via* peristalsis [65,66]. The following intestinal tract is divided into the small and the large intestine [65]. With a length of approx. 4 m, the small intestine is the longest part of the GIT [66]. It consists of the duodenum, the jejunum and the ileum, and is responsible for food digestion and absorption of nutrients [65,66]. In the large intestine, consisting of colon and rectum with a total length of approx. 1.5 m, water and electrolytes are reclaimed and the feces are formed [65,66]. In addition to its digestive and absorptive function, the GIT is an important immunological system providing appropriate immune responses by functioning as a barrier against enteropathogens and, at the same time, mediating tolerance to harmless commensals and food antigens [62,65,68].

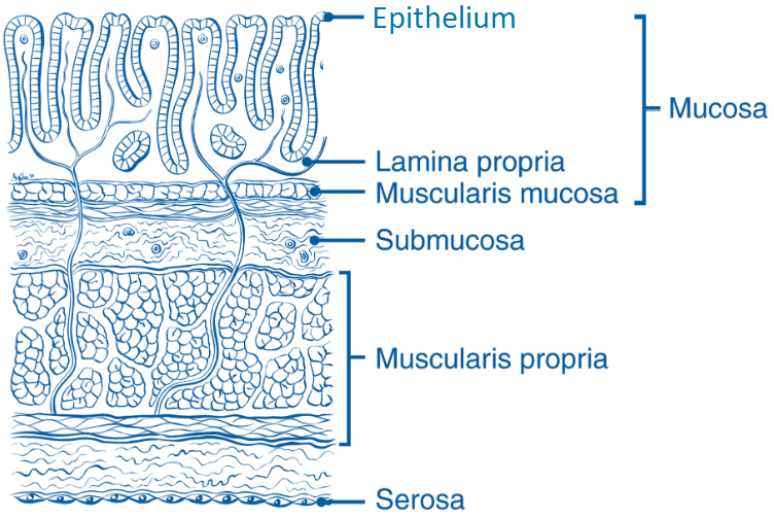

Figure 2: Schematic section of the GIT tissue. Each segment of the GIT can be classified into four layers, which are quite similar among the segments. The serosa represents the outer layer, followed by the smooth muscle cells of the muscularis propria and the vascular network in the submucosa. The mucosa forms the innermost layer and consists of the muscularis mucosa, the lamina propria and the epithelial cells facing the lumen. Adapted from the American Joint Committee on Cancer (https://cancerstaging.org/references-tools/quickreferences/Documents/ColonMedium.pdf) [69].

The segments of the GIT share similarities regarding their anatomy, as they consist of four layers, and are interconnected by connective tissue, neural and vascular elements (Figure 2) [65,66]. Whereas the outer surface, the serosa, serves as a protective layer and consists of squamous epithelial cells, the adjacent muscularis propria, containing smooth muscle cells, is responsible for the contractile peristaltic movement [65]. The adjoining submucosa contains a vascular network, which is essential for oxygen delivery and nutrient transport, and comprises a variety of immune cells [6,62,66]. The innermost layer of the GIT, the mucosa, is the most complex and most important layer as it has an adsorptive function and faces the content of the intestinal lumen [65]. The mucosa contains a sheet of smooth muscle cells, the muscularis mucosae, lying at the base of the lamina propria which consists of connective tissue and lymph nodes [62,65]. Attached to this basement membrane, a single layer of epithelial cells and intraepithelial immune cells forms the inner layer of the GIT [62,65].

1.3.1. The intestinal epithelium

Besides being the largest mucosal surface of the human body [62], the intestinal epithelium is the most vigorously self-renewing tissue of adult mammals [70,71]. It consists of a single layer of columnar epithelial cells which are organized into crypts and villi, with the latter being present only in the small intestine [62,72] (Figure 3).

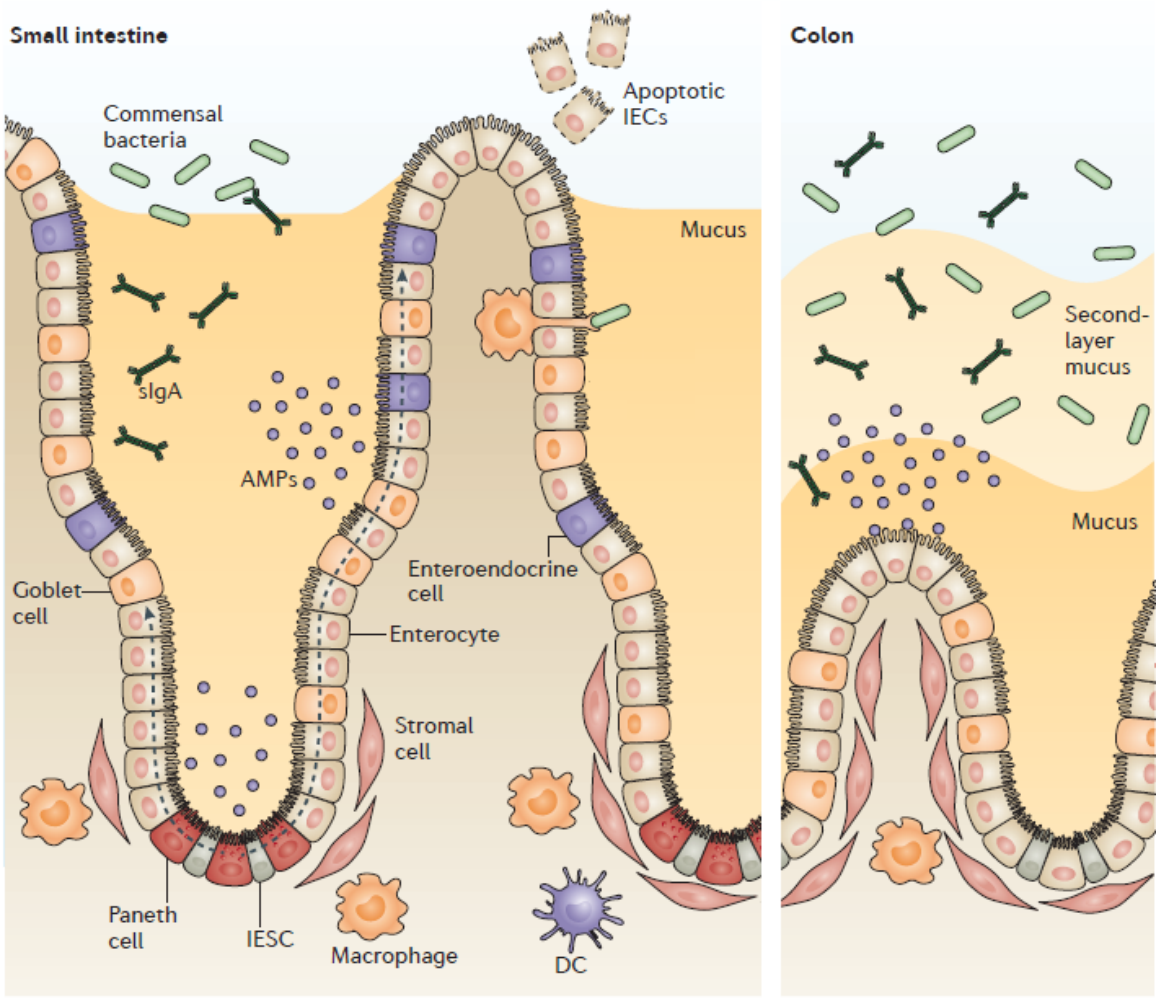

Figure 3: Structure of the intestinal epithelium. Intestinal epithelial stem cells (IESCs) reside in the crypts and differentiate into absorptive enterocytes, enteroendocrine cells, goblet cells and Paneth cells. During their differentiation, these cells migrate toward the lumen, as indicated by dashed arrows, and are shed into the lumen from the top of the villi in the small intestine or from the surface between the crypts in the colonic epithelium. The exception therefor are Paneth cells which stay at the bottom of the crypts in the small intestine. The production of mucus and antimicrobial peptides (AMPs) by intestinal epithelial cells (IECs) contributes to the intestinal mucosal barrier as well as secretory Immunoglobulin A (sIgA) produced by lymphocytes from the lamina propria. Adapted from Peterson and Artis, 2014 [62].

The intestinal epithelial layer is continually renewed by intestinal epithelial stem cells (IESCs) residing in the base of the crypts [62,70-72]. The IESCs give rise to a pool of multipotent progenitor cells which are highly proliferative und undifferentiated [72,73]. When these progenitor cells begin to differentiate, they migrate toward the lumen and are shed either from the tip of the intestinal villi or from the mucosal surface between the crypts of the colonic epithelium [67,70]. Thus, the crypts of the intestinal epithelium are the proliferative but immature compartment whereas the villi contain differentiated epithelial cells which are unable to divide [67,70,72,73]. The IESCs can differentiate into four specialized

cell types: the absorptive enterocytes being highly polarized and characterized by a luminal brush border, the goblet cells which produce a protective mucus barrier, the hormone-secreting enteroendocrine cells regulating digestion, and the Paneth cells which secrete antimicrobial peptides (AMPs) [62,70-73]. The latter are absent in the colonic epithelium where absorptive enterocytes ensure the AMP secretion [71,72,74]. Whereas absorptive enterocytes, goblet cells and enteroendocrine cells migrate toward the intestinal lumen, Paneth cells stay at the bottom of the crypts [71,72].

1.3.2. The intestinal mucosal barrier

The intestinal epithelium contributes to the mucosal barrier function *via* the secretion of a mucus layer by goblet cells, and the release of AMPs, like defensins, cathelicidins and lysozyme, which can be secreted by all intestinal epithelial cells (IECs) but particularly by Paneth cells [62,74-76]. Between IECs tight junctions ensure a tight paracellular barrier preventing the movement of ions and solutes but also microbes and intraluminal pathogens from the intestinal lumen to the underlying tissue [68,77,78]. These intercellular junctions are the most apical structures of the junctional complex which further comprises adherens junctions and desmosomes [79,80]. Furthermore, the gut associated lymphoid tissue (GALT), comprising mesenteric lymph nodes, Peyer's patches and lymphoid cells, contributes to the intestinal barrier by inducing the initial mucosal immune response [32,62,81,82]. The GALT is the largest component of lymphoid systems protecting the GIT from the stomach to the colon [32,82]. The large amount of scattered lymphoid cells (B and T cells), macrophages and dendritic cells in the lamina propria and the intestinal epithelium are responsible for the local immune response and provide a disseminated immunity throughout the intestine [32,81]. These effector sites for example produce secretory Immunoglobulin A (sIgA) *via* plasma B cells which is transported across the epithelial barrier *via* transcytosis [32,62]. The Peyer's patches, which are lymphoid aggregates in the submucosa containing dendritic, B and T cells, are covered by the follicle-associated epithelium consisting of microfold (M) cells amongst other IECs [62,81].These M cells, which also overlay isolated lymphoid follicles [62], are a specialized population of epithelial cells and mediate the uptake, transport and presentation of luminal antigens and microorganisms to the underlying lymphoid tissue [62,73,81]. The uptake of antigens by M cells leads to the induction of antigen-specific sIgA, which prevents microbial adhesion to epithelial cells suppressing pathogenic infection, and thus contributes to the mucosal immunosurveillance [83].

1.4. Oxygen availability in the gut

The intestinal epithelium is subjected to profound fluctuations in blood flow on regular intervals throughout a day due to food intake and fasting periods [84-87]. The blood flow in the small intestine increases after meals, known as postprandial hyperaemia, necessary to facilitate efficient absorption and transport of nutrients [86,88]. In contrast, the blood flow in the colon is influenced by short-chain fatty acids, like acetic and butyric acid, which are produced by the gut microbiota [4,63,86]. Furthermore, there is also a steep oxygen gradient along the crypt-to-villus axis due to the vascular oxygen supply; this is mediated by the rich vascularization of the subepithelial mucosa, the exposure of epithelial cells to the anoxic lumen, and the countercurrent shunt (Figure 4) [84-88].

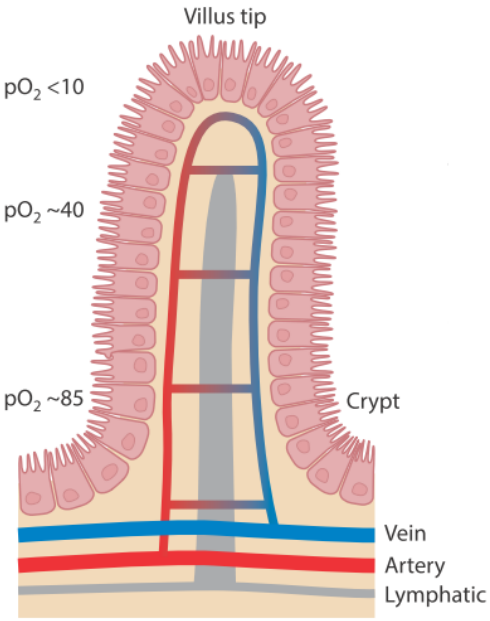

Figure 4: Schematic model of blood flow and oxygen availability in the intestinal epithelium. A countercurrent shunt is responsible for the generation of a steep oxygen gradient along the crypt-to-villus axis. Oxygen diffuses from the arterial blood to the adjacent venules. Thus, the oxygen gradient ranges from ~ 15 % - 8 % O_2 at the border to the submucosa to almost anoxic conditions in the intestinal lumen. Adapted from Colgan *et al.*, 2016 [89].

The countercurrent blood flow in the intestinal villi leads to the diffusion of oxygen from the arterial blood to the adjacent venules which reduces the oxygen content reaching the epithelium surface or the villus tip, respectively [86,89]. Thus, the oxygen availabilities range from 15 % - 8 % O_2 at the border to the submucosa to 3 % - 1 % O_2 at the tip of the villus while almost anoxic conditions occur in the intestinal lumen [6,85-87,89]. The luminal oxygen concentration furthermore decreases along the longitudinal axis from the duodenum to the colon [86].

1.4.1. Oxygen availability during pathophysiological situations

Besides the temporal fluctuation and the wide range of physiological oxygen availability in the GIT, a variety of pathophysiological situations like mesenteric arterial embolism, major surgery, organ transplantation, trauma, shock or sepsis affects the oxygen levels in the GIT, leading to intestinal ischemia, followed by reperfusion if the underlying condition improves or resolves [90-92]. Depending on the duration of the ischemic period, the intestinal epithelial barrier can be severely impaired by hypoxia [93,94]. However, the subsequent period of reoxygenation during reperfusion leads to even more severe cellular damage, tissue disruption and inflammation, which can induce a multiple organ dysfunction syndrome [90,91,93-95]. Thereby, ischemia-reperfusion (IR) injury leads to high morbidity and mortality rates [90].

The production of ROS during intestinal IR, especially during the reperfusion period, severely damages the cellular membranes *via* lipid peroxidation leading to severe tissue injury and loss of barrier integrity [92,95-98]. During physiological conditions, enzymes of the endogenous antioxidant defense system, like Sods and glutathione (GSH), prevent cellular damage by ROS [95,98]. However, these mechanisms are attenuated during pathophysiological IR due to the decreased effectiveness of the antioxidant defense system or since the production of ROS exceeds the capacity of antioxidant enzymes [98]. Furthermore, toxic metabolic byproducts accumulate intracellularly during the ischemic period, are flushed into the blood stream and are transported to distant organs when the tissue is reperfused, thereby leading to tissue dysfunction [94,99]. The impairment of the intestinal epithelial barrier integrity increases the intestinal permeability which enhances bacterial translocation, thereby leading to infectious complications after IR [90,92,95].

1.4.2. Regulation of oxygen responses by HIF-1α

The adaptation of human cells to low oxygen conditions is mediated by the hypoxia-inducible factor (HIF), the key regulator of hypoxic adaptation [100]. Its transcriptional activity is determined by the HIF-1α subunit which is constitutively translated but post-translationally modified in an oxygen-dependent manner [101,102] (Figure 5).

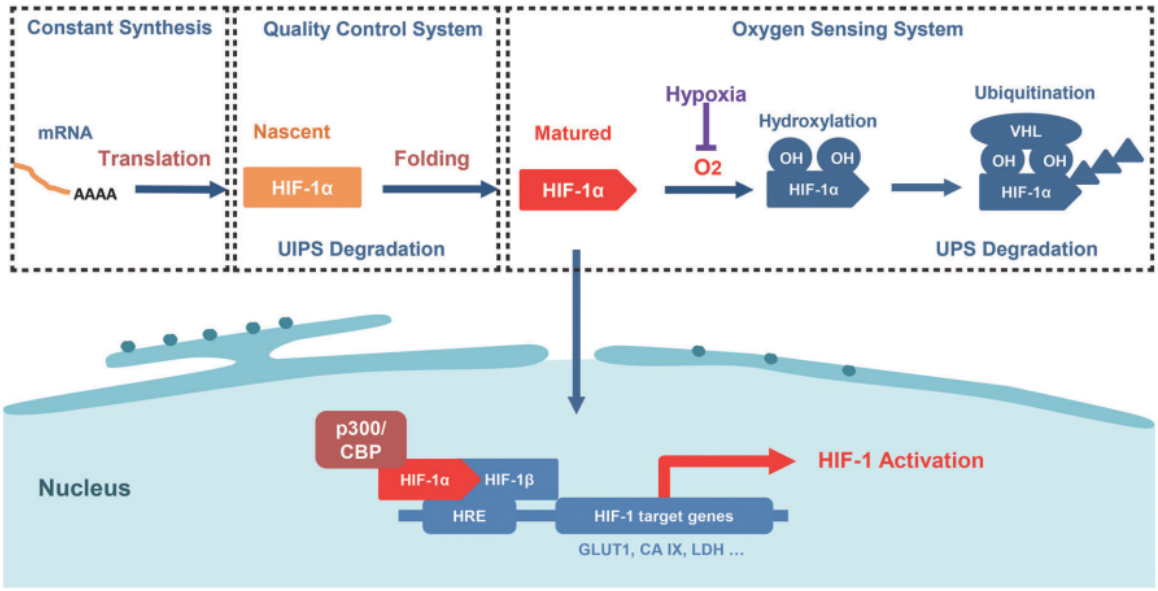

Figure 5: Post-translational regulation of HIF-1α stability. The constitutively translated HIF-1α subunit is subject to an oxygen-dependent post-translational modification. During oxygen-rich conditions, HIF-1α is hydroxylated and, thus, ubiquitinated *via* the von Hippel Lindau protein (VHL). This leads to the proteasomal degradation of HIF-1α. In contrast, during hypoxia this α-subunit is stabilized, translocates to the nucleus and, with the constitutively expressed and stable HIF-1β, it forms the heterodimer HIF. This transcription factor binds to hypoxic responsible elements (HRE) inducing the expression of its target genes. Adapted from Chen *et al.*, 2016 [101].

The HIF-1α stability is regulated by prolyl hydroxylases (PHDs). In the presence of oxygen, PHDs modify proline residues of HIF-1α *via* hydroxylation leading to polyubiquitination by the von Hippel Lindau protein (VHL), an ubiquitin ligase, which initiates the subsequent proteasomal degradation of HIF-1α [101-103]. In the absence of oxygen, HIF-1α is stabilized and accumulated, and translocates to the nucleus where it dimerizes with the constitutively expressed HIF-1β subunit [100,103,104]. The resulting heterodimeric basic helix-loop-helix transcription factor HIF now binds to hypoxic responsible elements (HRE) in the promotor regions of its target genes [100,101,104]. Thereby, HIF orchestrates the metabolic shift to anaerobic glycolysis and increased lactic acid production to maintain cellular energy production at hypoxia [100,103,104]. HIF is involved in the regulation of angiogenesis, glucose transport, glycolysis, erythropoiesis, migration, and cell proliferation and survival [100,103-106]. Furthermore, due to its decisive role for the transcriptional activity of HIF, HIF-1α contributes to the stability of the intestinal epithelium barrier and mucosal immunity al low oxygen by promoting the production of AMPs and pro-inflammatory cytokines [87,89,107]. In addition, HIF-1α is involved in the protection and defense against fungal and bacterial infections [107-110].

1.5. Interaction of *C. albicans* with epithelial cells

C. albicans is a common member of the gut microbiota and therefore in close proximity with the intestinal epithelial cell layer interacting with these enterocytes [111]. The initial interaction step is the adhesion of *C. albicans* yeast cells to epithelial cells *via* the interaction of fungal cell wall components with the surface of the host cells [40,112]. These interactions are on the one hand non-specific due to hydrophobicity, Brownian movement forces or repulsive effects of the electrical double layer of cells [22,40]. In addition, specific protein-protein interactions mediate adhesion of *C. albicans* to epithelial cells e.g. *via* binding of the fungal adhesion protein Als3 to the adherens junction protein E-Cadherin or the covalently linkage of the adhesin Hwp1 to epithelial surface proteins [40,112,113]. The adhesion of yeast cells to the epithelium triggers the filamentation of *C. albicans* which can adhere more strongly to the epithelial cells due to the enhanced expression of adhesins [40]. The formation of hyphae on host cells is associated with the subsequent invasion of *C. albicans* into epithelial cells [114]. This is realized by both induced endocytosis and active penetration [113,115]. Whereas induced endocytosis occurs early during this interaction and is a host driven-mechanism involving Als3/Ssa1-E-Cadherin interaction and host actin cytoskeleton redistribution [40,44,113,115-117], active penetration is fungal-mediated by hyphae invading into epithelial cells supported by secreted hydrolases, like the Sap family, affecting epithelial cell-cell-junctions [40,113,118,119]. Both invasion routes occur in oral epithelial cells [115]. In contrast, the main invasion route of *C. albicans* into IECs is active penetration [115,120]. Only if tight junctions are impaired, induced endocytosis can contribute to invasion into enterocytes [115,121]. Fungal invasion leads to tissue destruction in which candidalysin plays a key role by directly damaging epithelial cells [39,120]. These processes lead to fungal translocation *via* the transcellular route due to decreased epithelial barrier integrity and tight junction impairment [120,122].

2. Aims of this study

The *C. albicans* population in the GIT is the main source of disseminated *Candida* infections; in hospitalized patients subjected to major surgeries or traumatic shock situation the development of IR which results in the dysfunction of the intestinal epithelial barrier and increased barrier permeability enhances bacterial translocation. An *in vivo* rat model furthermore demonstrated *C. albicans* translocation and dissemination during IR injury [123]. This suggests that the shifts in oxygen availability during IR might affect *C. albicans* translocation and subsequent dissemination. Although several studies investigated in the interaction of *C. albicans* with enterocytes with regard to the translocation process and fungal factors involved [120,122], these *in vitro* investigations were conducted at ambient (~ 21 % O_2) conditions. Thus, this study aimed to investigate the role of physiological oxygen levels on fungal-host interaction and the impact of oxygen shifts mimicking hypoxic shock or reoxygenation as they occur during IR.

3. Materials and Methods

3.1. Materials

3.1.1. *C. albicans* strains

The *C. albicans* strains used in this study are listed in Table 1. Unless stated otherwise, the *C. albicans* wild-type (wt) strain SC5314 was used for experiments performed during this study.

Table 1: *C. albicans* strains used in this study

Strain	Genotype	Parental strain	Reference
SC5314	Prototrophic clinical isolate	–	[124]
CAF2-1	*ura3::imm^{434}/ura3::URA3*	SC5314	[125]
Parental strain of deletion mutants complemented for auxotrophies	*arg4::dpl200/arg4::dpl200 leu2::dpl200/LEU2 his1::hisG/HIS1 ura3::imm^{434}/ura3::URA3 iro1::imm^{434}/iro1::IRO1*	SN152	[126,127]
*ssa1*ΔΔ	*ura3::imm^{434}/ura3::imm^{434} ssa1::FRT/ssa1::FRT ssa2::FRT::URA3::SSA2/SSA2*	CAF4-1	[44,128]
*ssa1*ΔΔ + *SSA1*	*ura3::imm^{434}/ura3::imm^{434} ssa1::FRT/ssa1::FRT ssa2::FRT/SSA2 rps10::URA3::SSA1/RPS10*	*ssa1*ΔΔ	[44]
*ace2*ΔΔ	*ace2::C.d.HIS1/ace2::C.m.LEU2*	SN152	[126]
*efg1*ΔΔ	*efg1::C.d.HIS1/efg1::C.m.LEU2*	SN152	[126]
*tye7*ΔΔ	*tye7::C.d.HIS1/tye7::C.m.LEU2*	SN152	[126]
*upc2*ΔΔ	*upc2::C.d.HIS1/upc2::C.m.LEU2*	SN152	[126]

3.1.2. Cell lines

The human enterocyte cell lines listed in Table 2 were used as *in vitro* models to study the interaction of *C. albicans* with IECs. These cell lines were commercially obtained

from the “Deutsche Sammlung von Mikroorganismen und Zellkulturen” (DSMZ) or the American Type Culture Collection (ATCC®), respectively.

Table 2: human cell lines used in this study

Cell line	Cell type	Cultivation medium	Source/Nr.
Caco-2	Colon adenocarcinoma	DMEM (Dulbeccos Modified Eagle’s Medium), 10 % heat-inactivated FCS (fetal calf serum)	DSMZ/ACC 169
C2BBe1	Colon adenocarcinoma	DMEM, 10 % heat-inactivated FCS, 10 µg/ml human holotransferrin	ATCC®/CRL-2102™

3.1.3. Antibodies

Table 3: Antibodies used in this study

Antibody	Produced in	Company	Application
Anti-*C. albicans*	Rabbit	Acris Antibodies	Adhesion/Invasion
Anti-rabbit Alexa Fluor® 488	Goat	Invitrogen	Adhesion/Invasion
Phalloidin DyLight® 594	–	Invitrogen	Adhesion
Anti-rabbit Alexa Fluor® 647	Chicken	Invitrogen	Invasion
Anti-HIF-1α	Mouse	BD Transduction Laboratories™	Western Blot
Anti-Claudin-4 (clone 3E2C1)	Mouse	Invitrogen	Western Blot
Anti-Occludin	Rabbit	Invitrogen	Western Blot
Anti-E-Cadherin	Goat	R&D Systems	Western Blot
Anti-pan-Actin (clone D18C11)	Rabbit	Cell Signaling Technology®	Western Blot
Anti-CEACAM1 (clone C5-1X)	Mouse	ReliaTech GmbH	Western Blot
Anti-CEACAM6 (clone 1H7-4B)	Mouse	EMD Millipore	Western Blot
Anti-14-3-3 (clone H8)	Mouse	Santa Cruz	Western Blot
Anti-goat-HRP	Rabbit	Invitrogen	Western Blot

Anti-rabbit-HRP	Goat	Cell Signaling Technology®	Western Blot
Anti-mouse-HRP	Horse	Cell Signaling Technology®	Western Blot
Anti-mouse-HRP	Goat	Dianova	Western Blot

3.1.4. Media and chemicals

All media, buffers, commercially available kits, chemicals and enzymes used in this study are listed in Table 4 – Table 7.

Table 4: Media used in this study

Medium	Composition	Application
YPD medium	1 % yeast extract, 2 % D-glucose, 2 % peptone	*C. albicans* growth curves and overnight cultures
YPD agar	1 % yeast extract, 2 % D-glucose, 2 % peptone, 2 % agar-agar	Cultivation of *C. albicans*
DMEM with phenol red	Commercially obtained from Gibco®; see [129]	Enterocyte cultivation, infection experiments
DMEM without phenol red	Commercially obtained from Gibco®; see [130]	Translocation Assay

Table 5: Buffers used in this study

Buffer	Composition	Application
PBS II	140 mM NaCl; 2.7 mM KCl; 10 mM Na_2HPO_4; 1.8 mM KH_2PO_4; pH 7.4	All experiments as indicated
PBST	PBS II; 0.01 % Tween20	Adhesion/Invasion
RIPA lysis buffer (Merck Millipore)	50 mM Tris-HCl, pH 7.4; 150 mM NaCl; 0.25 % Deoxycholic acid; 1 % NP-40; 1 mM EDTA	Cell lysis for protein quantification by SDS-PAGE/ Western Blot
1x Sample lysis buffer (1x SLB)	10 % Glycerol; 2 % SDS; 5 % β-mercaptoethanol; 62.5 mM Tris, pH 6.8; Bromophenol blue only for SDS-PAGE	Cell lysis for HIF-1α quantification by SDS-PAGE/Western Blot; Denaturation of

		proteins for SDS-PAGE
Separation gel buffer (SGB)	2 M Tris, pH 8.8	SDS-PAGE
Sollection gel buffer (CGB)	0.5 M Tris, pH 6.8	SDS-PAGE
5x Lämmli buffer	50 % Glycerol; 14.5 % SDS; 0.3 M Tris, pH 6.8; 0.015 % Bromophenol blue	SDS-PAGE
SDS-PAGE buffer	200 mM Glycine; 25 mM Tris; 3.5 mM SDS	SDS-PAGE
Blotting buffer	200 mM Glycine; 25 mM Tris	Western Blot
TBST, pH 7.6	10 mM Tris; 100 mM NaCl; 0.9 mM Tween 20	Western Blot

Table 6: Kits used in this study

Kit	Company	Application
Cytotoxicity Detection Kit	Roche	Damage Assay
Pierce™ BCA Protein Assay Kit	Thermo Fisher Scientific	Protein concentration determination
Human IL-8 ELISA	eBioscience	IL-8 quantification
Human IL-6 ELISA	eBioscience	IL-6 quantification
Human MCP-1 ELISA	eBioscience	MCP-1 quantification
Human LL-37 ELISA	Hycult®Biotech	LL-37 quantification
DCFDA Cellular ROS Detection Assay Kit	Abcam®	Quantification intracellular ROS production

Table 7: Chemicals and enzymes used in this study

Name	Company	Application
FCS	Bio&Sell	Enterocyte cultivation
Human holo transferrin	Calbiochem®	Enterocyte cultivation
Gibco™ collagen I rat protein	Thermo Fisher Scientific	Coating of microwell plates
Accutase®	Capricorn	Enterocyte cultivation
Triton X-100	Sigma-Aldrich®	Enterocyte permeabilization
HCl	Carl Roth®	Damage Assay
Sodium lactate (60 % w/w syrup)	Sigma-Aldrich®	Damage Assay/Hyphal length determination

$CoCl_2$	Sigma-Aldrich®	Damage Assay/Western Blot
BAY 87-2243	Selleckchem	Damage Assay/Western Blot
4 % Roti®-Histofix	Carl Roth®	Adhesion/Invasion
Bovine serum albumin (BSA)	Serva	Adhesion/Invasion/Western Blot
Tween20	Carl Roth®	Adhesion/Invasion/Western Blot
ProLong Antifade Reagent	Thermo Fisher Scientific	Adhesion/Invasion
Rhodamine B isothiocyanate (RITC) dextran, 10 kDa	Sigma-Aldrich®	Permeability determination
Zymolyase® (*Arthrobacter luteus*)	amsbio	Fungal cell detachment/separation
Glycerol	Carl Roth®	-80 °C storage/SDS-PAGE
sodium dodecyl sulfate (SDS)	Carl Roth®	SDS-PAGE
Acrylamide/Bis 37.5:1 30 % (w/v) (AB 30 %)	Serva	SDS-PAGE
Ammonium persulfate (APS)	Serva	SDS-PAGE
N,N,N',N'-tetramethyl-ethylendiamine (TEMED)	Serva	SDS-PAGE
β-mercaptoethanol	Carl Roth®	SDS-PAGE
Bromophenol blue	Carl Roth®	SDS-PAGE
PageRuler™ Prestained Protein Ladder	Thermo Fisher Scientific	SDS-PAGE/Western Blot
Tris	Carl Roth®	SDS-PAGE/Western Blot
Glycine	Carl Roth®	SDS-PAGE/Western Blot
NaCl	Carl Roth®	SDS-PAGE/Western Blot
Protease Inhibitor Mix	Jena Bioscience	Enterocyte lysis
Milk powder	Carl Roth®	Western Blot
Western Lightning® Plus-ECL solution	Perkin Elmer	Western Blot
Glucose	Carl Roth®	Hyphal length determination

3.2. Methods

3.2.1. *C. albicans* cultivation and infection

The *C. albicans* strains were kept at - 80 °C for long term storage in YPD medium supplemented with 50 % (v/v) glycerol. These glycerol stocks were used for inoculation of YPD agar plates which were incubated for two days at 30 °C and stored for up to three weeks at 4 °C as short term storage.

For experiments, one single colony from the short term storage YPD plate was re-streaked on an YPD agar plate and incubated for two days at 30 °C. The obtained single colonies were then used to inoculate YPD medium. After incubation at 30 °C and 180 rpm in a shaking incubator overnight, the cells were harvested by centrifugation at 14,000 rpm for 2 min and washed twice with PBS II before the desired concentration was adjusted with DMEM.

For the infection of enterocytes with *C. albicans* strains, the cultivation medium of the host cells was replaced with DMEM prior to infection to prevent the FCS-induced filamentation of *C. albicans*. This ensures that the fungal filamentation only depends on the oxygen regime, DMEM, and the presence of enterocytes.

3.2.2. *C. albicans* growth analysis

The cultivation in YPD medium and on YPD agar plates was performed to investigate the influence of oxygen on *C. albicans* growth.

For growth curve analysis, overnight cultures were harvested by centrifugation at 14,000 rpm for 2 min and washed twice with PBS II. The fungal cell suspension was diluted in YPD medium to an optical density (OD) of 0.2 at 600 nm (OD_{600} = 0.2) and transferred to three 96-well plates with technical triplicates per plate. The fungal cells were then cultivated at 37 °C, 5 % CO_2 and oxygen levels ranging from 0.2 % to 21 % in oxygen-adjustable incubators (CO_2 Incubator INCOmed 153, Memmert). A temperature-controlled Hypoxystation (H35, Don Whitley Scientific) was used in some experiments, predominantly for cultivation of cells at oxygen levels at or below 2 % O_2. The growth of *C. albicans* was monitored measuring the OD at 600 nm every 30 min for a time course of 14 h using a microplate reader (Infinite® M200 pro, TECAN). Therefore, three microtiter plates per experiment were prepared: for each OD measurement, the upper plate was carried to the microplate reader and placed back below the two remaining plates after measurement. This procedure ensured that the fungal cells had enough time to re-adapt to the respective oxygen level prior to the next measurement since the cells

had to face ambient (~ 21 %) oxygen shortly for the time of measurement which took approximately 3 min to 4 min.

To analyze the colony morphology of *C. albicans* in dependence of the oxygen availability, a maximum of 100 fungal cells resuspended in PBS II were plated on YPD agar plates and incubated for five days at 37 °C, 5 % CO_2 and oxygen levels ranging from 0.2 % to 21 % O_2. The colony morphology was recorded using a binocular microscope (Stemi 2000-C, Carl Zeiss Microscopy GmbH) and the software AxioVision. For examination of single cell morphology, colony parts were dispensed in water droplets and documented using an inverse light microscope with software ZEN 2 (Carl Zeiss Microscopy GmbH).

3.2.3. Cultivation of enterocytes

The colorectal adenocarcinoma cell lines Caco-2 and C2BBe1 (brush border expressing sub-clone of Caco-2) were used in this study. Caco-2 cells are able to undergo an absorptive enterocyte-like differentiation with the expression of brush borders mimicking the situation in the small intestine although they origin from the colon [131,132]. However, not all cells express brush borders resulting in a highly heterogeneous morphology within the population [133]. In contrast, the Caco-2 sub-clone C2BBe1 exhibits little morphological heterogeneity and, hence, stability in brush border expression, representing an authentic *in vivo* structure of the human colon [133]. Therefore, C2BBe1 cells were used for all infection experiments performed in this study. Additionally, the Caco-2 cell line was used in the initial Damage Assays (see Chapter 3.2.6) for comparison because these cells were extensively used as a model for the intestinal epithelial barrier over the last decades [134]. In the following chapters, both cell lines will be termed as enterocytes since they exhibit brush borders which are characteristic for absorptive enterocytes [132,133].

Both cell lines were stored in liquid nitrogen. After thawing at 37 °C, enterocytes were added to 9 ml of the respective cultivation medium (see Table 2; heat-inactivation of FCS for 20 min at 56 °C using a water bath) and centrifuged for 5 min at 200 × g to remove dimethyl sulfoxide (DMSO) which was used as a cryoprotectant during cryopreservation [135]. The cells were resuspended in cultivation medium and added to cultivation medium provided in a 25 cm^2 cell culture flask (CELLSTAR®, greiner bio-one) to a total volume of 8 ml. The cultivation medium was exchanged after cultivation for 24 h at 21 % O_2, 37 °C and 5 % CO_2. After confluency was reached, the cultivation medium was removed and the cells were washed with 5 ml PBS II and detached with 1 ml Accutase® at 37 °C for 10 min. The enterocytes were then seeded in 19 ml of respective cultivation medium in a 75 cm^2 cell culture flask (CELLSTAR®, greiner bio-one). Routine

cultivation of Caco-2 and C2BBe1 cells was performed at 21 % O_2, 37 °C and 5 % CO_2 for a maximum of 15 passages.

The passaging of enterocytes was performed after confluency was reached. Therefore, the cells were washed with 8 ml PBS II, detached with 2 ml Accutase® at 37 °C for 20 min and resuspended with 4 ml fresh cultivation medium. Depending on the experimental procedure, 0.5 ml – 3 ml of detached cells were transferred in fresh cultivation medium (total volume of 20 ml) to a new 75 cm^2 cell culture flask.

3.2.4. Cultivation of enterocytes for experiments

Enterocytes were seeded in multiple wells, which were collagen I-coated for C2BBe1 cells. In order to coat the wells, a 10 µg/ml collagen I-solution in bis-distilled water (ddH_2O) was added to the wells so that the bottom of the well was covered. After an incubation time of 2 h at RT, the wells were washed twice with ddH_2O and left at RT until the wells were dried. Unless indicated otherwise, the seeded enterocytes were incubated for seven days at 37 °C, 5 % CO_2 with defined oxygen concentrations ranging from 5 % to 21 % in oxygen-adjustable incubators. The incubation of enterocytes at oxygen levels at or below 2 % was performed using the Hypoxystation. The cultivation medium was exchanged every third day. In order to simulate hypoxic shock, the cells were shifted from high to low oxygen levels. Shifts from low to high oxygen levels were performed to mimic reoxygenation. The oxygen change was performed 1.5 h prior to the infection with *C. albicans* or mock-infection (no fungal inoculation was performed but cultivation medium was exchanged with DMEM) by placing the respective cell culture samples into a different incubator. During this adaptation phase, and all experiments, the enterocytes were kept at 37 °C and 5 % CO_2.

3.2.5. Determination of enterocyte proliferation

In order to quantify the proliferation of enterocytes, C2BBe1 cells were seeded in 6-well plates with 5×10^5 cells per well. 24 h after mock-infection, enterocytes were washed with PBS II, detached with 250 µl Accutase® (Capricorn) at 37 °C for up to 40 min, and counted with a Neubauer chamber.

3.2.6. Damage Assays

Severely damaged necrotic cells release intracellular proteins, including the cytosolic enzyme lactate dehydrogenase (LDH). LDH catalyzes the conversion from pyruvate to lactate, and was shown to be stable at a wide range of temperatures and to be expressed in a variety of cells [136,137]. Thus, the release of LDH into the supernatant was

used to quantify epithelial cell damage as the activity of this enzyme correlates with the grade of cell damage [138,139]. For Damage Assays, Caco-2 and C2BBe1 cells were seeded into 96-well plates at 2×10^4 cells per well. For infection, the cultivation medium was replaced with DMEM containing 8×10^4 *C. albicans* cells; DMEM without fungal cells was used for mock-infected controls. Supernatants were collected 24 h and 48 h post infection (p.i.) and analyzed using the Cytotoxicity Detection Kit from Roche according to the manufacturer's instructions using a LDH standard. Briefly, a catalyst solution containing diaphorase and NAD^+ and a dye solution containing iodotetrazolium chloride (INT) and sodium lactate were mixed at a ratio of 1:45, added to the sample supernatants diluted in PBS II, and incubated for up to 15 min in the dark at room temperature (RT). In this reaction, the LDH-catalyzed conversion of lactate to pyruvate causes the reduction of NAD^+ to $NADH/H^+$. Diaphorase then catalyzes the transfer of H/H^+ from $NADH/H^+$ to INT which results in the production of the water-soluble dye formazan. The enzymatic reaction was stopped by adding HCl to a final concentration of 200 µM. The absorption of the formazan dye was measured spectrophotometrically at 490 nm using a microplate reader. To determine the maximum of LDH release (high control), the cells were lysed with 10 µl of 5 % Triton X-100. The damage of *C. albicans*-infected enterocytes was calculated as percentage of high control after the values of mock-infected controls were subtracted from both infected enterocytes and high control.

In order to investigate in the influence of lactate on the damage caused by *C. albicans*, C2BBe1 cells were supplemented with different lactate concentrations (5 mM, 10 mM, 15 mM, 20 mM, 25 mM) in parallel to infection with the fungus. Therefore, sodium lactate in DMEM was added to the epithelial cells directly before inoculation with *C. albicans*.

Furthermore, the influence of HIF-1α on the damage phenotype of *C. albicans*-infection was analyzed. Therefore, C2BBe1 cells were seeded into 6-well plates at 5×10^5 cells per well. Prior to infection, the cells were treated with either 200 µM $CoCl_2$ for 24 h or 100 nM BAY 87-2243 for 5 h in cultivation medium. For infection, 2×10^6 *C. albicans* cells were used. In parallel to infection with the fungus or mock-infection, respective C2BBe1 cells were again treated with 100 nM BAY 87-2243 in DMEM for the time of infection (24 h). To obtain high damage control samples, enterocytes were lysed with 275 µl 5 % Triton X-100.

3.2.7. Analysis of adhesion and invasion

In order to investigate the adhesion and invasion of *C. albicans*, C2BBe1 cells were seeded onto collagen I-coated 15 mm glass cover slips in 24-well plates at 1×10^5 cells

per well. Enterocytes were infected with 1×10^5 *C. albicans* cells and fixed with 4 % Roti®-Histofix after 30 min (adhesion) or 4.5 h (invasion), respectively.

Adhesion assay

Following overnight fixation at 4 °C, the cover slips were washed three times for 1 min with PBS II and incubated with 5 % bovine serum albumin (BSA) in PBS II for 10 min on a shaking incubator at 50 rpm. After a second washing step with PBS II for three times 1 min, adherent *C. albicans* cells were stained using a polyclonal rabbit anti-*Candida* primary antibody (2 µg/ml in PBS II) and an Alexa Fluor® 488 conjugated anti-rabbit secondary antibody (0.4 µg/ml in PBS II). After each staining step, the cells were washed carefully three times for 1 min with PBS II supplemented with 0.01 % Tween20 (PBST). In order to differentiate areas with and without enterocytes for automatic image analysis of adherent *C. albicans* cells, the actin filaments of the enterocytes were stained. For this purpose phalloidin was used. This phallotoxin stabilizes actin filaments by binding to these and preventing their depolymerization [140]. Therefore, epithelial cells were permeabilized with 0.5 % Triton X-100 for 5 min and carefully washed three times for 1 min with PBST. Afterwards, the cells were incubated with DyLight® 594 Phalloidin (5 units/ml) in 5 % BSA in PBS II for 30 min in the dark. The cells were washed carefully three times for 1 min with PBST. The cover slips were mounted onto microscope slides using ProLong Antifade Reagent. Adherent *C. albicans* cells were quantified using a fluorescent microscope (Axio Observer Z1, Zeiss) with filter sets to detect Alexa Fluor® 488 and DyLight™ 594. The resulting images were quantified using an automated image analysis (see 3.2.8). The percentage of adherent *C. albicans* cells was calculated as follows:

$$\frac{\textit{C. albicans}\text{ cells per image section} \times \text{area of whole cover slip}}{\textit{C. albicans}\text{ cells used for infection} \times \text{area of image section}}$$

Invasion assay

In order to quantify the invasion of *C. albicans* into enterocytes, both adherent and invasive fungal cells were stained. Therefore, the cells were treated as described above for adherent *C. albicans* cells. Following host cell permeabilization with 0.5 % Triton X-100 and a washing step with PBST for three times 1 min, the invasive fungal cells were stained using a polyclonal rabbit anti-*Candida* antibody as primary antibody (2 µg/ml in PBS II) followed by incubation with an Alexa Fluor® 647 conjugated anti-rabbit

secondary antibody (0.4 µg/ml in PBS II). After each staining step, the cells were washed carefully three times for 1 min with PBST. The cover slips were mounted onto microscope slides using ProLong Antifade Reagent. Invasive *C. albicans* cells were quantified using a fluorescent microscope (Axio Observer Z1, Zeiss) with filter sets to detect Alexa Fluor® 488 and Alexa Fluor® 647. The percentage of invasion was determined as the ratio of invading cells to the number of adherent cells. A minimum of 150 fungal cells were counted per cover slip.

3.2.8. Quantification of fungal adhesion to enterocytes using automated image analysis

The microscopy images from the adhesion assays were used for automated image analysis. This analysis method was performed by Stefanie Dietrich from the Research Group of Applied Systems Biology at the Hans Knöll Institute Jena, who kindly provided the protocol for this procedure.

The number of adherent fungal cells was quantified using an automated image analysis workflow written in the Python programming language (version 2.7.13) combined with OpenCV library (version 3.1.0 [141]) and Numpy (version 1.11.3, as part of the SciPy [142]). The two fluorescence channels were processed separately: Void areas in the epithelial cell layer were segmented in the first channel and fungal cells were segmented in the second. The results from both channels were combined to distinguish adherent from non-adherent fungal cells, whereby fungal cells were considered to be non-adherent, if located within void areas.

To segment the void areas, images were processed in groups of four. The images were converted to grayscale, normalized and gamma corrected with $\gamma = 0.3$ to improve contrast. Denoising was performed using a Gaussian filter of 7×7 pixels with the width $\sigma = 3$ pixels. Otsu's thresholding was used to discriminate between void areas with low intensity values and the cell layer with high intensity values. The threshold was calculated using the histogram of the pixel intensity values in the intensity range [0,127]. Only void areas with an area of more than 1000 pixels were taken into account, in order to avoid false positives. Watershed segmentation was used to refine the contours of the void areas.

The intensity values in the green-fluorescent channel were converted to grayscale, normalized and Otsu-thresholded to locate clusters of fungal cells. To improve the accuracy of the cell contours and to remove noise, adaptive thresholding implemented in the OpenCV library was used. Exact contours are a prerequisite for the application of the

cluster splitting method adopted from Farhan *et al.* [143] as implemented in Brandes *et al.* [144]. Before the cluster splitting, hyphal structures were removed by morphological closing with an elliptical kernel of 9×9 pixels. Only cells with a minimal area of 50 pixels were taken into account, in order to exclude budding cells and segmentation artefacts. Single cells that were removed in the previous closing step were re-inserted based on missing overlap with other cells.

Finally, adherent and non-adherent fungal cells were discriminated: A cell was classified as being non-adherent, if at least one half of its area overlapped with a void area region. The number of adherent cells was then normalized by the total pixel area of the epithelial cells in this image.

3.2.9. Translocation Assay

In order to determine the enterocyte barrier integrity and the translocation of *C. albicans*, the recently described *in vitro* translocation model by Allert *et al.* [120] was used and adapted. Briefly, 24-well plates with polycarbonate membrane Transwell® Inserts with 5 µm pore size (Corning) were used. Inserts were coated with collagen I and seeded with 2×10^4 C2BBe1 cells. The cultivation medium was exchanged after four days of incubation and every second day afterwards. The transepithelial electrical resistance (TEER) was measured from day one until day 13 every second day and at day 14 to monitor the establishment of the barrier integrity [122] using a chopstick electrode connected to the Epithelial Voltohmmeter EVOM^2 (World Precision Instruments). Blank values from empty inserts without epithelial cells were subtracted from sample values. In order to monitor TEER kinetics after infection with 1×10^5 *C. albicans* cells or mock-infection, measurements were performed prior to both oxygen switch and infection/medium exchange as well as 30 min, 4.5 h, 12 h and 24 h after infection.

To determine the permeability of the enterocyte monolayer, 10 µl of 50 mg/ml Rhodamine B isothiocyanate (RITC) dextran (10 kDa), dissolved in ddH_2O, were added to the upper compartment 24 h p.i. After 4 h of incubation, the fluorescence of the lower compartment was measured at 600 nm using a microplate reader and concentrations were calculated with the help of a RITC dextran standard. To prevent signal interferences from phenol red, DMEM without phenol red was used for infection and mock-infection in these experiments.

In order to quantify *C. albicans* translocation, 20 U/ml Zymolyase® were added to the lower transwell compartment 24 h p.i. Due to its lytic activity on the fungal cell wall [145], translocated *C. albicans* hyphae were detached from the bottom side of the Transwell®

Inserts and separated. After incubation for 2 h at 37 °C, the cell suspensions were serially diluted and plated in duplicates onto YPD agar. After one day incubation at 30 °C, the colony forming units (CFUs) were counted. Toni Förster from the Department of Microbial Pathogenicity Mechanisms supported the translocation analysis by performing the Zymolyase® treatment and plating CFUs.

3.2.10. Protein isolation from enterocytes

C2BBe1 cells were seeded in 6-well plates with 5×10^5 cells per well. Following the infection with 2×10^6 *C. albicans* cells per well or mock-infection (24 h), cell culture supernatants from both mock-infected and *C. albicans*-inoculated C2BBe1 cells were removed carefully and cleared from cellular debris by centrifugation at 3,000 × g for 10 min at 4 °C. The cells were washed with ice-cold PBS and lysed with either RIPA lysis buffer for adherens/tight junction proteins and CEACAMs or 1× sample lysis buffer (1× SLB) for HIF-1α. Both lysis buffers were supplemented with Protease Inhibitor Mix, which consists of phenylmethylsulfonylfluorid (PMSF), pefabloc, aprotinin and pepstatin A. The cell lysates used for CEACAM detection were incubated on ice for 1h. HIF-1α samples were incubated at 98 °C for 10 min. All cell lysates were centrifuged for 15 min at 4 °C and 20,000 × g to remove cellular debris.

The protein concentration of cleared cell lysates was determined using the Pierce™ BCA Protein Assay Kit. A BSA standard ranging from 0 – 2 mg/ml was prepared according to manufacturers' instructions. A Working Reagent (WR) was prepared using solution A, containing bicinchoninic acid (BCA), and solution B, containing cupric sulfate, with a ratio of 50:1. 25 µl of each standard concentration, and each sample were mixed with 200 µl of WR and incubated for 30 min at 37 °C. Proteins reduce Cu^{2+} to Cu^{+} which is known as biuret reaction. The cuprous ion then chelates two BCA molecules leading to a purple-colored reaction product. The absorbance of this water-soluble complex was measured at 562 nm using a microplate reader.

3.2.11. SDS-PAGE

The proteins were separated *via* a sodium dodecyl sulfate polyacrylamide gel electrophoresis (SDS-PAGE) using the Biometra Eco-Mini system from Analytik Jena. Protein gels (see Table 8) with appropriate concentrations of acrylamide were used according to the proteins of interest: the percentage of acrylamide was lowered with increasing protein size.

Table 8: components of protein gels

% acrylamide	AB 30 %	CGB/SGB	SDS	APS	TEMED
4 % (collection gel)	13.3 %	25 %	0.1 %	0.12 %	0.08 %
7.5 %	25 %				
10 % (separation gel)	33.3 %	19 %	0.1 %	0.08 %	0.08 %
12.5 %	41.6 %				

Prior to protein separation, the samples were heated either to 98 °C for 10 min with 1× SLB with bromophenol blue (adherens/tight junctions) or to 95 °C for 5 min with 5× Lämmli buffer (CEACAMs). The gels were loaded with 5 µg protein per adherens/tight junction sample and 15 µl per HIF-1α cell lysate sample (determination of protein concentration was not possible due to β-mercaptoethanol in 1× SLB). To detect CEACAM proteins, 10 µg protein per cell lysate (except for reoxygenation samples of *C. albicans*-infected enterocytes, where the protein concentrations allowed for only 1 µg, respectively) and corresponding volumes of the cell culture supernatants were used. Additionally to protein samples, 5 µl of PageRuler™ Prestained Protein Ladder were applied per protein gel as a molecular weight marker. Two gels were run in SDS-PAGE buffer at 25 mA and 140 V for ~ 2 h.

3.2.12. Western Blot

The SDS-PAGE-separated proteins were transferred to polyvinylidenfluorid (PVDF) membranes (Amersham Hybond P 0.45, GE Healthcare) *via* Tank Blot (Bio-Rad). The protein transfer was performed in Blotting buffer for 1 h at 350 mA. The membranes were blocked with 1 % BSA (junction proteins) and 5 % milk powder (HIF-1α) in TBST or 10 % milk powder (CEACAMs) in TBS. After a washing step with TBST for three times 10 min, the primary antibody incubation was performed overnight at 4 °C in the respective blocking solution or in TBST (CEACAMs). The membranes were washed three times for 10 min with TBST. The incubation with the horseradish peroxidase (HRP)-conjugated secondary antibodies was performed at RT for 1 h using the respective blocking solution or TBST (CEACAMs). Afterwards, the membranes were washed three times for 10 min with TBST. Bound HRP-conjugated secondary antibodies were detected *via* chemiluminescence using the Western Lightning® Plus-ECL solution according to manufacturer's instructions. The quantification of adherens/tight junction and HIF-1α protein expression was performed using the ImageJ software with normalization to the pan-Actin loading control. The CEACAM signal intensities were quantified using the

Image Studio Lite Software (V3.1, LI-COR), adjusted to 14-3-3 signal intensities (loading control for CEACAM cell lysates) and fold signal intensities (=normalized expression) of the respective CEACAM bands compared to mock-infected C2BBe1 cells kept at 21 % O_2 were calculated.

3.2.13. Lactate and glucose measurements

In order to investigate the oxygen-dependent changes in the enterocyte metabolism, both the lactate production and the glucose consumption of C2BBe1 cells was quantified. Therefore, the lactate and glucose concentrations in the supernatants from both *C. albicans*-infected and mock-infected C2BBe1 cells were determined 24 h p.i. The supernatants were centrifuged for 20 min at 4 °C and 1,000 × g. The analysis was performed by Cora Richert from the Institute for Clinical Chemistry and Laboratory Diagnostic at the Jena University Hospital using the Abbot Architect ci8200 Integrated System (Abbot Laboratories) according to the manufacturers' instructions.

3.2.14. Quantification of cytokine production

It has been shown that IECs are able to produce cytokines in response to bacterial and fungal infection, lipopolysaccharide (LPS)-stimulation or inflammatory diseases. Among the produced cytokines, interleukin (IL)-8, monocyte chemoattractant protein-1 (MCP-1), granulocyte-macrophage colony-stimulating factor (GM-CSF), tumor necrosis factor α (TNFα), IL-33, IL-1β and IL-6 showed the highest abundance [62,146-149]. To determine whether these cytokines are expressed in C2BBe1 cells following *C. albicans* infection, the cell culture supernatants from mock-infected, *C. albicans*-inoculated and LPS-stimulated (2.5 µg/ml) C2BBe1 cells 24 h p.i. were centrifuged for 20 min at 4 °C and 1,000 × g and analyzed using a ProcartaPlex® Immunoassay (affymetrix eBioscience) performed according to manufacturers' instruction. In principle, this assay uses distinct dye-labeled magnetic beads with each type of bead covered with a distinct specific primary antibody. This allows the detection of several targets within one sample since the targets can be discriminated *via* the different dyes. The amount of each target is determined by the secondary detection antibody which binds to all targets.

For the quantification of detectable cytokines, enzyme-linked immunosorbent assays (ELISAs) with supernatants generated as stated above were performed using Kits from eBioscience according to manufacturers' instruction (see Table 6).

3.2.15. Quantification of LL-37 production

The cathelicidin LL-37 was shown to have a candidacidal effect and to reduce *C. albicans* adhesion [150,151]. Furthermore, its secretion by enterocytes is at least partly mediated by HIF-1α [109]. In order to determine whether the production of this AMP was influenced by the different oxygen regimes used in this study, LL-37 concentrations were determined in the cell culture supernatants from both mock-infected and *C. albicans*-inoculated C2BBe1 cells 24 h p.i. These supernatants were centrifuged for 20 min at 4 °C and 1,000 × g and analyzed using the human LL-37 ELISA Kit from Hycult®Biotech according to manufacturer's instructions.

3.2.16. Quantification of ROS production

In order to analyze the intracellular ROS production in enterocytes, the DCFDA Cellular ROS Detection Assay Kit was used. Therefore, C2BBe1 cells were seeded into white 96-well plates with clear bottom (µCLEAR®, greiner bio-one) at 2×10^4 cells per well. Following infection with 8×10^4 *C. albicans* cells or mock-infection for 24 h, the ROS production was quantified using the Kit according to the manufacturers' instructions. Briefly, the enterocytes were incubated with 10 µM 2'7'-dichlorofluorescein diacetate (DCFDA) for 30 min. DCFDA is able to diffuse through cell membranes and to be converted by cellular esterases. The resulting non-fluorescent compound can be oxidized by ROS into the highly fluorescent 2'7'-dichlorofluorescein (DCF). Additionally, the enterocytes were incubated with 250 µM tert-butyl hydrogen peroxide (TBHP) for 3 h as a positive control to induce ROS. As background control non-infected C2BBe1 cells without addition of DCFDA were used. All incubation steps were performed under the indicated oxygen concentrations. ROS levels were quantified by measuring the fluorescence intensity at an excitation and emission maximum of 495 nm and 529 nm, respectively. The background control was subtracted from all measured values.

3.2.17. Determination of fungal burden

In addition to growth curves, the determination of fungal burden was used as a parameter to analyze fungal growth under different experimental conditions. Therefore, 4×10^5 *C. albicans* cells per well were added to collagen I-coated 24-well plates with or without host cells (C2BBe1 seeded at a density of 1×10^5 cells per well, pre-incubated for seven days) and incubated for 4.5 h or 24 h at 37 °C, 5 % CO_2, at the indicated oxygen concentrations. Afterwards, the cells were treated with 1 mg/ml Zymolyase® for 30 min at 37 °C, vortexed rigorously and incubated again at 37 °C for 30 min. The cell

suspension was vortexed again, serially diluted, and plated onto YPD agar in duplicates. The CFUs were counted after one day incubation at 37 °C.

3.2.18. Determination of hyphal length

To investigate the influence of oxygen concentrations on the hyphal length of *C. albicans*, collagen I-coated wells with and without enterocytes as described above (3.2.17) were inoculated with 1×10^5 fungal cells. The hyphal length was measured after 4.5 h for 100 *C. albicans* hyphae per well using an inverse light microscope with the software ZEN 2 (Carl Zeiss Microscopy GmbH). In addition to fresh DMEM, supernatants from both enterocytes and *C. albicans* cells were used in some experiments. Therefore, infected and mock-infected enterocytes as well as *C. albicans* cells were cultivated in DMEM for 24 h at the indicated oxygen concentrations.

In order to test the influence of lactate and glucose on hyphal length, *C. albicans* cells were cultivated in DMEM with or without 25 mM glucose supplemented with 0 mM, 5 mM or 20 mM sodium lactate.

3.2.19. Statistical analyses

All experiments were performed in at least three biological replicates and their resulting mean value was depicted either as Whisker-Box-Plot (horizontal line with interquartile range; experiments with at least four biological replicates) or as mean with standard deviation (SD). Technical duplicates or triplicates within biological replicates were averaged. The statistical analyses were performed using GraphPad Prism® 7 for Windows. Comparisons between selected data sets were determined using a one-way analysis of variance (ANOVA) with a follow-up test for multiple comparisons (Tukey's correction). The statistical comparisons to control mean values were performed using a one-way ANOVA with Dunnett's multiple comparisons test as follow-up test. The analysis of two selected data sets was performed using an unpaired two-sided *t*-test. *P* values ≤ 0.05 were considered as significant. * $P < 0.05$, ** $P < 0.01$, *** $P < 0.001$.

4. Results

The influence of oxygen availabilities, ranging from constant oxygen supplies to oxygen shifts from high to low oxygen levels (hypoxic shock) or *vice versa* (reoxygeation), on the interaction of enterocytes with *C. albicans* was investigated. The results are shown in this section. In order to distinguish between the effects induced by oxygen availability on either host or fungal cells, respectively, and the effects of the combination of all of these factors, the impact of the oxygen regimes on both the enterocytes and *C. albicans* cultivated alone was also explored and will be presented first.

4.1. The influence of oxygen on *C. albicans* growth

The impact of oxygen on the growth of *C. albicans* cultivated without enterocytes was analyzed to differentiate between direct effects of oxygen and indirect effects mediated by the response of enterocytes to oxygen availability. Previous studies showed that at almost anaerobic conditions (0.1 % O_2 or 0.2 % O_2) growth rates of *C. albicans* were similar but biofilm mass was reduced in YPD medium compared to 21 % O_2 [52,53]. However, no comprehensive analysis of growth across a range of oxygen concentrations and in cell culture media has been published to date. Since the study presented here aimed to characterize the impact of different oxygen availabilities on the host-fungus interaction, the fungal growth analysis were performed using physiological oxygen concentrations present in the GIT (1 % - 10 % O_2) as well as almost anaerobic conditions (0.2 % O_2) present in the gut lumen [2,6,86]. In addition, atmospheric oxygen (~ 21 %) was used as a control condition which is commonly used for the cultivation of *C. albicans*.

4.1.1. *C. albicans* growth in YPD

The growth of *C. albicans* in liquid YPD medium was investigated in 96-well plates over a time course of 14 h by measuring the OD_{600} every 30 min. As the microplate reader used for OD-measurements was not oxygen-adjustable, fungal cultures had to be cultivated in oxygen-adjustable incubators and a Hypoxystation, respectively. Thus, every measurement was done manually by transferring each plate with the fungal cultures from the incubator/Hypoxystation to the microplate reader and *vice versa*. To ensure a proper re-adaptation of *C. albicans* to the respective oxygen concentration, as the fungus was exposed to atmospheric oxygen for a few minutes during the measurement procedure, three microwell plates were used per oxygen level and biological replicate.

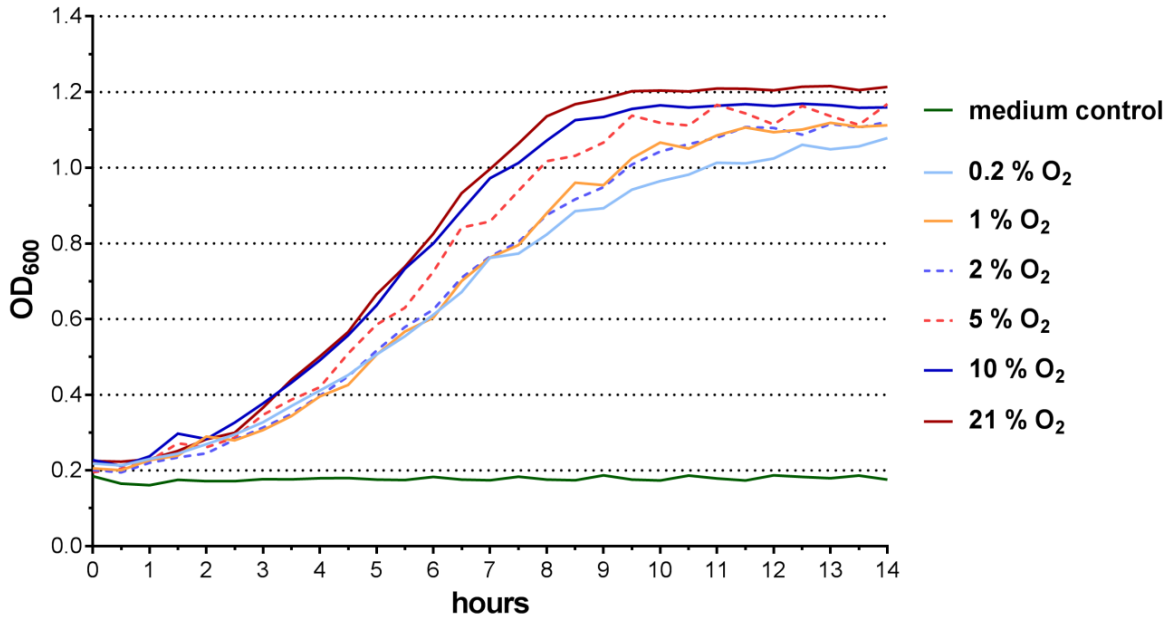

Figure 6: The growth of *C. albicans* is slightly delayed at ≤ 5 % O_2, but is not severely impaired. *C. albicans* was cultivated at indicated oxygen levels in YPD medium at 37 °C and 5 % CO_2 for 14 h. The OD_{600} was measured manually every 30 min. Data of three biological replicates each performed in triplicates are presented as mean.

The *C. albicans* growth in YPD medium was not severely impaired at any oxygen concentration tested (Figure 6). For oxygen levels at or below 5 %, a slight growth delay was observed during the exponential log phase (4 h – 11 h), which was more pronounced for hypoxic conditions (0.2 % to 2 % O_2), whereas the fungal growth at 10 % O_2 was comparable to the growth at atmospheric oxygen. At the stationary phase (11 – 14 h), no major differences were observed between the oxygen concentrations with OD values ranging from approx. 1.05 at 0.2 % O_2 to ~ 1.2 for 21 % O_2.

4.1.2. Colony and single cell morphology of *C. albicans* on YPD

Besides the growth speed of *C. albicans* in liquid medium, the fungal morphology on solid YPD medium was analyzed at different oxygen levels. The colony phenotypes of *C. albicans* on YPD agar differed depending on the oxygen concentration (Figure 7 and Figure 8).

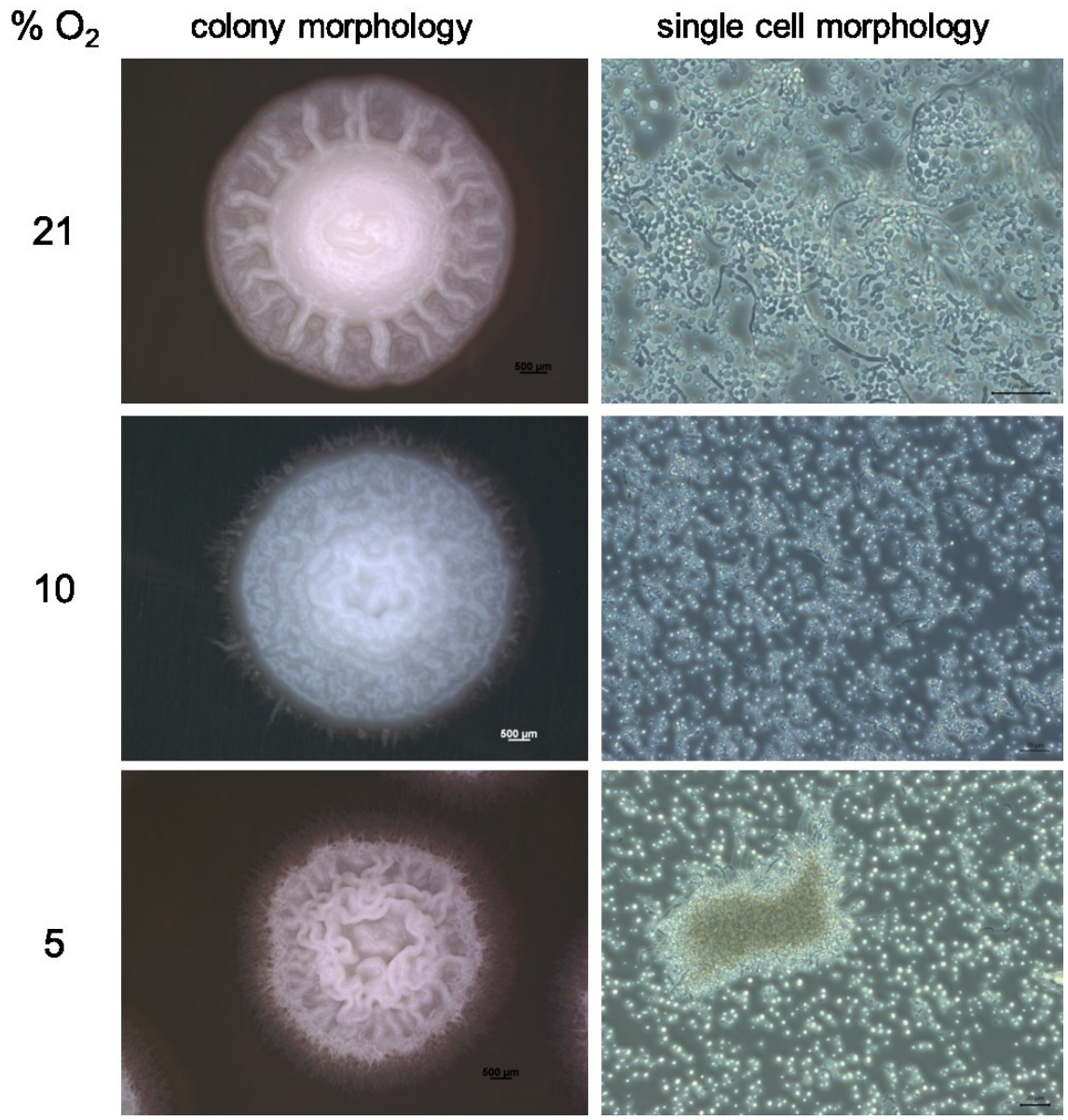

Figure 7: Reduced oxygen supply leads to wrinkled and smaller *C. albicans* colonies and longer filaments. *C. albicans* was grown on YPD agar plates at 21 %, 10 % and 5 % O_2, 5 % CO_2 and 37 °C for five days. Colony parts were dispensed in water to examine single cell morphology. Scale bar: 500 µm (colony), 20 µm (single cells). Representative pictures of colonies and single cells are shown.

The colonies appeared to be smaller in diameter with decreasing oxygen concentration. This would be consistent with the delayed growth of *C. albicans* at hypoxic conditions observed for the growth curve analysis (see Figure 6). In addition, while the colonies grown at atmospheric ambient (~ 21 %) oxygen exhibited smooth and wrinkled parts with a sharp colony boundary, the cultivation of *C. albicans* at 10 % and 5 % O_2 led to solely wrinkled colony phenotypes and extensions of the colony boundary (Figure 7). This effect was more pronounced at 5 % O_2 and was even stronger at oxygen concentrations

at or below 2 % (Figure 8). The colonies grown at these hypoxic conditions showed a so called “fuzzy” phenotype which was already described for oxygen concentrations at or below 5 % [55]. Since wrinkled and fuzzy colonies are associated with a strong filamentation [55,57], the single cell morphology of the respective colonies was analyzed. Indeed, the colonies grown at oxygen concentrations at or below 2 % exhibited more and longer hyphae compared to the growth at 5 %, 10 % and ambient O_2.

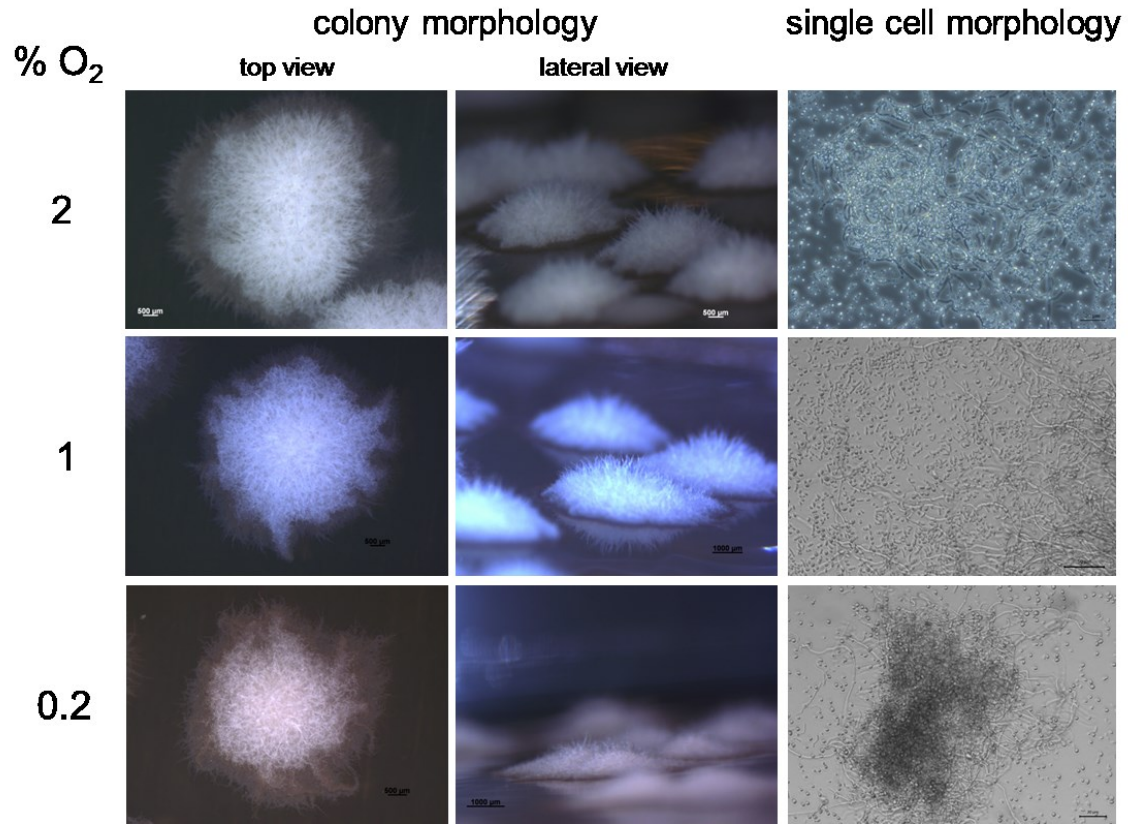

Figure 8: Reduced oxygen supply leads to wrinkled and smaller *C. albicans* colonies and longer filaments. *C. albicans* was grown on YPD agar plates at 2 %, 1 % and 0.2 % O_2, 5 % CO_2 and 37 °C for five days. Colony parts were dispensed in water to examine single cell morphology. Scale bar: 500 µm (colony; except 0.2 % and 1 % O_2 lateral view: 1,000 µm), 20 µm (single cell; except 1 % O_2: 50 µm). Representative pictures of colonies and single cells are shown.

These results showed that hypoxic conditions induced a stronger filamentation but led to slightly delayed growth of *C. albicans*.

4.1.3. *C. albicans* growth in cell culture-like conditions

In order to investigate the fungal growth under conditions mimicking the *in vitro* enterocyte infection model used in this study, *C. albicans* was seeded on collagen I-coated well plates in DMEM, the medium used for the infection experiments of enterocytes with *C. albicans*. The fungal burden was determined as colony forming units

(CFUs) per well after 4.5 h and 24 h, and the hyphal length was measured after 4.5 h incubation at 37 °C, 5 % CO_2 and the indicated oxygen concentrations.

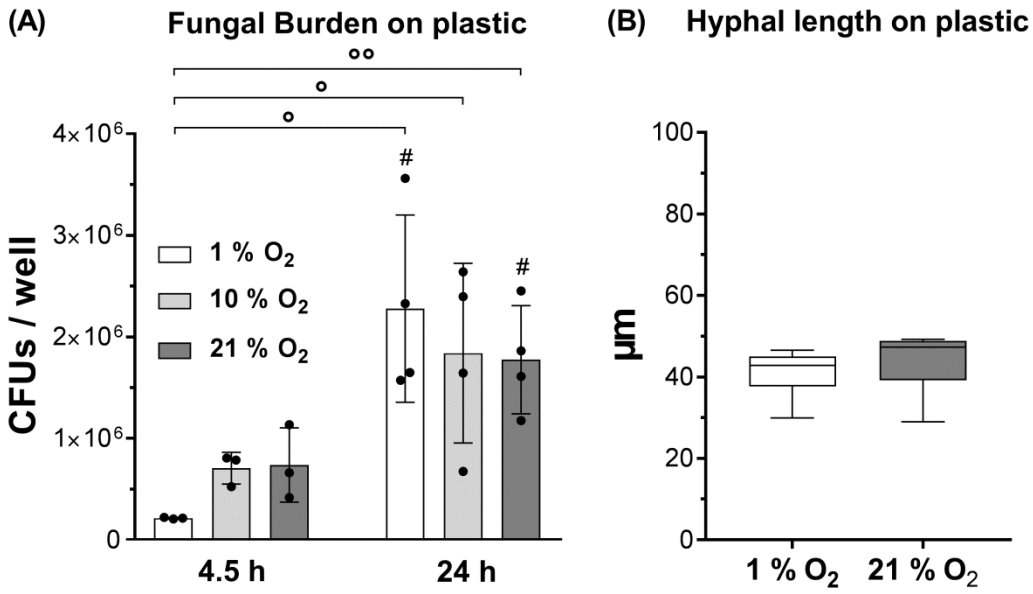

Figure 9: Hypoxia leads to an initial growth reduction of *C. albicans* on plastic but does not influence hyphal length. *C. albicans* was inoculated on collagen I-coated wells without enterocytes in DMEM. **(A)** Cultivation for 4.5 h and 24 h at 37 °C, 5 % CO_2 and indicated oxygen concentrations. CFUs/well was determined after Zymolyase® treatment. Results of at least three biological replicates each performed in duplicates are shown as mean ± SD. Statistically significant differences between 4.5 h and 24 h were determined by unpaired two-tailed *t*-test. ° Significant differences as indicated by lines (° $P < 0.05$, °° $P < 0.01$). # Significant differences to 10 % and 21 % O_2 at 4.5 h ($P < 0.05$). **(B)** Hyphal length was measured for 100 *Candida* hyphae per well after incubation for 4.5 h at 1 % and 21 % O_2, 5 % CO_2 and 37 °C. Results of nine biological replicates each performed in duplicates are depicted as a Whisker-Box-Plot. An unpaired two-tailed *t*-test revealed to statistical significance.

The CFUs from *C. albicans* cells grown on plastic without epithelial cells were initially (4.5 h) reduced at hypoxia (1 % O_2) but similar for 10 % and ambient O_2 (Figure 9, A). After 24 h, however, the fungal load was similar independent of the oxygen concentration. The growth of *C. albicans* on plastic led to similar hyphal lengths at hypoxia and ambient O_2 (Figure 9, B).

Consistent with the results obtained from the growth curve analysis (see chapter 4.1.1, Figure 6), these data suggest that hypoxic conditions do not lead to a general growth reduction but rather to a prolonged adaptation phase from the growth at ambient oxygen used to prepare the fungal pre-culture for inoculation.

4.2. The influence of oxygen on enterocytes

During their life span, enterocytes migrate from the crypts to the top of the villi [6,62,71]. This migration is accompanied with a strong reduction of available oxygen: the oxygen level in the gut decreases from 15 % - 10 % in the crypts to 2 % - 1 % at the tip of the villi [2,6,86]. Therefore, the effect of oxygen availability within this physiological range on the barrier function of enterocytes was assessed. 0.2% O_2, a concentration below the assumed physiological range, was included as a condition representing pathophysiological hypoxia.

4.2.1. Basal LDH release of enterocytes

The intestinal epithelium is regenerated every three to eight days *via* the migration of enterocytes from the crypts to the top of the villi [6,67,70,71]. During their migration, these epithelial cells differentiate and are exposed to a decreasing amount of oxygen. The Caco-2 and C2BBe1 cell lines are able to differentiate and establish a polarized monolayer within two to three weeks [122,133,134]. In order to investigate the sensitivity of these enterocyte cell lines to oxygen, the amount of released LDH was determined, which is used as a marker for cell damage. In addition, to determine whether the differentiation stage of the enterocytes affects the oxygen sensitivity, the Caco-2 and C2BBe1 cells were cultivated for two, seven and 14 days.

In order to mimic either hypoxic shock or reoxygenation, the respective cell cultures were shifted to different incubators 1.5 h prior to the mock-infection, which represents a medium exchange to DMEM to mimic infection conditions. The damage assays with C2BBe1 (Figure 10, Figure 11) and Caco-2 (Figure 12) cells were performed 24 h and 48 h after mock-infection, respectively.

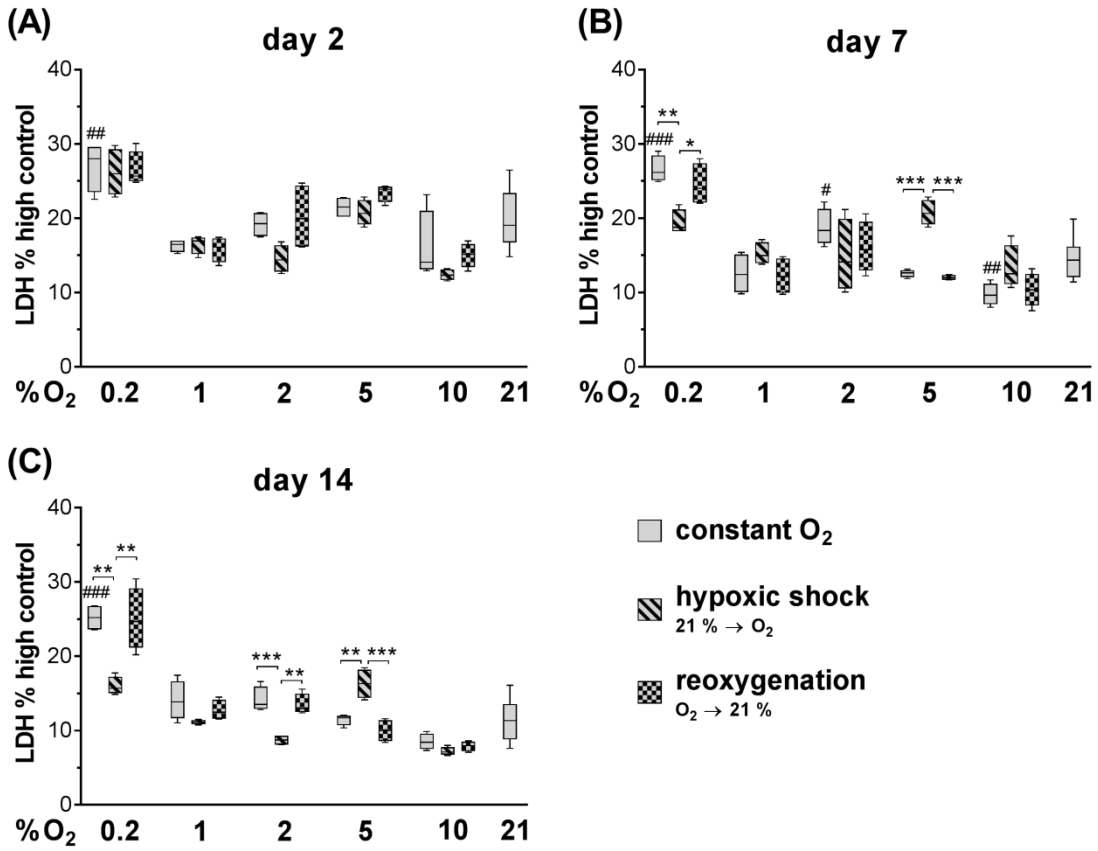

Figure 10: Almost anoxic conditions (0.2 % O_2) increase the basal LDH release of mock-infected C2BBe1 cells 24 h after mock-infection independent of the differentiation stage. The LDH release is shown as percentage relative to the high control. Mock-infection was performed 1.5 h after oxygen shifts using **(A)** two, **(B)** seven and **(C)** 14 days old C2BBe1 cultures. Results of four biological replicates each performed in triplicates are shown as Whisker-Box-Plot. Statistical analysis within an oxygen concentration was performed using one-way ANOVA with Tukey's multiple comparisons test (* $P < 0.05$, ** $P < 0.01$, *** $P < 0.001$). Statistical comparison of constant oxygen (0.2 % – 10 % O_2) to 21 % O_2 was performed using one-way ANOVA with Dunnett's multiple comparisons test (# $P < 0.05$, ## $P < 0.01$, ### $P < 0.001$).

For C2BBe1 cells, the differentiation stage did not influence their LDH release in dependence of oxygen: a slight increase in LDH levels at all oxygen concentrations was observed for two days old enterocytes (Figure 10 and Figure 11, A) compared to seven and 14 days of cultivation (Figure 10 and Figure 11, B and C). Apart from this, the LDH release was similar between the differentiation stages. In addition, the LDH release of C2BBe1 cells was comparable for 24 h (Figure 10) and 48 h (Figure 11) after mock-infection, except for 0.2 % and 5 % O_2 (constant O_2, hypoxic shock, reoxygenation), which led to a slight increase in LDH release at 24 h independent of the differentiation stage. In general, the LDH release increased at all conditions that included 0.2 % O_2 (constant O_2, hypoxic shock and reoxygenation) with the lowest LDH values for hypoxic

shock. This indicates that very low oxygen availability is indeed harmful to the cells. This is supported by the observation that, even after seven days, cells cultured under these conditions rarely reached confluency, and holes were observed in the cell layer at longer periods of incubation (data not shown). Significant differences were also observed for oxygen regimes within the range of 1 % to 21 % O_2, however without a clear trend.

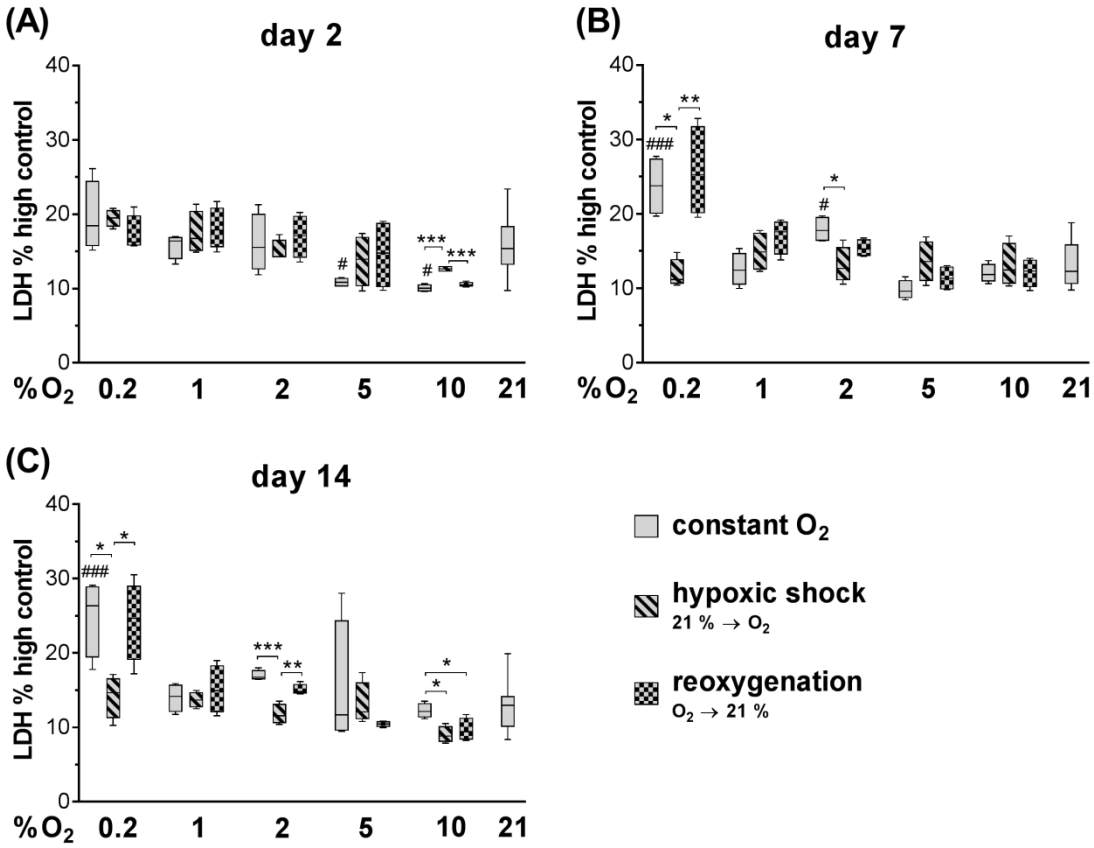

Figure 11: Almost anoxic conditions (0.2 % O_2) increase the basal LDH release of mock-infected C2BBe1 cells 48 h after mock-infection independent of the differentiation stage. The LDH release is shown as percentage relative to the high control. Mock-infection was performed 1.5 h after oxygen shifts using **(A)** two, **(B)** seven and **(C)** 14 days old C2BBe1 cultures. Results of four biological replicates each performed in triplicates are shown as Whisker-Box-Plot. Statistical analysis within an oxygen concentration was performed using one-way ANOVA with Tukey's multiple comparisons test (* $P < 0.05$, ** $P < 0.01$, *** $P < 0.001$). Statistical comparison of constant oxygen (0.2 % – 10 % O_2) to 21 % O_2 was performed using one-way ANOVA with Dunnett's multiple comparisons test (# $P < 0.05$, ### $P < 0.001$).

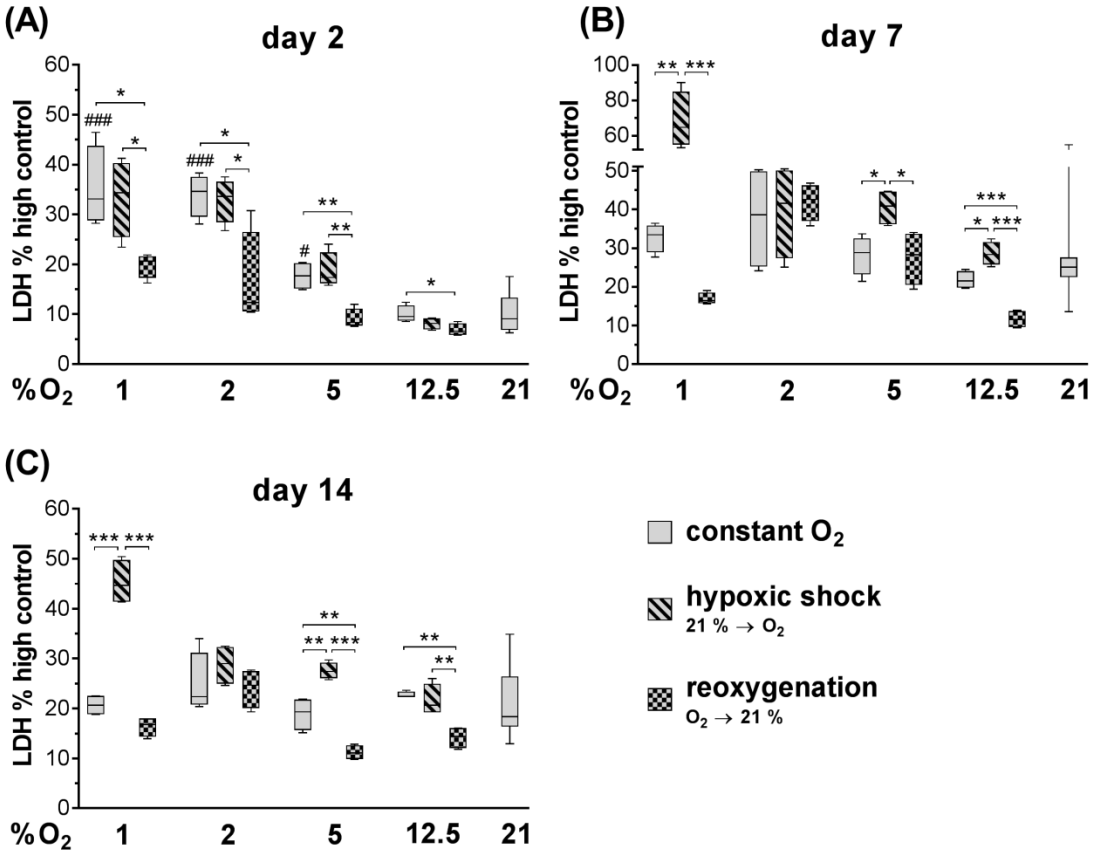

Figure 12: The basal LDH release of mock-infected Caco-2 cells decreases progressively with raised oxygen levels from 1 % - 21 % 48 h after mock-infection. The LDH release is shown as percentage relative to the high control. Mock-infection was performed 1.5 h after oxygen shifts using **(A)** two, **(B)** seven and **(C)** 14 days old Caco-2 cultures. Results of four biological replicates each performed in triplicates are shown as Whisker-Box-Plot. Statistical analysis within an oxygen concentration was performed using one-way ANOVA with Tukey's multiple comparisons test (* $P < 0.05$, ** $P < 0.01$, *** $P < 0.001$). Statistical comparison of constant oxygen (1 % – 12.5 % O_2) to 21 % O_2 was performed using one-way ANOVA with Dunnett's multiple comparisons test (# $P < 0.05$, ### $P < 0.001$).

The LDH release of mock-infected Caco-2 cells decreased progressively from 1 % to 21 % O_2 conditions (Figure 12). This was more pronounced for less differentiated cells (Figure 12, A) compared to later differentiation stages (Figure 12, B and C). This suggests that these enterocytes are more susceptible to low oxygen levels at an early differentiation phase. In contrast to C2BBe1 cells, a differentiation-dependent phenotype was observed for Caco-2 cells. The least differentiated enterocytes showed significantly reduced LDH levels during hypoxic shock and a comparable LDH release for reoxygenation and constant oxygen (Figure 12, A). In contrast, a significant increase in LDH release was observed during reoxygenation compared to both constant oxygen and

hypoxic shock for differentiated cells at almost all oxygen concentrations (Figure 12, B and C). Additionally, the amount of released LDH was significantly higher for Caco-2 cells compared to C2BBe1 enterocytes independent of their differentiation stage and the oxygen amount provided (Figure 13).

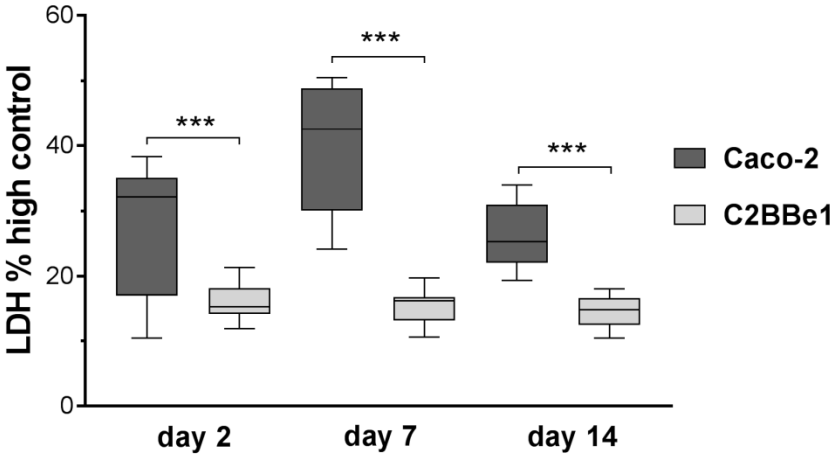

Figure 13: The basal LDH release is increased in Caco-2 cells compared to C2BBe1 cells. The LDH release was determined 48 h after mock-infection and is shown as percentage relative to the high control. Data from 2 % oxygen conditions (constant O_2, hypoxic shock and reoxygenation) were averaged per differentiation stage (day two, seven and 14) for both Caco-2 and C2BBe1 cells. These data are representative for all oxygen concentrations. Results are shown as Whisker-Box-Plot. Significant differences between basal LDH release of Caco-2 and C2BBe1 cells at respective differentiation stage were determined using an unpaired two-tailed *t*-test (* $P < 0.05$, *** $P < 0.001$).

Although the C2BBe1 cells originate from Caco-2 cells, these results indicate that both cell lines behave differently regarding their sensitivity to oxygen and their stage of differentiation. Whereas the C2BBe1 cells were quite robust to a large range of oxygen availabilities independent of their differentiation stage, except for pathophysiological hypoxia, the Caco-2 cells showed an increased sensitivity to physiological hypoxia which was most pronounced for the less differentiated cells. Previously it was shown that the C2BBe1 cells are more stable in their expression of brush borders and exhibit a less morphological heterogeneity compared to the Caco-2 cells [133]. Therefore, most of the following studies regarding the barrier function of enterocytes were performed using C2BBe1 cells only. Since the variability in LDH release was lowest for seven days old enterocytes and the LDH levels were comparable for 24 h and 48 h after mock-infection, further experiments were conducted using seven day old cells which were incubated for 24 h after mock-infection.

4.2.2. Enterocyte proliferation

To investigate a possible influence of oxygen on the proliferation ability of enterocytes, the number of C2BBe1 cells was determined 24 h after mock-infection (medium exchange to DMEM). 1.5 h prior to mock-infection, the respective cell cultures were switched from 10 %/21 % O_2 to hypoxia (hypoxic shock) or *vice versa* to simulate reoxygenation.

Enterocytes cultivated at 10 % O_2 yielded significantly higher cell numbers compared to hypoxia (Figure 14). This result implies that 10 % O_2 is the optimal growth condition for these enterocytes which is in the range of the physiological oxygen level in the crypts of the GIT [2,6,86]. Hypoxic shock and reoxygenation had no effect on the cell proliferation. The cell numbers for enterocytes cultivated at these oxygen shift conditions were comparable to cells grown at the respective constant oxygen levels which were set up before the oxygen shift was performed.

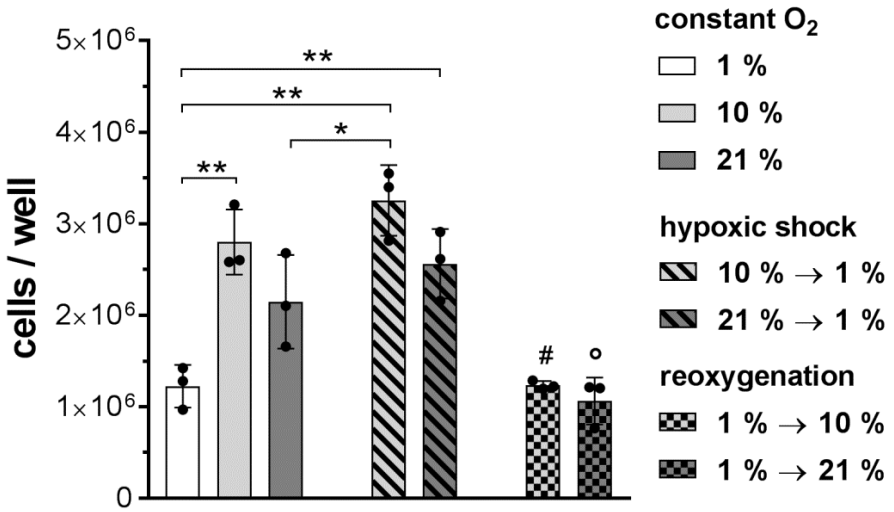

Figure 14: The proliferation of enterocytes is oxygen-dependent with highest cell numbers at 10 % O_2. The C2BBe1 cells were grown for seven days at 37 °C, 5 % CO_2 and indicated oxygen availabilities. Cell numbers were determined 24 h after mock-infection which was performed 1.5 h after oxygen shifts. Results of three biological replicates are shown as mean ± SD. Statistical analysis was performed across all data using one-way ANOVA with Tukey's multiple comparisons test. * Significant differences between two groups as indicated by lines (* $P < 0.05$, ** $P < 0.01$); # Significant differences to hypoxic shock and 10 % O_2 ($P < 0.01$); ° Significant differences to hypoxic shock, 10 % and 21 % O_2 ($P < 0.05$).

4.2.3. Expression of cellular junctions

In order to investigate the expression of the tight and adherens junctions that have an important role for epithelial barrier functions, C2BBe1 cells were lysed and the tight

junction proteins Claudin-4 and Occludin as well as the adherens junction protein E-Cadherin were analyzed *via* Western Blot.

While enterocytes cultured at different constant oxygen levels and reoxygenation showed comparable expression of the tight junction proteins Claudin-4 and Occludin, quantitative differences were observed for hypoxic shock with increased Claudin-4 levels and reduced expression of Occludin (Figure 15; see Appendix 8.1., Suppl. Figure 1 for representative protein bands). The adherens junction protein E-Cadherin was expressed at comparable levels for almost all oxygen availabilities, except for hypoxic shock 21 % → 1 % showing a slightly decreased expression level. The differences in single protein expression were not statistically significant. Despite the opposite expression pattern of Claudin-4 and Occludin during hypoxic shock, these results suggest that the tight junction complex is not impaired.

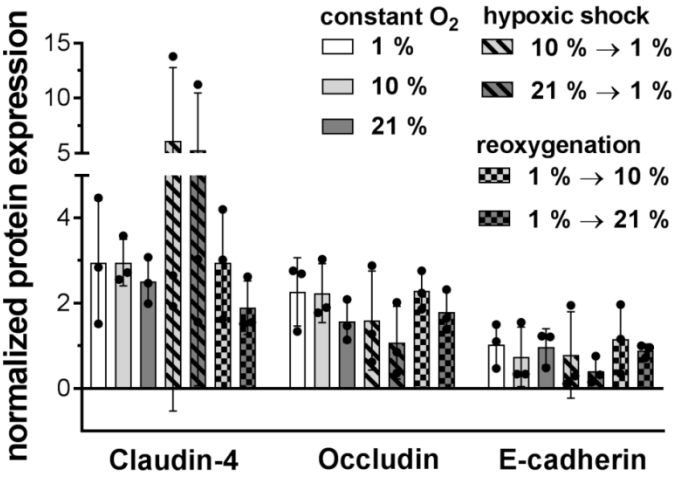

Figure 15: Hypoxic shock leads to a different expression pattern of tight junction proteins. The expression of tight junction (Claudin-4, Occludin) and adherens junction (E-cadherin) proteins in seven days old C2BBe1 cells was determined using whole cell lysates. Western Blot protein bands were quantified with ImageJ and normalized to the actin loading control. Results of three biological replicates are shown as mean ± SD. Statistical analyses using a one-way ANOVA with Tukey's multiple comparisons test showed no significant differences.

4.2.4. Intestinal epithelial barrier integrity

The impairment of tight junctions is accompanied by a decrease in transepithelial electrical resistance (TEER) [121]. Impaired barrier function furthermore allows an increased translocation of macromolecules such as dextran. Therefore, the determination of TEER and permeability for Rhodamine B isothiocyanate (RITC) dextran was performed in mock-infected C2BBe1 cell layers cultured in Transwell® Inserts and undergoing mock-infection for 24 h.

During the progression of mock-infection, TEER levels showed no significant differences between the oxygen regimes (Figure 16, A). The RITC permeability did not differ significantly between the oxygen concentrations but was slightly increased at hypoxia (1 % O_2) and hypoxic shock (Figure 16, B). This suggests that the barrier function of enterocytes is not impaired by the differences in oxygen availability investigated, which support the hypothesis that the tight junction complex is not influenced by oxygen within the tested range. Thus, C2BBe1 cells appear to tolerate a wide range of oxygen availability and the barrier function is maintained at both constant and changing oxygen concentrations ranging from 1 % to 21 %.

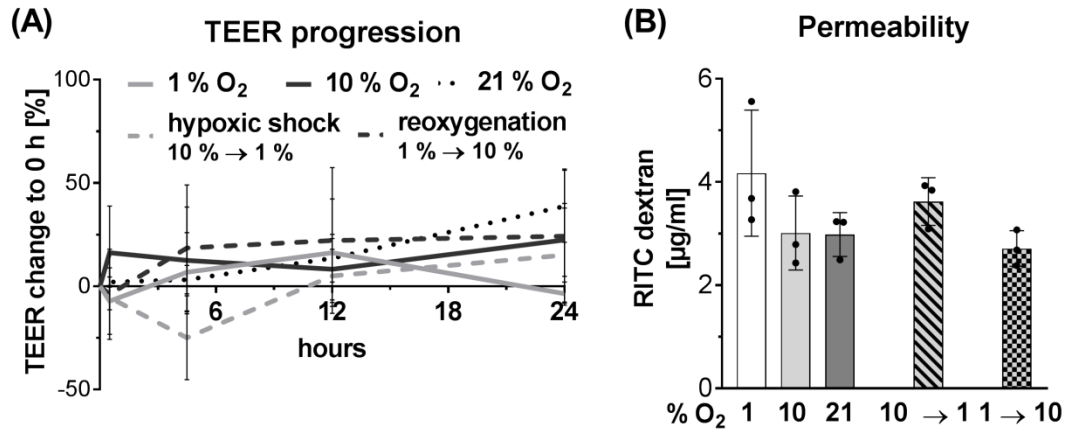

Figure 16: The barrier integrity of mock-infected enterocytes is not influenced by oxygen. The C2BBe1 cells were grown in Transwell® inserts for 14 days. Oxygen shifts were performed 1.5 h prior to mock-infection (medium exchange to mimic infection). (**A)** TEER was recorded for 24 h after mock-infection and measured values were normalized to respective TEER before medium exchange (0 h). Results of six biological replicates each performed at least in duplicates are shown as mean ± SD. Statistical analysis using a one-way ANOVA with Tukey's multiple comparisons test showed no significant differences. **(B)** Permeability of the C2BBe1 monolayer was determined 24 h after mock-infection by RITC dextran translocation into the lower compartment of transwell cultures. Concentrations were calculated using a RITC dextran standard. Results of three biological replicates each performed in triplicates are shown as mean ± SD. Statistical analysis using a one-way ANOVA with Tukey's multiple comparisons test showed no significant differences.

Taken together, the analyses performed to assess the effect of oxygen on enterocyte barrier function showed that C2BBe1 cells proliferate and mediate barrier function within the physiological range of available oxygen (1 % – 10 %) in the GIT, whereas nearly anoxic conditions (0.2 % O_2) are detrimental.

In the following sections, both 10 % O_2 and atmospheric oxygen (approx. 21 % O_2), which is commonly used for the cultivation of cell lines, will be referred to as ”normoxia” and 1 % O_2 as “hypoxia” even though this is still physiological normoxia in parts of the intestinal tissue.

4.3. The influence of oxygen on the *C. albicans*-enterocyte interaction

C. albicans is part of the microbiota in the GIT and interacts with enterocytes due to the close proximity of the fungus to the epithelial cell layer [111]. Since the oxygen availability in the GIT differs along gut length and diameter and greatly depends on food intake [6,86-88], the influence of physiological oxygen availabilities on the interaction of *C. albicans* with enterocytes was investigated.

4.3.1. Oxygen-dependent damage of enterocytes by *C. albicans* infection

To determine the *C. albicans*-mediated damage, the LDH release by C2BBe1 (Figure 17 and Figure 18) and Caco-2 (Figure 19) cells was quantified 24 h and 48 h after infection, respectively. Oxygen shifts were performed as described for mock-infected cells and enterocytes at different differentiation stages were used.

Interestingly, the LDH release was significantly increased after reoxygenation compared to both constant oxygen concentrations and hypoxic shock. The difference in LDH levels between reoxygenation and constant oxygen/hypoxic shock was more pronounced for hypoxic oxygen levels (0.2 % - 2 % O_2) and decreased with increasing oxygen concentration. In addition, lowest LDH levels were observed following hypoxic shock. These oxygen-dependent damage phenotypes were independent of the differentiation stage (two, seven or 14 days), the length of the infection period (24 h or 48 h) and the used cell line (C2BBe1 or Caco-2) (Figure 17 – Figure 19).

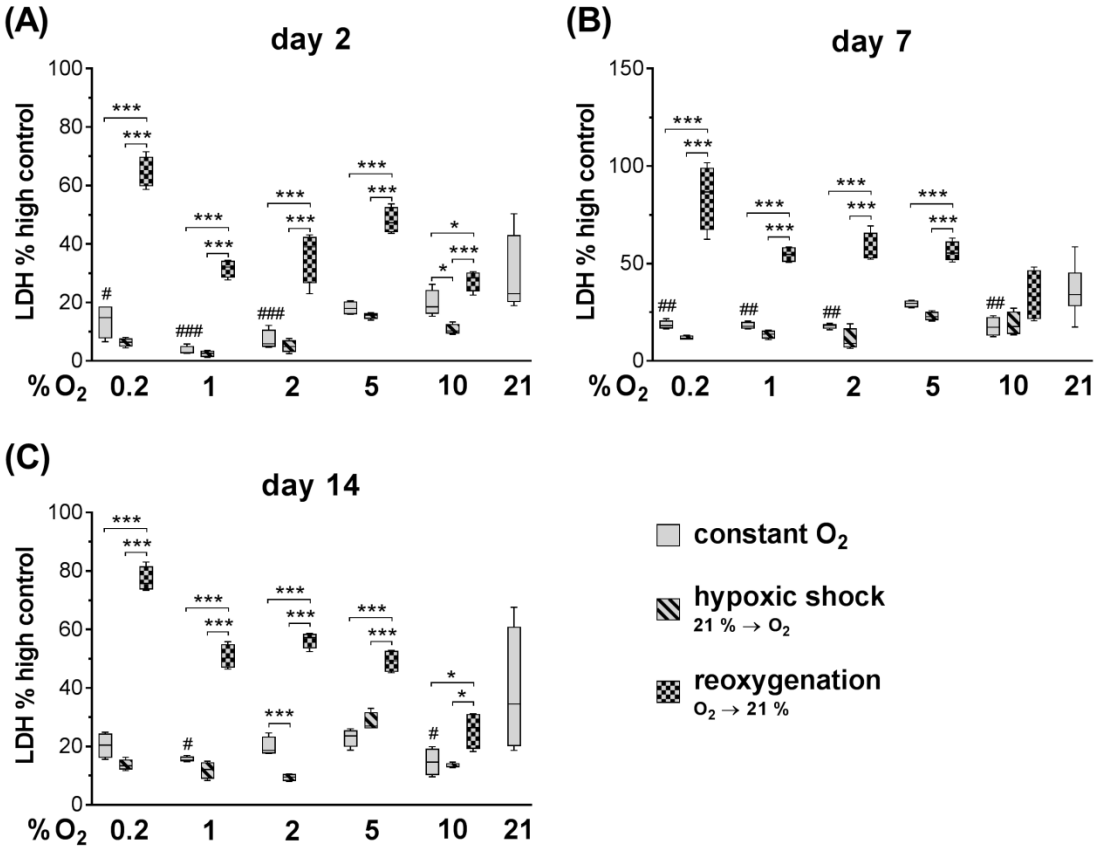

Figure 17: Reoxygenation leads to significantly increased LDH levels of *C. albicans*-infected C2BBe1 cells 24 h p.i. The LDH level is depicted as percentage of LDH release relative to the high control. LDH release from mock-infected cells was subtracted from all values. Infection with *C. albicans* was performed 1.5 h after oxygen shifts using **(A)** two, **(B)** seven and **(C)** 14 days old C2BBe1 cultures. Results of four biological replicates each performed in triplicates are shown as Whisker-Box-Plot. Statistical analysis within an oxygen concentration was performed using one-way ANOVA with Tukey's multiple comparisons test (* $P < 0.05$, *** $P < 0.001$). Statistical comparison of constant oxygen (0.2 % – 10 % O_2) to 21 % O_2 was performed using one-way ANOVA with Dunnett's multiple comparisons test (# $P < 0.05$, ## $P < 0.01$, ### $P < 0.001$).

Furthermore, the amount of LDH released by infected C2BBe1 cells increased from 24 h to 48 h p.i. (Figure 17, Figure 18), especially under constant oxygen supply and after hypoxic shock. Since the LDH release upon infection after reoxygenation was already high 24 h p.i. (Figure 17), reaching up to 100 % relative damage, it was not surprising that the elongation of the incubation time did not further increase the LDH level to a similar extent as observed for constant oxygen and hypoxic shock (Figure 18). In addition, 48 h of incubation led to higher variations of LDH levels especially for constant oxygen concentrations and hypoxic shock. Therefore, for further analysis 24 h was chosen as infection period.

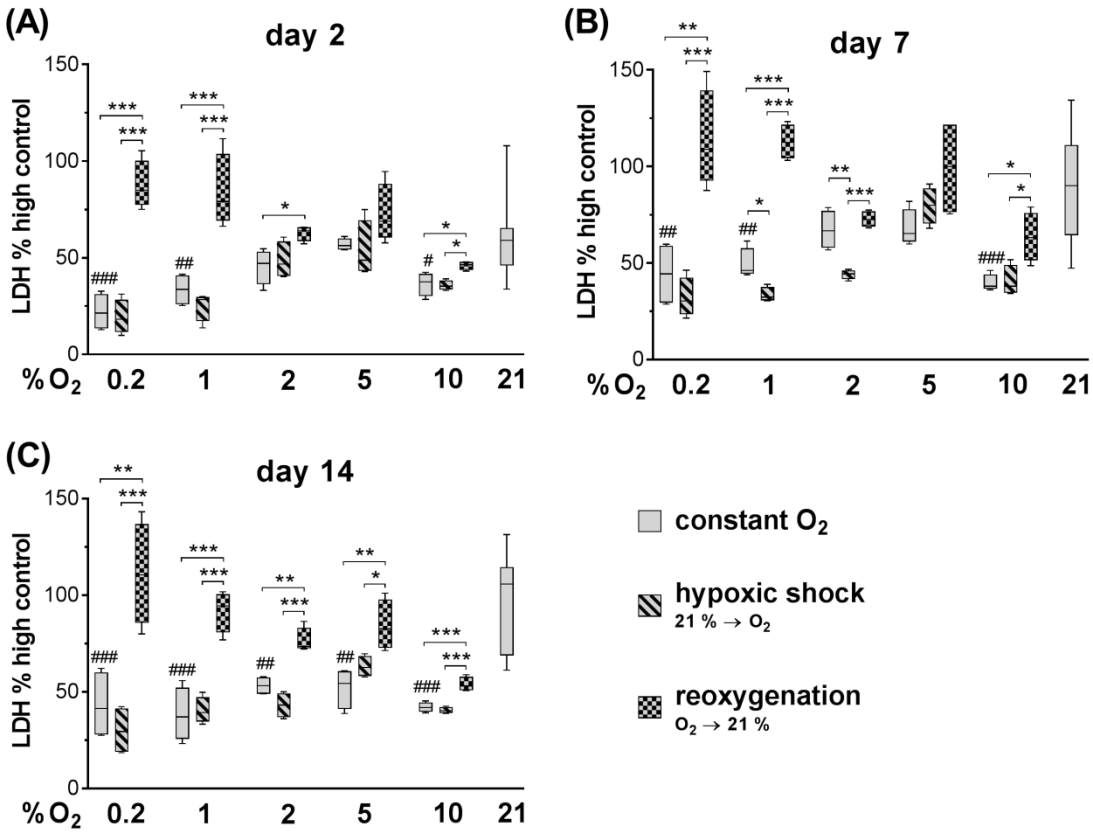

Figure 18: Reoxygenation leads to significantly increased LDH levels of *C. albicans*-infected C2BBe1 cells 48 h p.i. The LDH level is depicted as percentage of LDH release relative to the high control. LDH release from mock-infected cells was subtracted from all values. Infection with *C. albicans* was performed 1.5 h after oxygen shifts using **(A)** two, **(B)** seven and **(C)** 14 days old C2BBe1 cultures. Results of four biological replicates each performed in triplicates are shown as Whisker-Box-Plot. Statistical analysis within an oxygen concentration was performed using one-way ANOVA with Tukey's multiple comparisons test (* $P < 0.05$, ** $P < 0.01$, *** $P < 0.001$). Statistical comparison of constant oxygen (0.2 % – 10 % O_2) to 21 % O_2 was performed using one-way ANOVA with Dunnett's multiple comparisons test (# $P < 0.05$, ## $P < 0.01$, ### $P < 0.001$).

The comparison of LDH levels for C2BBe1 (Figure 18) and Caco-2 cells (Figure 19) 48 h p.i. showed a higher variation in LDH release for the Caco-2 cell line. This could be due to the higher heterogeneity of these cells compared to the C2BBe1 cell cultures [133], which was already mentioned above. Therefore, further analyses of the *C. albicans*-enterocyte interaction at different oxygen availabilities were conducted using the C2BBe1 cell line grown for seven days.

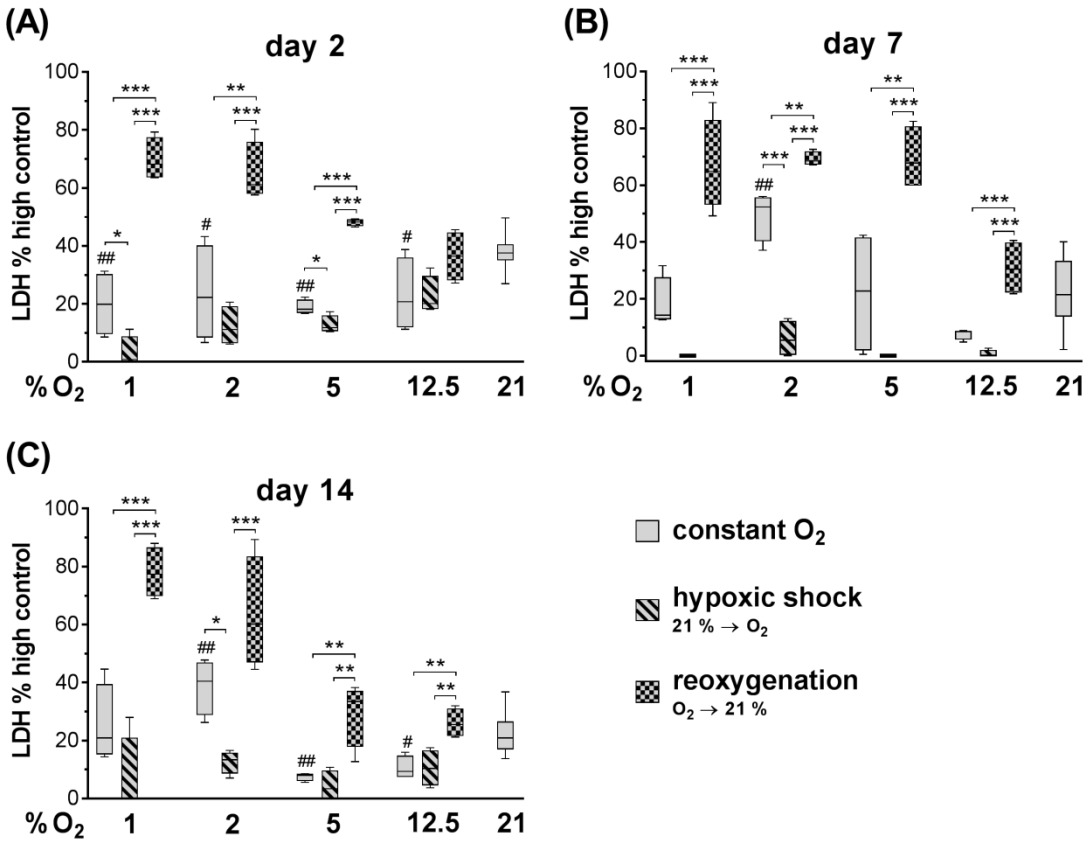

Figure 19: Reoxygenation leads to significantly increased LDH levels of *C. albicans*-infected Caco-2 cells 48 h p.i. The LDH level is depicted as percentage of LDH release relative to the high control. LDH release from mock-infected cells was subtracted from all values. Infection with *C. albicans* was performed 1.5 h after oxygen shifts using **(A)** two, **(B)** seven and **(C)** 14 days old Caco-2 cultures. Results of four biological replicates each performed in triplicates are shown as Whisker-Box-Plot. Statistical analysis within an oxygen concentration was performed using one-way ANOVA with Tukey's multiple comparisons test (* $P < 0.05$, ** $P < 0.01$, *** $P < 0.001$). Statistical comparison of constant oxygen (1 % – 12.5 % O_2) to 21 % O_2 was performed using one-way ANOVA with Dunnett's multiple comparisons test (# $P < 0.05$, ## $P < 0.01$).

In order to elucidate whether the damage outcome shown for oxygen shifts from low oxygen to 21 % (reoxygenation) or *vice versa* (hypoxic shock) depends on the dimension of the oxygen shift, cell cultures were also shifted from hypoxia (1 % O_2) to 5 % or normoxia (10 %, 21 % O_2) simulating reoxygenation or *vice versa* to mimic hypoxic shock. This would also mimic physiological oxygen availabilities to a greater extent. Furthermore, cell cultures subjected to hypoxic shock for 2 h were reperfused after fungal infection for 24 h to investigate the influence of reoxygenation on the low damage level observed after hypoxic shock.

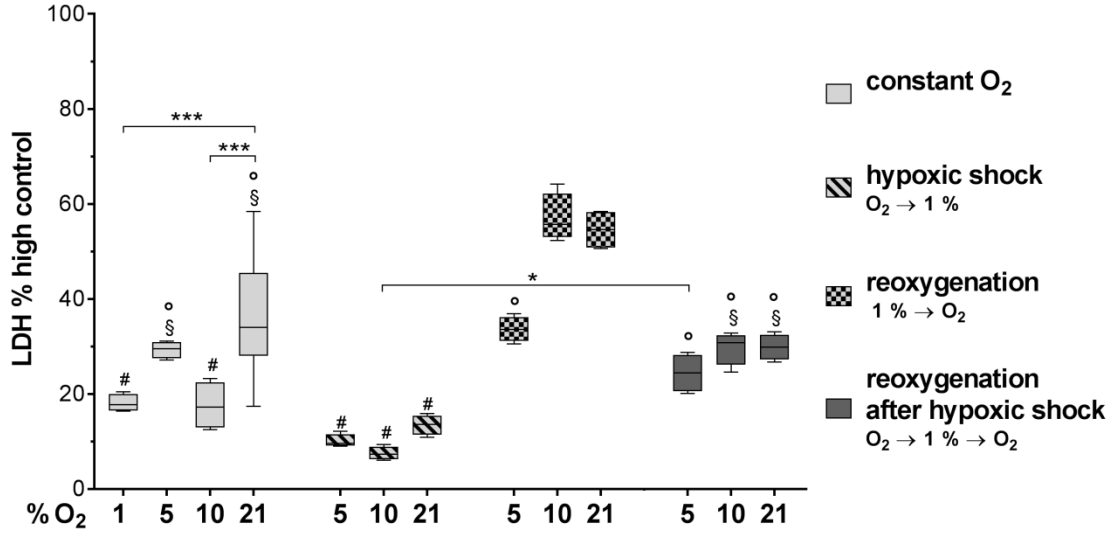

Figure 20: Physiological reoxygenation conditions significantly increase the LDH release of C2BBe1 cells 24 h p.i. with *C. albicans*. The LDH level is depicted as percentage of LDH release relative to the high control. LDH release from mock-infected cells was subtracted from all values. Infection with *C. albicans* was performed 1.5 h after oxygen shifts using seven days old C2BBe1 cultures. For reoxygenation after hypoxic shock, fungal infection was performed 2 h after hypoxic shock and then enterocytes were reperfused for 24 h. Results of four biological replicates each performed in triplicates are shown as Whisker-Box-Plot. Statistical analysis was performed across all data using one-way ANOVA with Tukey's multiple comparisons test. * Significant differences between two groups as indicated by lines (* $P < 0.05$, *** $P < 0.001$). # $P < 0.05$ compared to all reoxygenation conditions. ° $P < 0.01$ compared to reoxygenation except for 1 % → 5 %. § $P < 0.05$ compared to all hypoxic shock conditions.

In accordance with the damage phenotype observed for oxygen switches from 21 % O_2 to low oxygen levels or *vice versa*, simulating physiological hypoxic shock resulted in significantly reduced LDH levels whereas reoxygenation from hypoxia to 5 % O_2 or normoxia significantly increased the *C. albicans*-mediated LDH release of enterocytes (Figure 20). In addition, reoxygenation of cell cultures which were subjected to hypoxic shock led to significantly increased LDH release compared to hypoxic shock alone. However, the damage was lower than observed for enterocytes undergoing reoxygenation only.

Taken together, the damage phenotypes observed for physiological oxygen switches (Figure 20) were similar compared to those performed between 21 % O_2 and low oxygen levels (Figure 17 – Figure 19). Thus, further analyses were conducted using hypoxia (1 % O_2) and normoxia (10 % and 21 % O_2) for constant oxygen supply as well as for oxygen switches mimicking hypoxic shock or reoxygenation.

4.3.2. Barrier integrity of infected enterocytes

In order to determine the barrier function of enterocytes upon infection with *C. albicans* at different oxygen levels, both TEER and permeability for dextran were determined using Transwell® inserts. TEER was monitored for indicated time points after infection whereas permeability was determined 24 h p.i. In addition, fungal translocation was quantified 24 h p.i. as CFUs in the lower Transwell® compartment.

During the infection progression, TEER decreased for all oxygen regimes but with different kinetics and to a different extend (Figure 21, A). While TEER levels of cell cultures infected after reoxygenation and at 10 % O_2 were reduced by over 50 % already 12 h p.i., hypoxic shock led to rather stable TEER levels after a slight initial decrease. 24 h p.i., reduction in TEER of approx. 60 % - 85 % of the initial TEER value was observed at all conditions except hypoxic shock, for which the TEER reduction was significantly less pronounced (Figure 21, B). The strongest decrease in TEER after infection of enterocytes with *C. albicans* was observed for reoxygenation. These results were accompanied by an increased permeability for RITC dextran after infection at all conditions which was most pronounced during reoxygenation (Figure 21, C). Although the translocation was not further enhanced during reoxygenation compared to hypoxia and normoxia (Figure 21, D), these data overall indicate that reoxygenation renders enterocytes more susceptible to *C. albicans* damage significantly impairing the barrier function. In addition, hypoxic shock led to reduced fungal translocation (Figure 21, D) which is consistent with LDH release, TEER and the RITC dextran permeability, indicating that this condition has protective effects on the enterocyte barrier function during the interaction with *C. albicans*.

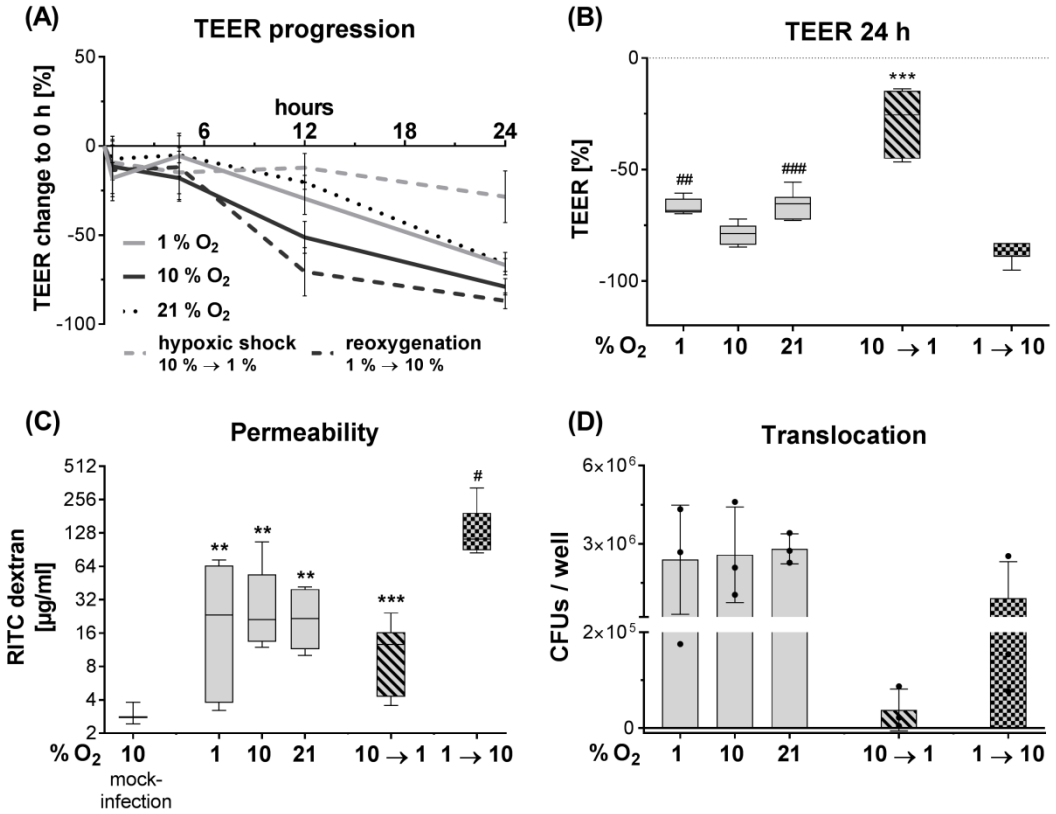

Figure 21: Reoxygenation significantly impairs the barrier integrity of infected enterocytes whereas hypoxic shock reduces the translocation ability of *C. albicans*. C2BBe1 cells were grown in Transwell® inserts for 14 days. Oxygen shifts were performed 1.5 h prior to infection with *C. albicans*. **(A)** TEER was recorded for 24 h p.i. and measured values were normalized to respective TEER prior to fungal infection (0 h). Results of six biological replicates each performed at least in duplicates are shown as mean ± SD. **(B)** Change in TEER 24 h p.i. is depicted as percentage relative to the respective TEER values prior to infection. Results of six biological replicates each performed at least in duplicates are shown as Whisker-Box-Plot. Statistical analysis was performed across all data sets using one-way ANOVA with Tukey's multiple comparisons test. *** $P < 0.001$ compared to all other conditions. # Significant difference compared to reoxygenation: ## $P < 0.01$, ### $P < 0.001$. **(C)** Permeability of mock-infected enterocytes at 10 % O_2 and of C2BBe1 monolayer 24 h after infection with *C. albicans*. Results of six biological replicates (except 10 % mock-infection: three biological replicates) are shown as Whisker-Box-Plot. Statistical analysis was performed across all data sets using a one-way ANOVA with Tukey's multiple comparisons test: ** $P < 0.01$, *** $P < 0.001$ compared to reoxygenation. # $P < 0.001$ compared to mock-infection at 10 % O_2 according to one-way ANOVA with Dunnett's multiple comparisons test. **(D)** Translocated *C. albicans* cells were determined as CFUs/well after Zymolyase® treatment of the lower transwell compartment. Results of three biological replicates each performed in triplicates are shown as mean ± SD. Statistical analysis using a one-way ANOVA with Tukey's multiple comparisons test showed no significant differences.

4.3.3. Adhesion and invasion potential of *C. albicans*

Since the adhesion and invasion of *C. albicans* are the initial steps of infection and thus influence the subsequent host cell damage, the impact of oxygen on both *C. albicans* adhesion to and invasion of enterocytes was investigated.

The incubation of C2BBe1 cells with *C. albicans* for 30 min revealed increased adhesion of fungal cells to enterocytes that underwent hypoxic shock compared to constant oxygen supply, whereas reoxygenation did not affect adherence (Figure 22, A). In contrast to adhesion, fungal invasion was significantly reduced during hypoxic shock (Figure 22, B). Reoxygenation, however, led to significantly increased invasion of *C. albicans* which could contribute to the higher damage observed at this condition.

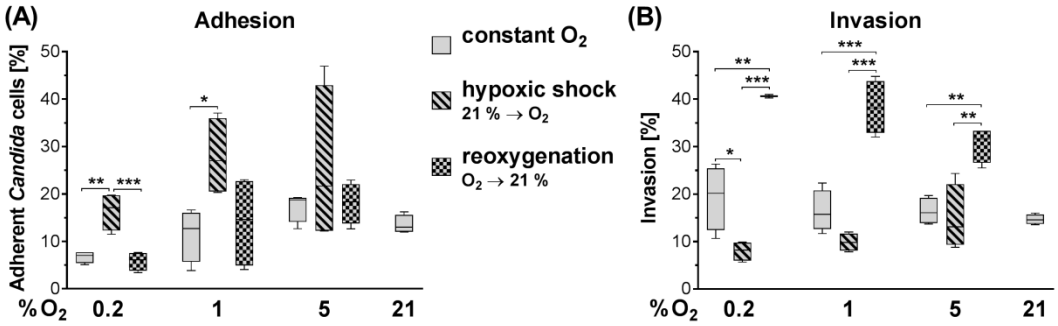

Figure 22: Hypoxic shock increases the number of adherent *C. albicans* cells whereas the fungal invasion ability of *C. albicans* to enterocytes is enhanced during reoxygenation. Seven days old C2BBe1 cells were inoculated with *C. albicans* and incubated at 37 °C, 5 % CO_2 and indicated oxygen concentration for **(A)** 30 min (depicted as percentage of adherent *Candida* cells) and **(B)** 4.5 h (depicted as percentage of invasive relative to adherent fungal cells). Results of four biological replicates each performed in duplicates are shown as Whisker-Box-Plot (except for (B) 0.2 % reoxygenation: two biological replicates). Statistical analysis was performed across all data sets within each oxygen condition using one-way ANOVA with Tukey's multiple comparisons test. * $P < 0.05$, ** $P < 0.01$, *** $P < 0.001$.

The impaired barrier function, determined by TEER and permeability *via* RITC dextran flux, and the increased fungal invasion ability during reoxygenation indicated impaired tight junctions which was shown previously [121]. Tight junction impairment provides access to the underlying adherens junctions, like E-Cadherin, and thus could mediate induced endocytosis. Even though no significant differences in expression of tight junctions and E-Cadherin expression was observed between the different oxygen regimes for mock-infected enterocytes, structural changes induced by reoxygenation alone or in combination with *C. albicans* infection could lead to accessibility of Cadherins. In order to test this hypothesis, a *C. albicans* mutant deficient for Ssa1, a

protein involved in mediating induced endocytosis [44], was investigated regarding its invasion ability and damage capability (Figure 23).

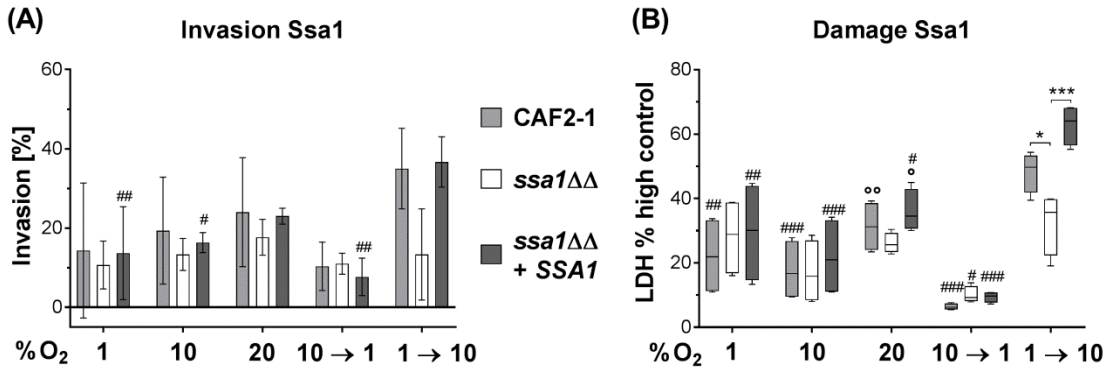

Figure 23: Deletion of *SSA1* reduces the fungal invasion ability exclusively at reoxygenation resulting in reduced host cell damage. Seven days old C2BBe1 cells were infected with *C. albicans* CAF2-1 wt, *ssa1*ΔΔ deletion and *ssa1*ΔΔ + *SSA1* revertant strain and were incubated at 37 °C, 5 % CO_2 and indicated oxygen regimes. Comparison of strains within each oxygen condition was performed using one-way ANOVA with Tukey's multiple comparisons test (* $P < 0.05$, *** $P < 0.001$). Comparison of differences between oxygen conditions was performed for each fungal strain using one-way ANOVA with Tukey's multiple comparisons test. # Significant differences compared to reoxygenation (1 → 10; # $P < 0.05$, ## $P < 0.01$, ### $P < 0.001$). ° Significant differences compared to hypoxic shock (10 → 1; ° $P < 0.05$, °° $P < 0.01$). **(A)** Invasion was determined 4.5 h p.i. and is depicted as percentage of invasive relative to adherent fungal cells. Results of three biological replicates are shown as mean ± SD. **(B)** The LDH level is depicted as percentage LDH release relative to high control. The LDH release from mock-infected enterocytes was subtracted from all values. Results of four biological replicates each performed in triplicates are shown as Whisker-Box-Plot. Invasion and Damage Assays with *C. albicans* CAF2-1 wt, *ssa1*ΔΔ deletion and *ssa1*ΔΔ + *SSA1* revertant strain were performed and analyzed by Rebecca Mikolajczyk, a former Master student of Research Group Microbial Immunology.

The deletion of *SSA1* caused reduced invasion only during reoxygenation (Figure 23, A). For all other oxygen regimes tested, the *ssa1*ΔΔ mutant showed the same invasion ability as its parental strain CAF2-1 and the revertant strain *ssa1*ΔΔ + *SSA1*. The decreased invasion ability seems to result in reduced damage capability as the *ssa1*ΔΔ mutant significantly diminished LDH levels released from enterocytes during reoxygenation (Figure 23, B). For all other oxygen regimes tested, the *ssa1*ΔΔ mutant lead to similar LDH release as CAF2-1 and *ssa1*ΔΔ + *SSA1*. Thus, this suggests that induced endocytosis contributes to fungal invasion and subsequent host cell damage during reoxygenation.

Taken together, the results indicate that reoxygenation renders enterocytes more susceptible to *C. albicans* infection whereas hypoxic shock exhibits protective effects on enterocyte barrier function.

4.4. Mechanistic analyses of oxygen-dependent *C. albicans*-enterocyte interaction

The oxygen availability within the physiological range of 1 % - 10 % O_2 did not impair the barrier function of mock-infected C2BBe1 cells (see 4.2.). Furthermore, hypoxia led to a prolonged adaptation phase in fungal growth assays but no general growth reduction at hypoxic conditions was observed (see 4.1.). While the latter together with altered invasion properties might contribute to the oxygen-dependent differences in *C. albicans*-mediated enterocyte damage (see 4.3.), it appeared unlikely that a general oxygen-dependent effect on fungal growth alone would sufficiently explain differences in damage. Thus, the fungal and host response during infection at varying oxygen regimes was investigated in more detail in order to elucidate molecular mechanisms which cause the observed oxygen-dependent infection phenotypes.

4.4.1. Host response

4.4.1.1. Intracellular ROS production

ROS are known to be produced during IR injury and have destructive effects on epithelial cell membranes which mediate tissue damage [97,98,152]. It thus appeared likely that ROS injury contributed to the enhanced enterocyte susceptibility to *C. albicans* infection, and therefore, the intracellular ROS production was determined 24 h p.i.

Both mock-infected and *C. albicans*-infected enterocytes showed an increased ROS production at normoxia compared to hypoxia (Figure 24). The ROS production in mock-infected C2BBe1 cells was higher during reoxygenation than hypoxic shock (Figure 24, left). However, the infection of enterocytes with *C. albicans* led to similar ROS levels during reoxygenation and hypoxic shock (Figure 24, right). This could be due to surface-associated fungal ROS detoxification systems [153-155].

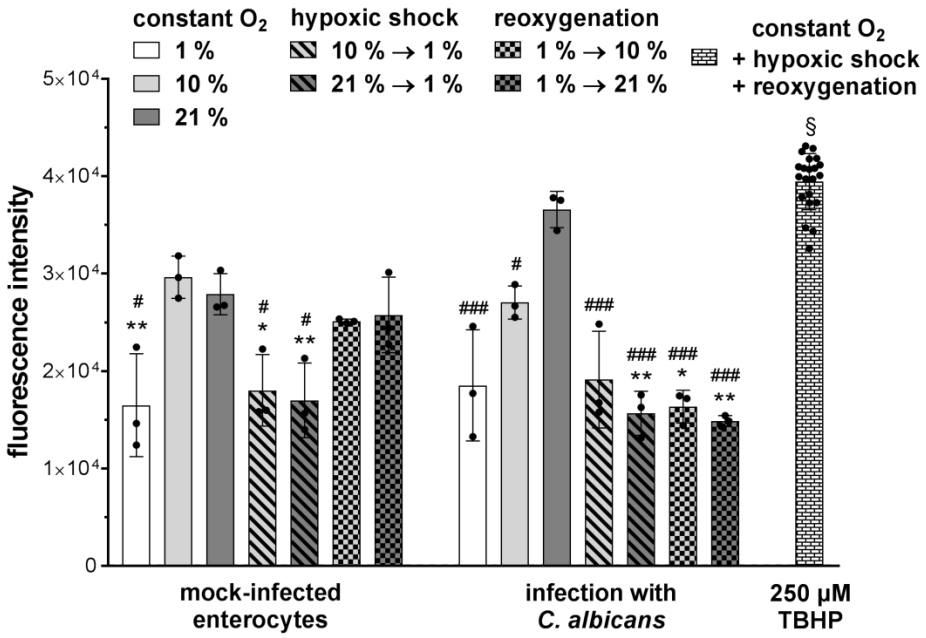

Figure 24: The increased intracellular ROS production during reoxygenation of mock-infected enterocytes is diminished after infection with *C. albicans*. ROS were determined in mock- and *C. albicans*-infected C2BBe1 cells 24 h p.i. using DCFDA. Results of three biological replicates each performed in triplicates are shown as mean ± SD. Tert-butyl hydrogen peroxide (TBHP) was used as positive control for ROS induction and results are depicted as mean ± SD from all oxygen regimes. Statistical analysis was performed across all data sets for mock- or fungal-infected enterocytes using a one-way ANOVA with Tukey's multiple comparisons test. * Significant differences compared to 10 % O_2 (* $P < 0.05$, ** $P < 0.01$). # Significant differences compared to 21 % O_2 (# $P < 0.05$, ### $P < 0.001$). § $P < 0.001$ compared to all other conditions (except for infected enterocytes at constant 21 % O_2) according to one-way ANOVA with Dunnett's multiple comparisons test.

Nevertheless, the increased ROS levels of mock-infected enterocytes during reoxygenation at the onset of infection could render these epithelial cells more susceptible to the *C. albicans* infection.

4.4.1.2. HIF-1α expression and its influence on the enterocyte susceptibility to *C. albicans* infection

HIF-1α, the key player of hypoxic adaptation in human cells, was shown to play an important role in the protection and defense against microbial pathogens [108-110,156]. Therefore, to analyze whether HIF-1α is involved in the protective effect observed during hypoxic shock, the protein expression of HIF-1α for both mock-infected and *C. albicans*-infected C2BBe1 cells was investigated.

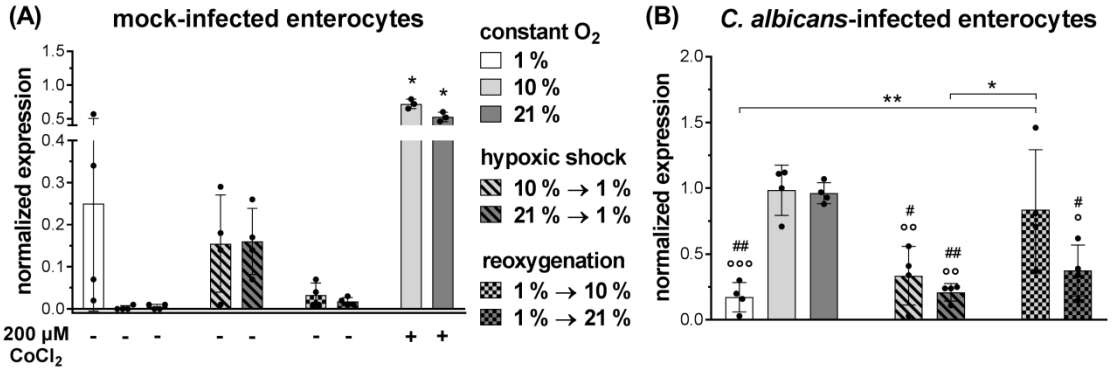

Figure 25: The HIF-1α protein expression is increased at low oxygen in mock-infected enterocytes but enhanced at normoxia and during reoxygenation after *C. albicans* infection. HIF-1α protein expression was determined in **(A)** mock-infected and **(B)** *C. albicans*-infected C2BBe1 cells using whole cell extracts. Western Blot protein bands were quantified with the ImageJ software and normalized to the actin loading control. 200 µM $CoCl_2$ was used as positive control for mock-infected enterocytes. Results of at least three biological replicates are shown as mean ± SD. Statistical analysis was performed across all data sets using a one-way ANOVA with Tukey's multiple comparisons test. **(A)** * $P < 0.05$ compared to all groups not treated with $CoCl_2$. **(B)** * Significant differences as indicated by lines (* $P < 0.05$, ** $P < 0.01$). # Significant differences to constant 21 % O_2 (# $P < 0.05$, ## $P < 0.01$). ° Significant differences to constant 10 % O_2 (° $P < 0.05$, °° $P < 0.01$, °°° $P < 0.001$).

24 h after mock-infection, HIF-1α was strongly expressed at both hypoxia and hypoxic shock compared to normoxia and reoxygenation (Figure 25, A; see Appendix 8.1., Suppl. Figure 2 A for representative protein bands). As expected, challenging C2BBe1 cells with the hypoxia-mimicking agent $CoCl_2$ resulted in a strong increase of HIF-1α expression at normoxia (Figure 25, A; see Appendix 8.1., Suppl. Figure 2 C for representative protein bands). This demonstrates the oxygen-dependent regulation of HIF-1α in the enterocytes used in this study. Furthermore, these results are consistent with previous findings for Caco-2 and HT-29 enterocytes [157]. The infection of C2BBe1 cells with *C. albicans* for 24 h significantly increased the HIF-1α expression at normoxia and during reoxygenation (Figure 25, B; see Appendix 8.1., Suppl. Figure 2 B for representative protein bands). These findings are consistent with previous studies showing that bacteria and *A. fumigatus* induce the HIF-1α expression in macrophages, dendritic cells and enterocytes at ambient and reperfusion conditions [108,157,158]. However, the expression levels of HIF-1α did not increase at hypoxia and hypoxic shock after infection.

To determine whether oxygen-dependent HIF-1α expression affects enterocyte susceptibility, the HIF-1α inducer $CoCl_2$ and the inhibitor BAY 87-2243 were used in infections experiments to induce or inhibit HIF-1α expression, respectively. The HIF-1α

inhibitor BAY 87-2243 was applied prior to and during mock-/infection. In contrast, $CoCl_2$ was used only before infection due to its negative effects on *C. albicans* filamentation (see Appendix 8.1., Suppl. Figure 3). The effect of both compounds on HIF-1α protein levels was determined after oxygen shifts immediately prior to mock-/infection (0 h) as well as 4.5 h and 24 h after mock- or fungal infection of enterocytes.

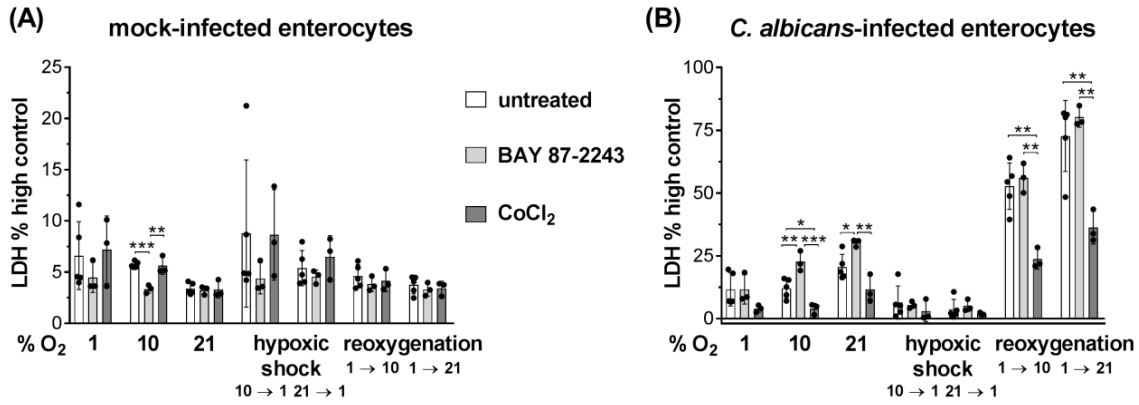

Figure 26: The HIF-1α inhibitor BAY 87-2243 and the inducer $CoCl_2$ do not affect LDH release of mock-infected enterocytes but $CoCl_2$ strongly decreases the LDH levels after *C. albicans* infection. Prior to mock- and fungal infection, C2BBe1 cells were treated with either 200 µM CoCl2 (24 h), an HIF-1α inducer, or with 100 nM BAY 87-2243 (5 h), an inhibitor of HIF-1α. 100 nM BAY 87-2243 was also included in the medium used for mock- and *C. albicans* infection. The LDH levels of **(A)** mock-infected and **(B)** *C. albicans*-infected C2BBe1 cells were determined 24 h p.i. and are depicted as LDH release relative to high control. For the calculation of LDH values after fungal infection, LDH release from mock-infected enterocytes were subtracted. Results of at least three biological replicates are shown as mean ± SD. Statistical analysis was performed across all data sets for each oxygen regime using one-way ANOVA with Tukey's multiple comparisons test. * $P < 0.05$, ** $P < 0.01$, *** $P < 0.001$.

The LDH release of mock-infected enterocytes was not influenced by $CoCl_2$ and was only slightly reduced after the treatment with BAY 87-2243 at all oxygen regimes (Figure 26, A). However, $CoCl_2$-treatment prior to infection significantly reduced the LDH release of enterocytes at normoxia and during reoxygenation (Figure 26, B). Furthermore, the relatively low LDH levels of untreated C2BBe1 cells at hypoxia and hypoxic shock were further decreased after the treatment of enterocytes with $CoCl_2$. However, the treatment of C2BBe1 cells with the inhibitor BAY 87-2243 led to significantly increased LDH levels only at normoxia (Figure 26, B). Nevertheless, these findings indicate that HIF-1α indeed affects the susceptibility of enterocytes to *C. albicans* infection.

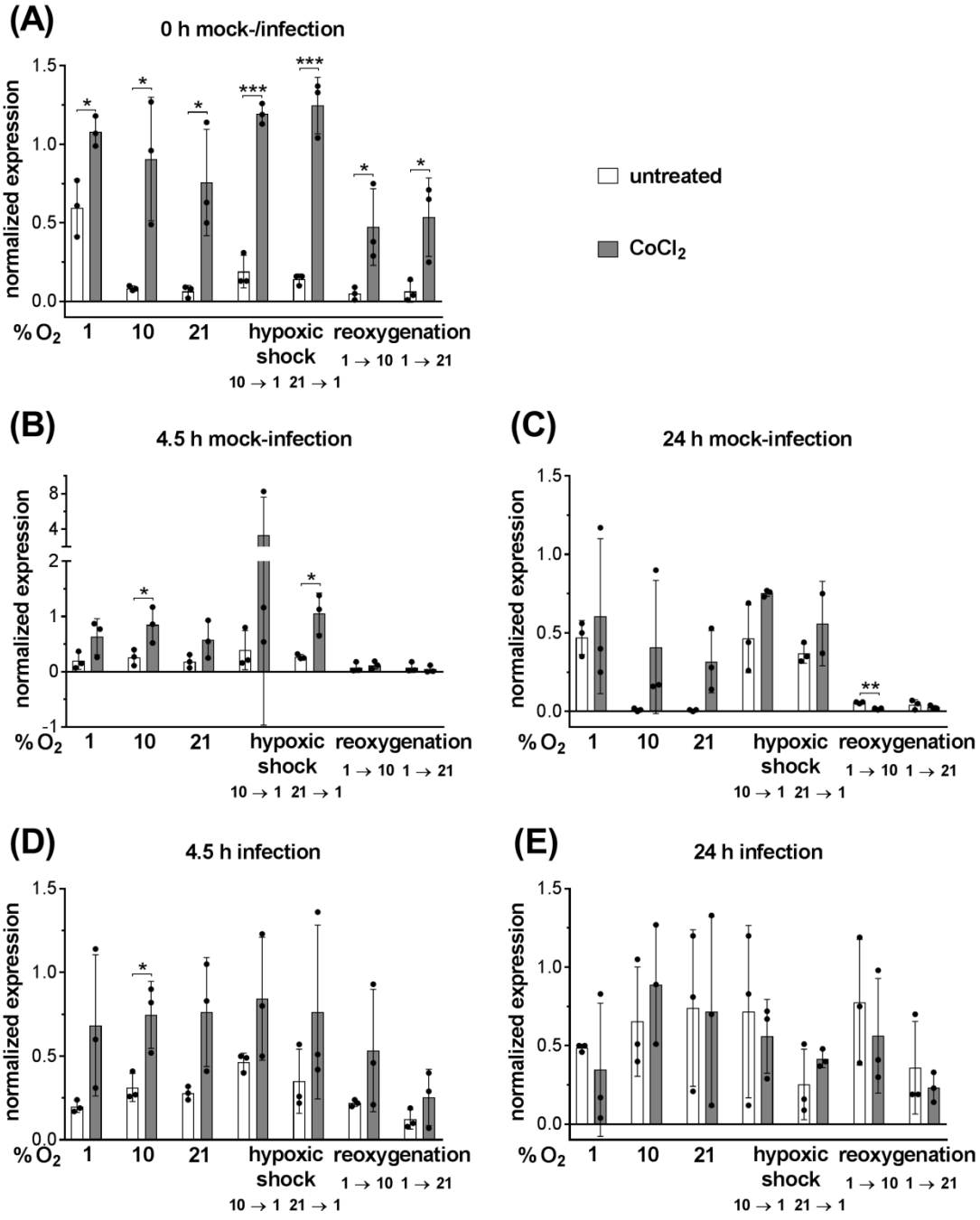

Figure 27: The $CoCl_2$-treatment increases the protein expression of HIF-1α prior to and 4.5 h after mock- or *C. albicans* infection of enterocytes. The HIF-1α protein expression was determined by Western Blot. Protein bands were quantified with the ImageJ software and normalized to the actin loading control. Prior to mock- and fungal infection, C2BBe1 cultures were treated with 200 µM $CoCl_2$ (for 24 h) or left untreated, respectively. HIF-1α expression was determined **(A)** immediately before mock-infection (1.5 h after oxygen shifts), **(B)** 4.5 h and **(C)** 24 h after mock-infection, and **(D)** 4.5 h and **(E)** 24 h after infection with *C. albicans*. Results of three biological replicates are shown as mean ± SD (except for (C) 21 → 1 with $CoCl_2$: two

biological replicates). Statistical significance of $CoCl_2$-treatment was determined using an unpaired two-tailed *t*-test. * $P < 0.05$, ** $P < 0.01$, *** $P < 0.001$.

The analysis of HIF-1α expression prior to fungal and mock-infection (0 h) confirmed that $CoCl_2$ significantly increased HIF-1α expression (Figure 27, A; see Appendix 8.1., Suppl. Figure 4 for representative proteins bands). As $CoCl_2$ was not included in the media during mock- and fungal infection, this effect declined over time (Figure 27, B and C; see Appendix 8.1., Suppl. Figure 5 A and B for representative protein bands). However, the pretreatment of enterocytes with $CoCl_2$ was still effective 4.5 h p.i. leading to increased HIF-1α levels at all oxygen concentrations tested (Figure 27, D; see Appendix 8.1., Suppl. Figure 6 A for representative protein bands). This effect was followed by a decreased HIF-1α expression 24 h after infection with *C. albicans* (Figure 27, E; see Appendix 8.1., Suppl. Figure 6 B for representative protein bands).

The treatment of enterocytes with BAY 87-2243 prior to fungal and mock-infection led to decreased HIF-1α expression levels at constant oxygen and reoxygenation (Figure 28, A; see Appendix 8.1., Suppl. Figure 4 for representative proteins bands). The effect of BAY 87-2243 was also maintained 4.5 h (Figure 28, B; see Appendix 8.1., Suppl. Figure 5 A for representative protein bands) and 24 h (Figure 28, C; see Appendix 8.1., Suppl. Figure 5 B for representative protein bands) after mock-infection as the inhibitor was present throughout the experiments. During hypoxic shock, however, HIF-1α expression was slightly increased 4.5 h after mock-infection in BAY 87-2243-treated cells compared to the untreated enterocytes (Figure 28, B). Interestingly, the infection of C2BBe1 cells with *C. albicans* abolished the inhibitory effect of BAY 87-2243 leading to increased HIF-1α levels at almost all oxygen regimes 4.5 h (Figure 28, D; see Appendix 8.1., Suppl. Figure 6 A for representative protein bands) and 24 h p.i. (Figure 28, E; see Appendix 8.1., Suppl. Figure 6 B for representative protein bands).

Altogether, these data suggest that the HIF-1α induction prior to (Figure 27, A and Figure 28, A) and at early time points of infection (4.5 h; Figure 27, D) reduces *C. albicans* damage to enterocytes and thereby contributes to the protective effect of hypoxic shock against *C. albicans* infection.

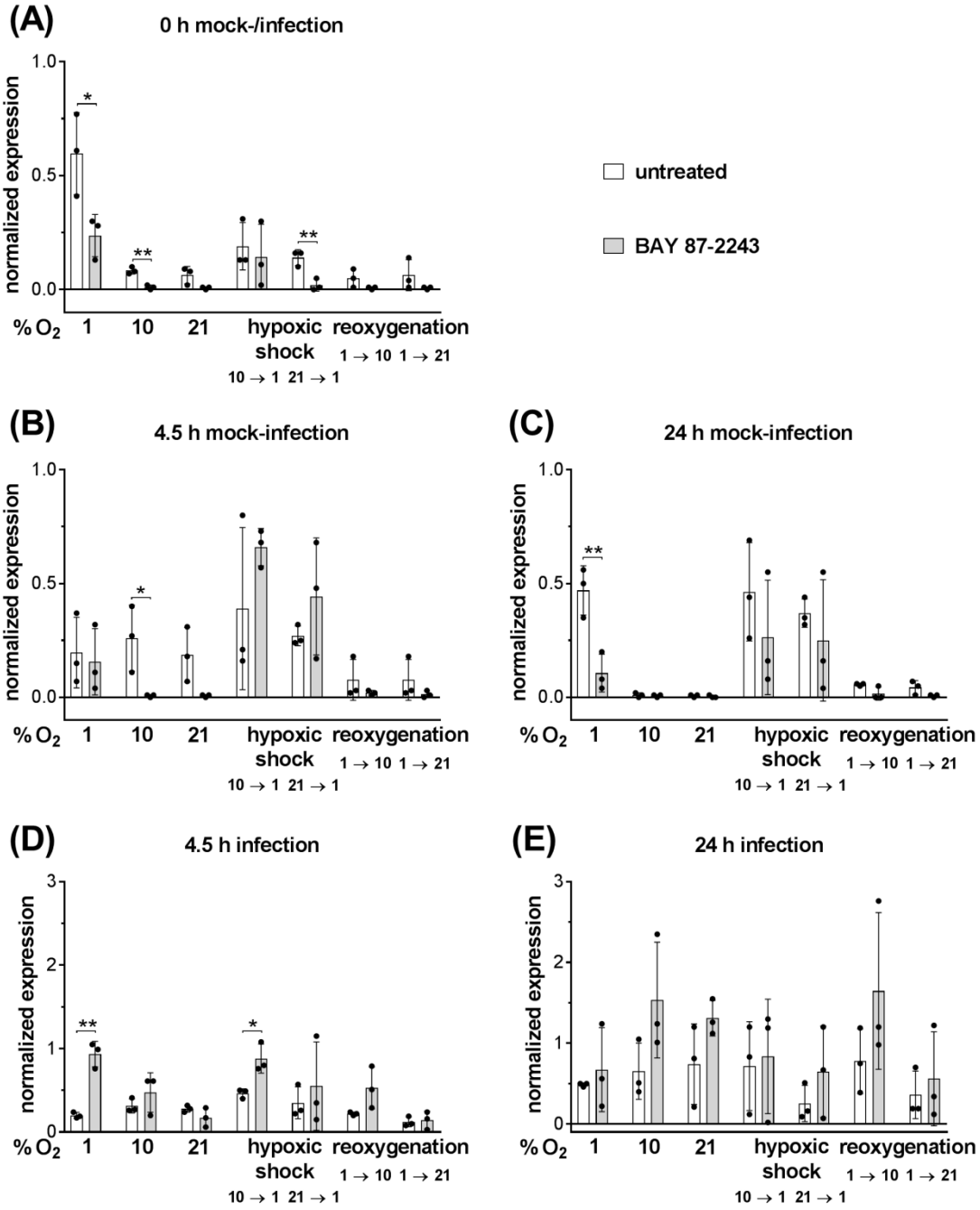

Figure 28: The treatment of enterocytes with BAY 87-2243 reduces the HIF-1α protein expression prior to and after mock-infection but has no inhibitory effect after fungal infection. The HIF-1α protein expression was determined by Western Blot. Protein bands were quantified with the ImageJ software and normalized to the actin loading control. Prior to mock- and fungal infection, C2BBe1 cultures were treated with 100 nM BAY 87-2243 (for 5 h) or left untreated, respectively. 100 nM BAY 87-2243 was also included in the medium used for mock- and *C. albicans* infection. HIF-1α expression was determined **(A)** immediately before mock-infection (1.5 h after oxygen shifts), **(B)** 4.5 h and **(C)** 24 h after mock-infection, and **(D)** 4.5 h and **(E)** 24 h after infection with *C. albicans*. Results of three biological replicates are shown as mean

± SD. Statistical significance of treatment with BAY 87-2243 was determined using an unpaired two-tailed *t*-test. * $P < 0.05$, ** $P < 0.01$.

4.4.1.3. Secretion of LL-37

Previous studies revealed that HIF-1α executes its antimicrobial activities at least partly by inducing the antimicrobial cathelicidin LL-37 [109,158]. As the induction of HIF-1α at early time points of infection (0 h and 4.5 h p.i.) contributes to the protective effect during hypoxic shock (see 4.4.1.2.), it appeared possible that HIF-1α-mediated increased LL-37 secretion contributed to protection. Therefore, the secretion of this AMP was quantified in the supernatants from both mock- and *C. albicans*-infected C2BBe1 cells 4.5 h and 24 h p.i.

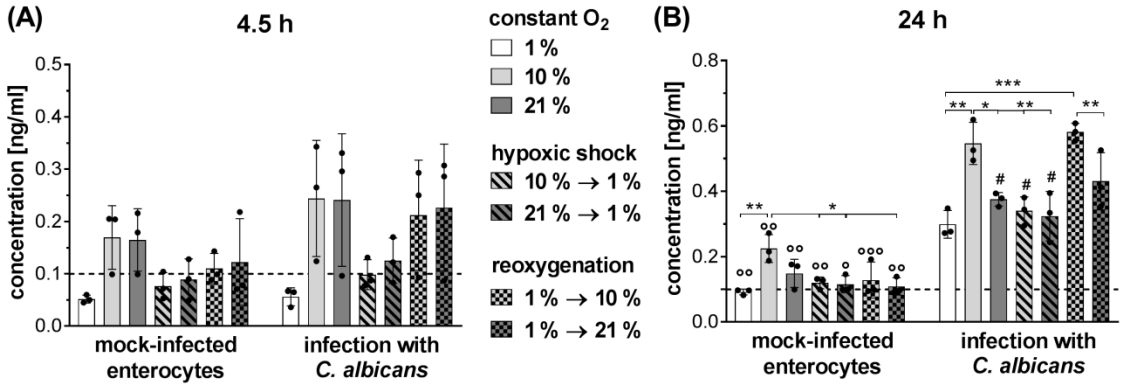

Figure 29: LL-37 secretion of mock- and *C. albicans*-infected enterocytes is increased at normoxia and reoxygenation. LL-37 concentrations were determined using supernatants of mock- and *C. albicans*-infected C2BBe1 cultures **(A)** 4.5 h and **(B)** 24 h after mock-/infection. Results of three biological replicates are shown as mean ± SD. Dashed line indicates detection limit of LL-37 (0.1 ng/ml). Statistical analysis was performed across all data sets for mock- or fungal-infected enterocytes using one-way ANOVA with Tukey's multiple comparisons test. * Significant differences as indicated by lines (* $P < 0.05$, ** $P < 0.01$, *** $P < 0.001$); # significant differences compared to reoxygenation (1 % → 10 %; # $P < 0.01$). To determine whether significant differences exist between mock- and *C. albicans*-infected enterocytes, an unpaired two-tailed *t*-test was performed. Significant differences are indicated by ° (° $P < 0.05$, °° $P < 0.01$, °°° $P < 0.001$).

At the early time point of infection (4.5 h; Figure 29, A), both mock- and *C. albicans*-infected enterocytes secreted increased amounts of LL-37 at normoxia and reoxygenation which was more pronounced after fungal infection. The LL-37 levels at hypoxia and hypoxic shock were below or close to detection limit (0.1 ng/ml) after both mock- and *C. albicans* infection.

The secretion of LL-37 after mock-infection was not increased after a prolonged incubation time (24 h; Figure 29, B): The LL-37 levels were still close to the detection limit except for constant oxygen supply at 10 % O_2. This slightly increased concentration could be due to the increased proliferation rate of enterocytes at this condition (see 4.2.2., Figure 14). However, *C. albicans* infection significantly increased the secretion of LL-37 irrespective of oxygen availability (Figure 29, B), with highest concentrations at 10 % O_2 and reoxygenation.

Thus, as secretion of LL-37 was highest upon infection during normoxia and after reoxygenation, the condition associated with highest fungal-mediated damage of enterocytes (see 4.3.1.), it appears unlikely that the protective effect of hypoxic shock is mediated by this AMP.

4.4.1.4. Expression of CEACAM1 and CEACAM6 in response to *C. albicans* infection

Recently, it was shown that *C. albicans* can bind to CEACAMs expressed on the surface of C2BBe1 cells which leads to an increased expression of CEACAMs and is associated with an immunomodulatory response [159]. As oxygen-dependent differences of infection phenotypes were observed, the possibility whether this is caused by an altered fungal recognition by host cells was tested. Therefore, the protein expression of CEACAM1 and CEACAM6 was determined at varying oxygen concentrations for both mock- and *C. albicans*-infected C2BBe1 cells using whole cell lysates and cell culture supernatants.

The expression of membrane-bound (Figure 30, A and C; see Appendix 8.1., Suppl. Figure 7 A for representative protein bands) and secreted (Figure 30, B and D; see Appendix 8.1., Suppl. Figure 7 B for representative protein bands) CEACAMs in C2BBe1 cells was not influenced by oxygen 24 h after mock-infection. However, the *C. albicans* infection caused an increased expression of both CEACAMs especially during reoxygenation. This was more pronounced for secreted CEACAMs (Figure 30, B and D).

These results suggest that the infection of enterocytes with *C. albicans* leads to an increased host response during reoxygenation.

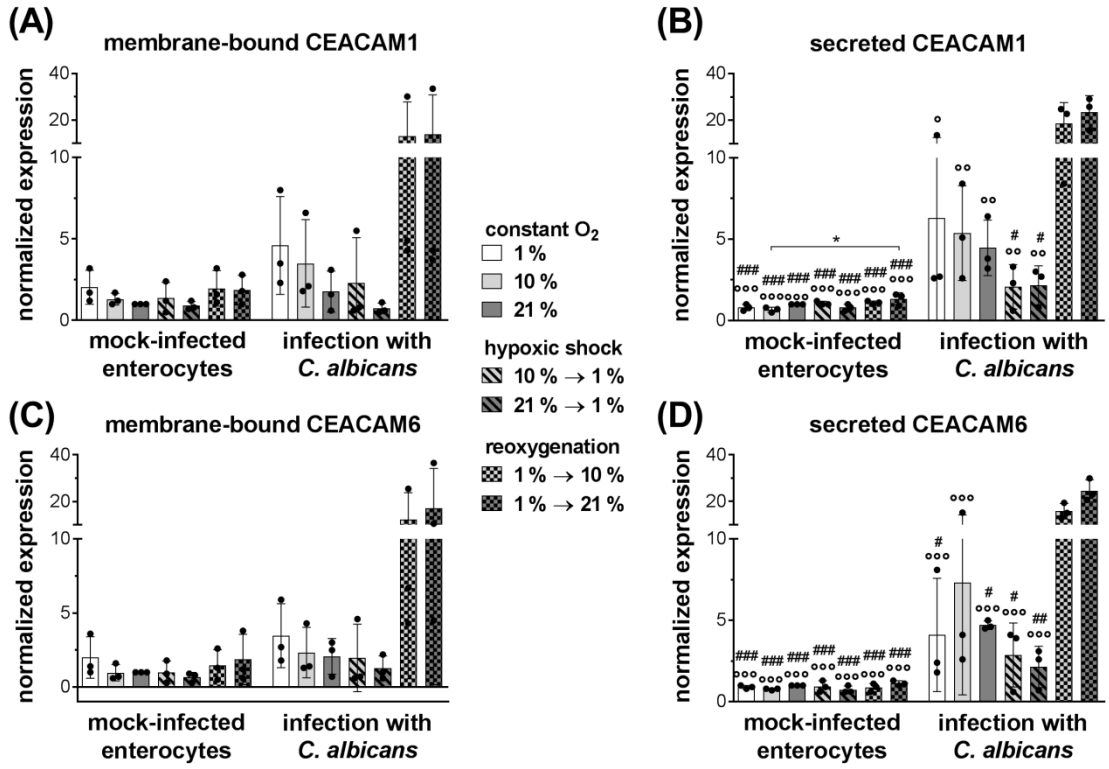

Figure 30: The expression of CEACAM1 and CEACAM6 is increased in *C. albicans*-infected enterocytes during reoxygenation. CEACAM1 **(A, B)** and CEACAM6 **(C, D)** expression of mock-infected and *C. albicans*-infected C2BBe1 cultures were determined by Western Blot using **(A, C)** whole cell lysates and **(B, D)** cell culture supernatants. The protein bands were quantified using the Image Studio Lite Software and adjusted to 14-3-3 loading control for whole cell lysates. Adjusted CEACAM1 and CEACAM6 signals were normalized to respective CEACAM signal intensities of mock-infected C2BBe1 cells at 21 % O_2. Results of three biological replicates are shown as mean ± SD. Statistical analysis was performed across all data sets using one-way ANOVA with Tukey's multiple comparisons test. * Significant difference as indicated by line (* $P < 0.05$). # Significant differences compared to infected enterocytes after reoxygenation from 1 % to 10 % O_2 (# $P < 0.05$, ## $P < 0.01$, ### $P < 0.001$). ° Significant differences compared to infected enterocytes after reoxygenation from 1 % to 21 % O_2 (° $P < 0.05$, °° $P < 0.01$, °°° $P < 0.001$). Western Blot analyses, quantification, adjustment and normalization of CEACAM protein bands were performed and kindly provided by Esther Klaile from Host Septomics.

4.4.1.5. Secretion of cytokines

Intestinal epithelial cells are able to produce cytokines in response to bacterial and fungal infection, to LPS-stimulation, or during inflammatory diseases, with high abundance for IL-8, MCP-1, GM-CSF, TNFα, IL-33, IL-1β and IL-6 [62,146-149]. Furthermore, a recent study showed that HIF-1α can modulate the pro-inflammatory cytokine response in dendritic cells upon exposure to *A. fumigatus* [108]. Therefore, the release of cytokines

into the supernatant by C2BBe1 cells upon infection with *C. albicans* at different oxygen levels was analyzed. First, a ProcartaPlex® Immunoassay for IL-8, MCP-1, GM-CSF, TNFα, IL-33, IL-1β and IL-6 was performed using LPS-treated C2BBe1 cells 24 h after stimulation as positive control. Concentrations above the detection limit were only detected for IL-6, MCP-1 and IL-8 (Figure 31). Thus, a detailed quantification by ELISA was performed for these three factors.

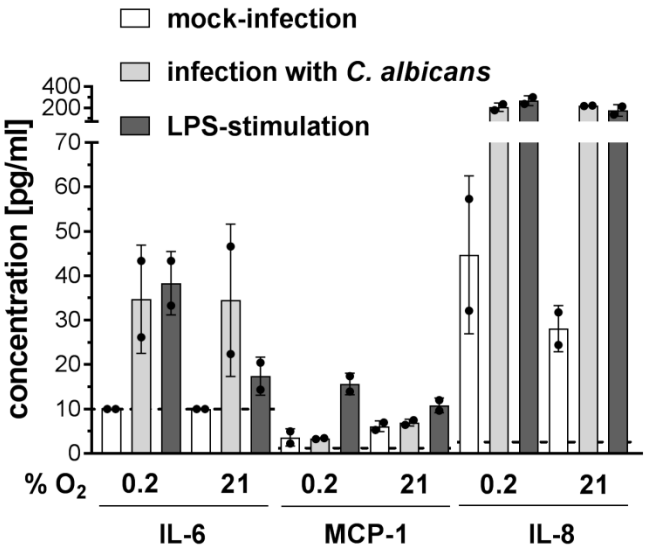

Figure 31: The production of IL-6, MCP-1 and IL-8 is increased in *C. albicans*-infected and LPS-treated enterocytes. Seven days old C2BBe1 cells were mock-infected, inoculated with fungal cells or treated with 2.5 µg/ml LPS for 24 h. Supernatants were used to determine IL-6, MCP-1 and IL-8 concentrations with a ProcartaPlex® Immunoassay. Results of one biological replicate performed in duplicates are shown as mean ± SD. Dashed lines indicate respective detection limit of IL-6 (10 pg/ml), MCP-1 (1.1 pg/ml) and IL-8 (2.5 pg/ml).

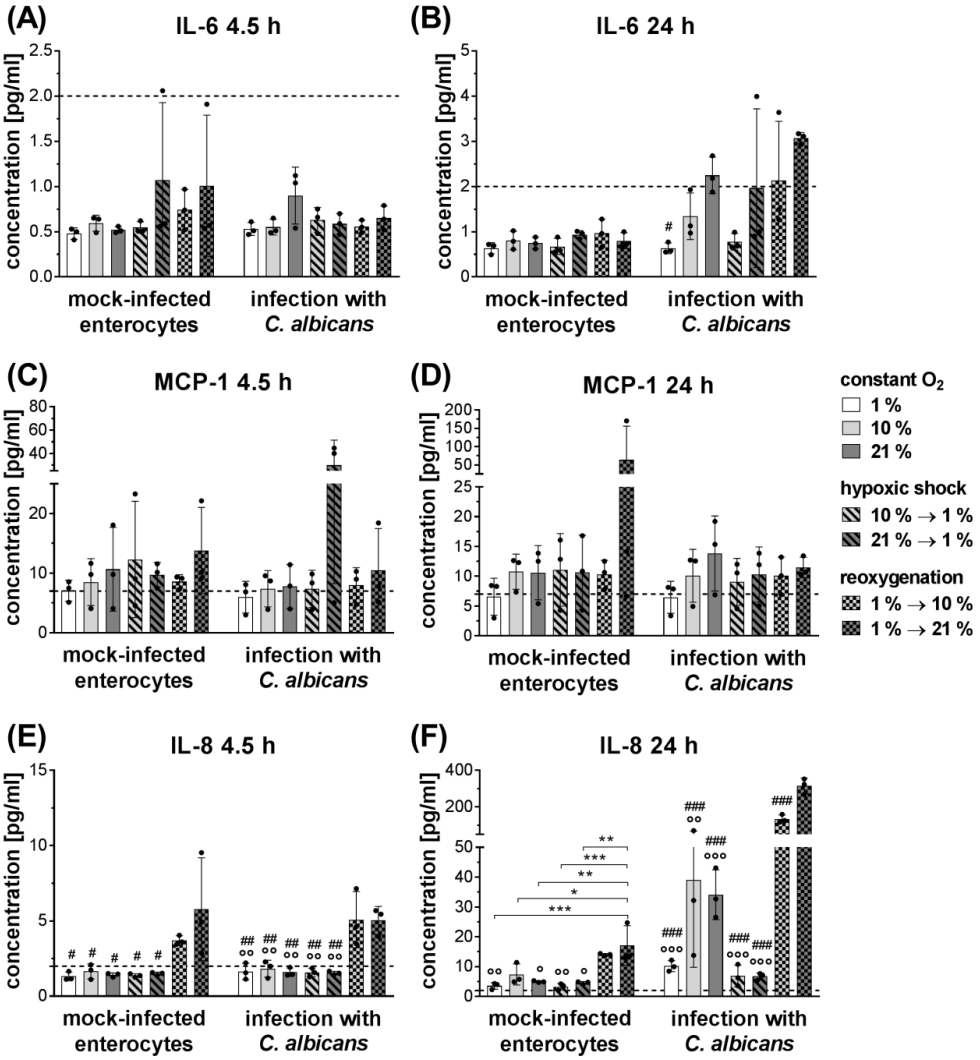

Figure 32: The secretion of IL-8 is increased during reoxygenation whereas IL-6 levels are below the detection limit and MCP-1 concentrations are not affected by both oxygen and incubation time. Supernatants of both mock-infected and *C. albicans*-infected C2BBe1 cultures were used to determine **(A, B)** IL-6, **(C, D)** MCP-1 and **(E, F)** IL-8 concentrations **(A, C, E)** 4.5 h and **(B, D, F)** 24 h after mock- and fungal infection. Results of three biological replicates are shown as mean ± SD. Dashed lines indicate detection limit of IL-6 (2 pg/ml), MCP-1 (7 pg/ml) and IL-8 (2 pg/ml), respectively. Statistical analysis was performed across all data sets for mock- or fungal-infected enterocytes using one-way ANOVA with Tukey's multiple comparisons test. * Significant difference indicated by line (* $P < 0.05$, ** $P < 0.01$, *** $P < 0.001$). ° Significant difference compared to reoxygenation from 1 % to 10 % O_2 (° $P < 0.05$, °° $P < 0.01$, °°° $P < 0.001$). # Significant difference compared to reoxygenation from 1 % to 21 % O_2 (# $P < 0.05$, ## $P < 0.01$, ### $P < 0.001$).

In contrast to the results of the ProcartaPlex® Immunoassay, IL-6 levels were found to be below the detection limit (2 pg/ml) of the commercially available ELISA Kit used (see chapter 3.1.4., Table 6) for all groups 4.5 h p.i (Figure 32, A). 24 h p.i., detectable IL-6

concentrations were observed only for infected enterocytes at constant 21 % O_2 supply, during reoxygenation, and when cells were shifted from 21 % to 1 % O_2 (Figure 32, B). Therefore, these results allowed no further conclusions.

Similar to the results of the Immunoassay pre-test, the MCP-1 levels determined by ELISA (see chapter 3.1.4., Table 6) were close to or only slightly above the detection limit (7 pg/ml). Although the MCP-1 levels were increased during hypoxic shock 21 % → 1 % 4.5 h p.i. (Figure 32, C) and for mock-infected enterocytes 24 h p.i. during reoxygenation 1 % → 21 % (Figure 32, D), no clear trend of the MCP-1 secretion was observed irrespective of oxygen and incubation time. Thus, it seems that this cytokine does not contribute to the oxygen-dependent response of C2BBe1 cells to *C. albicans* infection.

In contrast to IL-6 and MCP-1, the IL-8 levels of mock-infected enterocytes were significantly increased during reoxygenation, both 4.5 h (Figure 32, E) and 24 h p.i. (Figure 32, F). Infection of enterocytes with *C. albicans* did not affect IL-8 secretion within the first 4.5 h p.i. (Figure 32, E), but led to a significant increase 24 h after fungal inoculation (Figure 32, F). The highest concentrations were observed at normoxia and during reoxygenation (Figure 32, F). This correlates with the extent of fungal damage (see 4.3.1). In addition, as it was shown that *C. albicans* binding to CEACAM1 induces IL-8 production [159], the increased CEACAM1 expression after fungal infection might contribute to enhanced IL-8 secretion during reoxygenation.

4.4.1.6. Availability of nutrients and metabolic changes

Nutrient availability, such as glucose, and the production of metabolites, like lactate, is known to affect *C. albicans* growth and filamentation [160,161]. Furthermore, fungal adaptation to different carbon sources significantly influences the host-fungus interaction [45]. Thus, oxygen-induced changes in enterocyte metabolism could have an impact on *C. albicans*, thereby influencing the *C. albicans*-enterocyte interaction and contributing to the oxygen-dependent differences in damage. In order to analyze changes in metabolism, the amount of lactate and glucose was determined in supernatants from C2BBe1 cells cultured at different oxygen regimes after mock- and fungal infection, respectively.

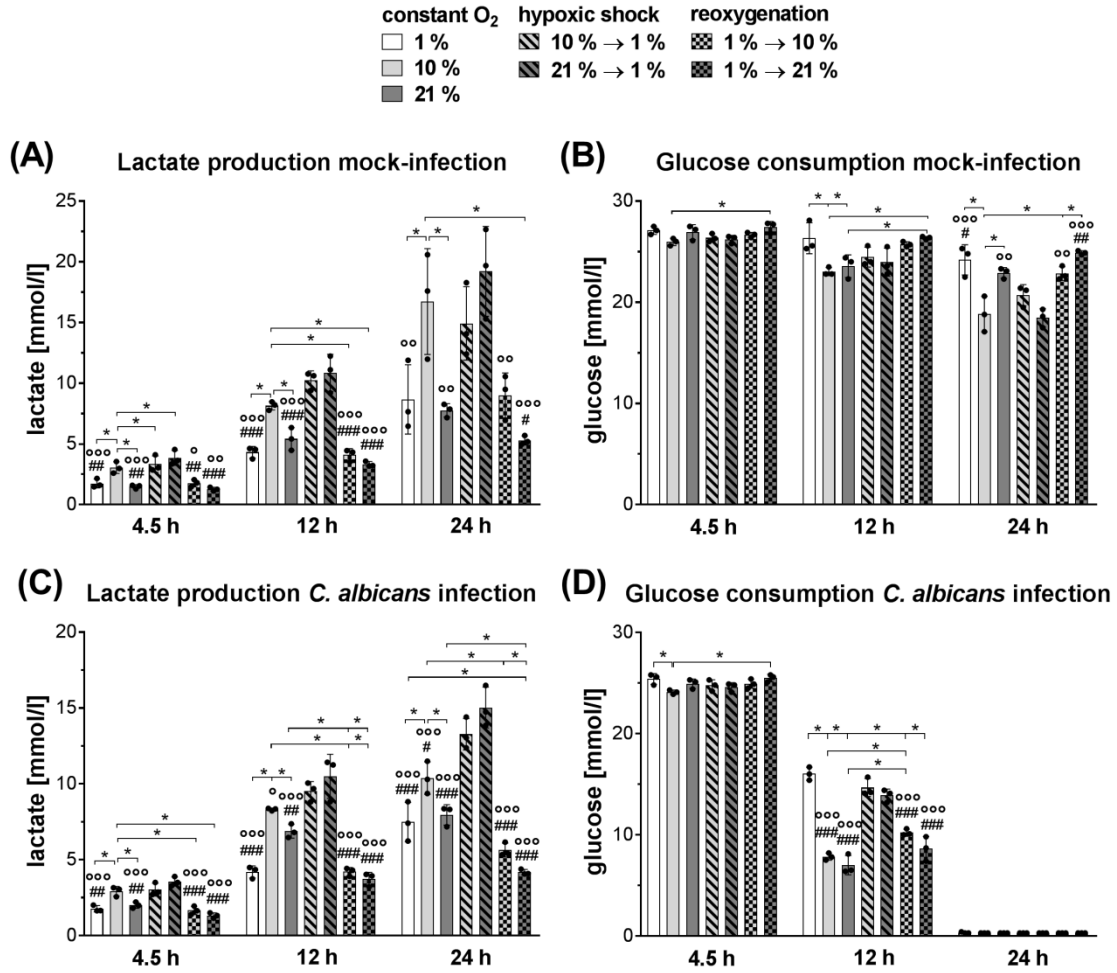

Figure 33: The lactate production is increased at 10 % O_2 and during hypoxic shock after mock- and fungal infection whereas the glucose levels are rapidly reduced in supernatants of *C. albicans*-infected enterocytes. (A, C) Lactate and **(B, D)** glucose levels were determined from supernatants of **(A, B)** mock-infected and **(C, D)** *C. albicans*-infected C2BBe1 cultures 4.5 h, 12 h and 24 h after infection. Data of three biological replicates are shown as mean ± SD. Statistical analysis was performed across all data sets within one time point using a one-way ANOVA with Tukey's multiple comparisons test. * Significant difference indicated by line (* $P < 0.05$). # Significant difference compared to shift from 10 % to 1 % O_2 (# $P < 0.05$, ## $P < 0.01$, ### $P < 0.001$). ° Significant difference compared to shift from 21 % to 1 % O_2 (° $P < 0.05$, °° $P < 0.01$, °°° $P < 0.001$).

Lactate production (Figure 33, A and C) and glucose consumption (Figure 33, B and D) increased over time in both mock-infected enterocytes and cells infected with *C. albicans*. As expected, significant higher lactate levels were observed during hypoxic shock as a result of the adaptation of enterocytes to reduced oxygen availability (Figure 33, A and C). The increased lactate levels observed at constant 10 % O_2 are likely due to the higher proliferation rate of enterocytes at this condition (see 4.2.2., Figure 14).

Whereas the lactate production was comparable for *C. albicans*- and mock-infected enterocytes, the glucose concentration was reduced more rapidly after fungal infection leading to full glucose depletion 24 h p.i. (Figure 33, D). This strong reduction in glucose levels is likely mediated by the fungal metabolism as *C. albicans* is known to efficiently utilize glucose [14,160,162]. The glucose consumption of mock-infected enterocytes was increased during hypoxic shock and at constant 10 % O_2 supply (Figure 33, B) which is consistent with the increased lactate production at these conditions, indicating metabolic adaptation.

In order to determine if increased lactate production during hypoxic shock contributes to the reduced *C. albicans*-mediated damage, C2BBe1 cells were exposed to different lactate concentrations in parallel to the infection with the fungus. However, lactate concentrations ranging from 5 mM to 25 mM did not affect damage at different oxygen regimes as determined by LDH release (Figure 34). These findings suggest that neither lactate production nor the reduction of glucose levels affect at least the fungal-mediated damage of enterocytes.

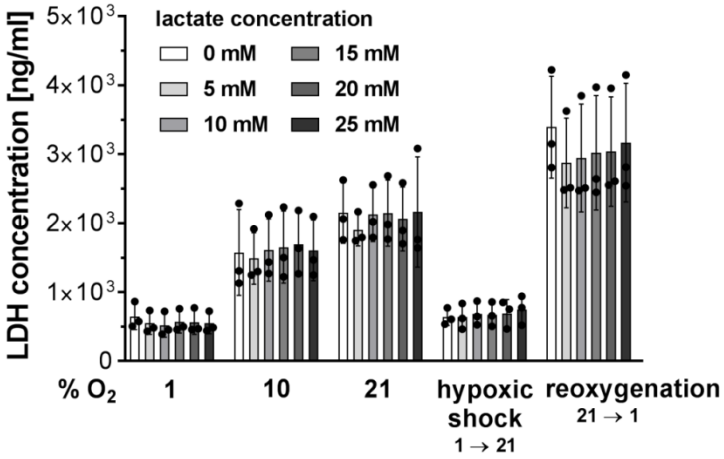

Figure 34: Lactate does not influence the LDH release of *C. albicans*-infected enterocytes. The LDH levels of *C. albicans*-infected C2BBe1 cells were determined after treatment of enterocytes with different lactate concentrations in parallel to fungal infection. LDH concentrations were determined 24 h p.i. using an LDH standard. Data of three biological replicates each performed in triplicates are shown as mean ± SD. No significant differences between data sets within each oxygen condition were observed using a one-way ANOVA with Tukey's multiple comparisons test.

4.4.2. Fungal response

While enterocytes were exposed to constant oxygen, hypoxic shock, and reoxygenation prior to infection, the fungus was added to the enterocytes 1.5 h after the oxygen shifts

took place. Thus, *C. albicans* had to face only different constant oxygen concentrations during the infection process. Consequently, the oxygen concentrations encountered by *C. albicans* were the same for constant low oxygen and hypoxic shock, and for constant normoxia and reoxygenation, respectively. The growth analysis of *C. albicans* mono-cultures revealed only a prolonged adaptation phase but no growth reduction at hypoxic conditions (0.2 % - 2 % O_2) compared to normoxia (see 4.1.). Nevertheless, significant differences were observed for the fungal adhesion and invasion ability, and the damage capability at the different oxygen regimes suggesting that enterocytes influence *C. albicans*. This raised the question if the behavior of the fungal cells is influenced by both the different oxygen regimes, used in this study, and the presence of enterocytes.

4.4.2.1. Growth and hyphal length of *C. albicans* in the presence of enterocytes

In order to analyze the growth of *C. albicans* on enterocytes, the fungal burden and the filamentation of *C. albicans* on C2BBe1 cells was quantified 4.5 h and 24 h p.i. by determining the CFUs and measuring hyphal length, respectively.

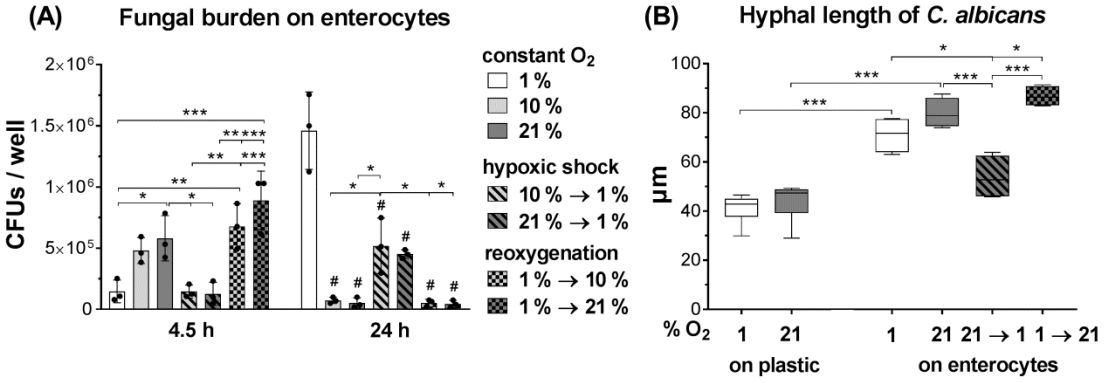

Figure 35: Hypoxic shock leads to reduced fungal CFUs and shorter filaments 4.5 h after infection of enterocytes with *C. albicans*. (A) *C. albicans* cells were incubated for 4.5 h and 24 h on C2BBe1 cells. The fungal burden was determined as CFUs/well after Zymolyase® treatment. Results of at least three biological replicates each performed in duplicates are shown as mean ± SD. Statistical analysis was performed across all data sets of each incubation time point using a one-way ANOVA with Tukey's multiple comparisons test. * Significant difference indicated by lines (* $P < 0.05$, ** $P < 0.01$, *** $P < 0.001$). # $P < 0.001$ compared to 1 % O_2. **(B)** Hyphal length of *C. albicans* incubated for 4.5 h on plastic and on C2BBe1 cells. 100 fungal cells were measured per well; results of nine (on plastic) or four (on enterocytes) biological replicates each performed in duplicates are shown as Whisker-Box-Plot. Statistical analysis of hyphal length on enterocytes was performed across all data sets using a one-way ANOVA with Tukey's multiple comparisons test. An unpaired two-tailed *t*-test was used for analysis of hyphal length on plastic

and for comparison of hyphal length on plastic and on enterocytes at the different oxygen concentrations. * $P < 0.05$, ** $P < 0.01$, *** $P < 0.001$.

The growth of *C. albicans* on enterocytes initially led to significantly reduced CFUs at hypoxia and during hypoxic shock (Figure 35, A). 24 h p.i., however, the number of CFUs was significantly increased at these conditions compared to normoxia and reoxygenation. This indicates no general growth defect at low oxygen on enterocytes but a prolonged adaptation phase, which is consistent with the findings for the growth of *C. albicans* on plastic surfaces (see 4.1.3., Figure 9). The hyphal length of *C. albicans* grown on enterocytes was significantly reduced on enterocytes that underwent hypoxic shock compared to normoxia and reoxygenation (Figure 35, B). Furthermore, the hyphae of fungal cells grown on enterocytes during hypoxic shock were also significantly shorter than those grown on enterocytes at hypoxia although the oxygen concentration for the fungus was identical. This suggests that enterocytes do affect the *C. albicans* filamentation. This is supported by the observation that *C. albicans* hyphae were significantly longer after growth on enterocytes (70 – 80 µm) compared to the growth on plastic surfaces (40 – 45 µm) at hypoxia and normoxia.

These results suggest that the oxygen-preconditioning of enterocytes affects the filamentous growth of *C. albicans*. Furthermore, the reduced fungal burden and hyphal length during early interaction with enterocytes that underwent hypoxic shock could indicate that the early interaction of *C. albicans* with enterocytes is the most important phase for damage outcome after 24 h. This would be consistent with the observations regarding HIF-1α (see chapter 4.4.1.2., Figure 26 – Figure 28).

4.4.2.2. The influence of nutrient availability and secreted factors on the filamentation of *C. albicans*

Enterocytes produced significantly higher amounts of lactate during hypoxic shock (see 4.4.1.6.; Figure 33, A and C) and fungal hyphae were significantly shorter for *C. albicans* cells grown on C2BBe1 cells exposed to this condition (see 4.4.2.1.; Figure 35). A previous study showed reduced filamentation rates of *C. albicans* in lactate-containing medium compared to fungal growth in the presence of glucose only [160]. Thus, the influence of lactate on the filamentation of *C. albicans* was analyzed even though this metabolite did not influence the fungal-mediated LDH release of enterocytes (see 4.4.1.6.; Figure 34). Therefore, fungal cells were cultivated in DMEM supplemented with 0 mM, 5 mM or 20 mM lactate. In addition, the influence of the nutrient availability was further investigated by cultivation in the presence or absence of 25 mM glucose.

C. albicans cells grown in DMEM without glucose exhibited significantly shorter hyphae compared to DMEM with glucose both at hypoxia and normoxia (Figure 36). The presence of different lactate concentrations did not influence hyphal length. But by trend, compared to filamentation at normoxia longer hyphae were observed at hypoxia in DMEM lacking glucose whereas the glucose supplementation resulted in slightly shorter hyphae at hypoxia.

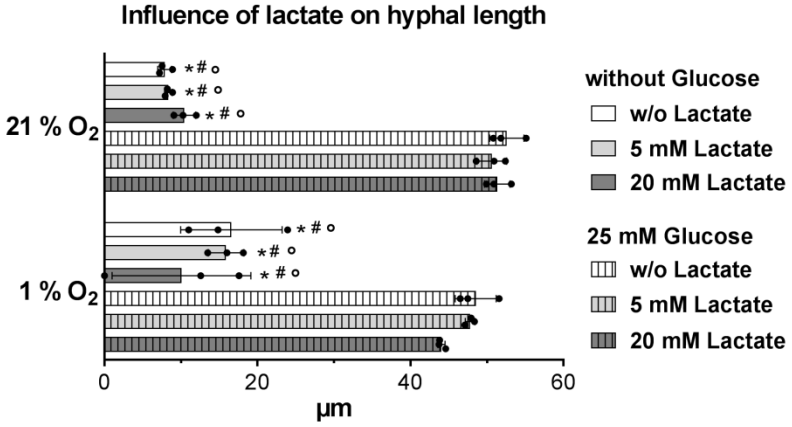

Figure 36: *C. albicans* hyphae are significantly shorter in the absence of glucose but their length is not significantly affected by lactate or oxygen. The hyphal length was determined after 4.5 h cultivation in DMEM on plastic with or without 25 mM glucose supplemented with 0, 5 or 20 mM lactate. For each technical replicate 100 hyphae were measured. Results of three biological replicates each performed in duplicate are shown as mean ± SD. Statistical analysis was performed across all data sets within each oxygen concentration using a one-way ANOVA with Tukey's multiple comparisons test. * $P < 0.001$ compared to respective 25 mM glucose without lactate. # $P < 0.001$ compared to respective 25 mM glucose + 5 mM lactate. ° $P < 0.001$ compared to respective 25 mM glucose + 20 mM lactate.

In order to determine whether other secreted enterocyte factors influence the hyphal growth of *C. albicans* in an oxygen-dependent manner, fungal cells were cultivated with supernatants of mock- and *C. albicans*-infected C2BBe1 cells, as well as with supernatants of *C. albicans* mono-cultures, grown under different oxygen concentrations. Supernatants of mock-infected enterocytes had no effect on hyphal length at any oxygen concentration (Figure 37, A). Hyphal length was reduced upon cultivation of *C. albicans* in supernatants of either infected enterocytes or *C. albicans* mono-cultures compared to fresh medium, but irrespective of oxygen availability (Figure 37, B and C). The significant reduction in hyphal length after the growth in these supernatants is likely caused by the reduction of nutrients, especially glucose (Figure 37, D; see 4.4.1.6., Figure 33, D for *C. albicans*-infected enterocytes), which results in the reduction of hyphal length (Figure 36).

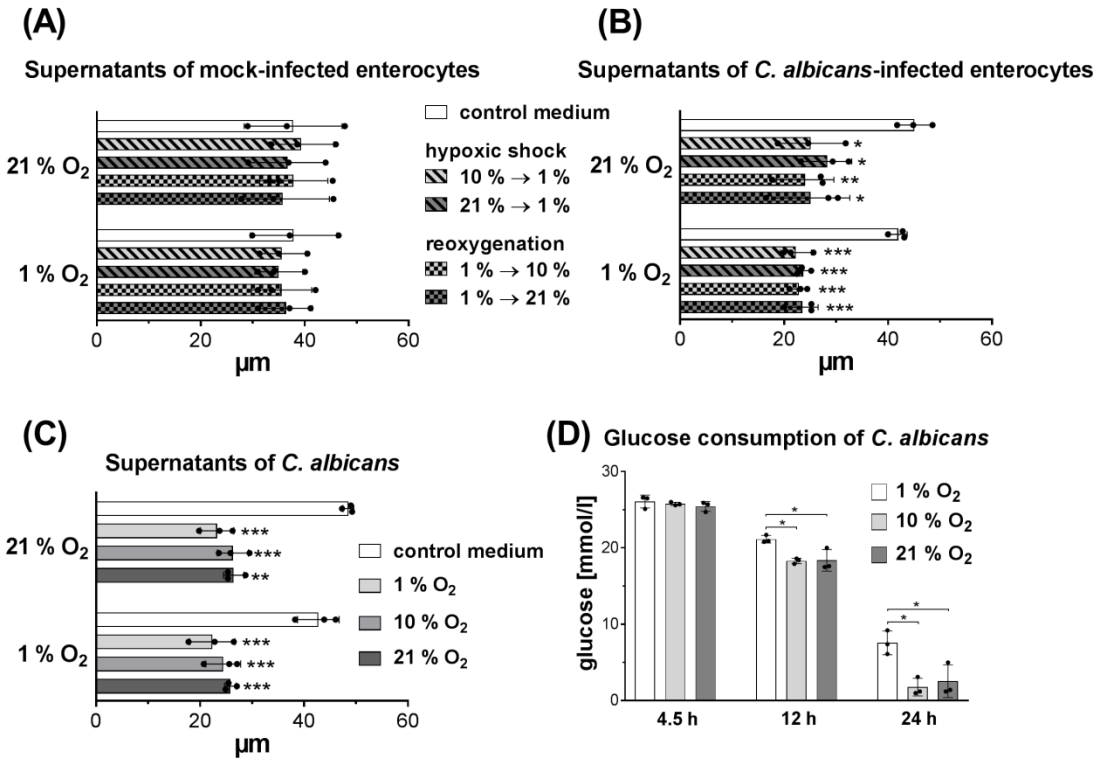

Figure 37: The supernatants of enterocyte and *C. albicans* co- and mono-cultures do not affect the hyphal length whereas the reduced glucose levels in *C. albicans* cultures reduce fungal filamentation. *C. albican*s cells were cultivated on collagen I-coated wells without enterocytes for 4.5 h in supernatants of **(A)** mock-infected C2BBe1 cells, **(B)** *C. albicans*-infected C2BBe1 cells or **(C)** *C. albicans* cells. The hyphal length was determined for 100 hyphae per technical replicate. Results of three biological replicates each performed in duplicates are shown as mean ± SD. Statistical analysis was performed across all data sets within each oxygen concentration using a one-way ANOVA with Tukey's multiple comparisons test. * $P < 0.05$, ** $P < 0.01$, *** $P < 0.001$ compared to respective medium control. **(D)** Glucose levels were determined from supernatants of *C. albicans* cells grown on plastic in DMEM 4.5 h, 12 h and 24 h after inoculation. Data of three biological replicates are shown as mean ± SD. Statistical analysis was performed across all data sets within one time point using a one-way ANOVA with Tukey's multiple comparisons test. * Significant difference indicated by line (* $P < 0.05$).

These findings indicate that neither specific secreted fungal nor host factors affect hyphal growth under the conditions used for enterocyte damage assays. Nutrient availability, especially glucose, has a significant impact on hyphal growth. However, the influence of host cells on the hyphal growth cannot be explained by glucose availability: The shortest hyphae were observed after hypoxic shock although glucose consumption was higher at constant normoxia. It thus seems that the impact of enterocyte preconditioning on hyphal growth requires direct cell-cell-contact.

4.4.2.3. The influence of fungal adaptation to hypoxia on the interaction with enterocytes

Most experiments described so far indicate that host cell adaptation rather than fungal factors contribute to the oxygen-dependent infection outcome. However, the ability of *C. albicans* to adapt to oxygen availabilities could also contribute to the observed differences. To test this hypothesis, fungal factors shown to be crucial for the hypoxic adaptation were analyzed regarding their contribution to enterocyte damage at different oxygen concentrations. Therefore, previously created *C. albicans* deletion mutants for *ACE2*, *EFG1*, *TYE7*, *UPC2* as well as a "wild-type" control strain [126] were used to infect enterocytes. In addition to damage analysis, the growth of deletions mutants was examined at different oxygen concentrations to ensure that the observed damage phenotypes are not due to general growth defects.

Consistent to the growth analysis of the *C. albicans* wt strain SC5314 (see 4.1.1.; Figure 6), the "wild-type" control strain used showed a slightly prolonged log-phase at hypoxia (Figure 38, A) compared to normoxia (Figure 38, B and C) but showed no considerable growth reduction. Independent of oxygen, the growth of *efg1*ΔΔ, *tye7*ΔΔ and *upc2*ΔΔ was clearly impaired compared to the growth of the "wild-type" control strain, with the strongest impairment observed for *upc2*ΔΔ (Figure 38). This growth reduction was most pronounced at hypoxia (Figure 38, A): *efg1*ΔΔ and *tye7*ΔΔ reached approx. 60 % of the "wild-type"-OD after a cultivation time of 14 h. The OD of *upc2*ΔΔ was even lower at this time point. The deletion of *ACE2* (*ace2*ΔΔ) led to an only slightly reduced growth compared to the control strain, resulting in approx. 90 % of the "wild-type"-OD irrespective of oxygen (Figure 38).

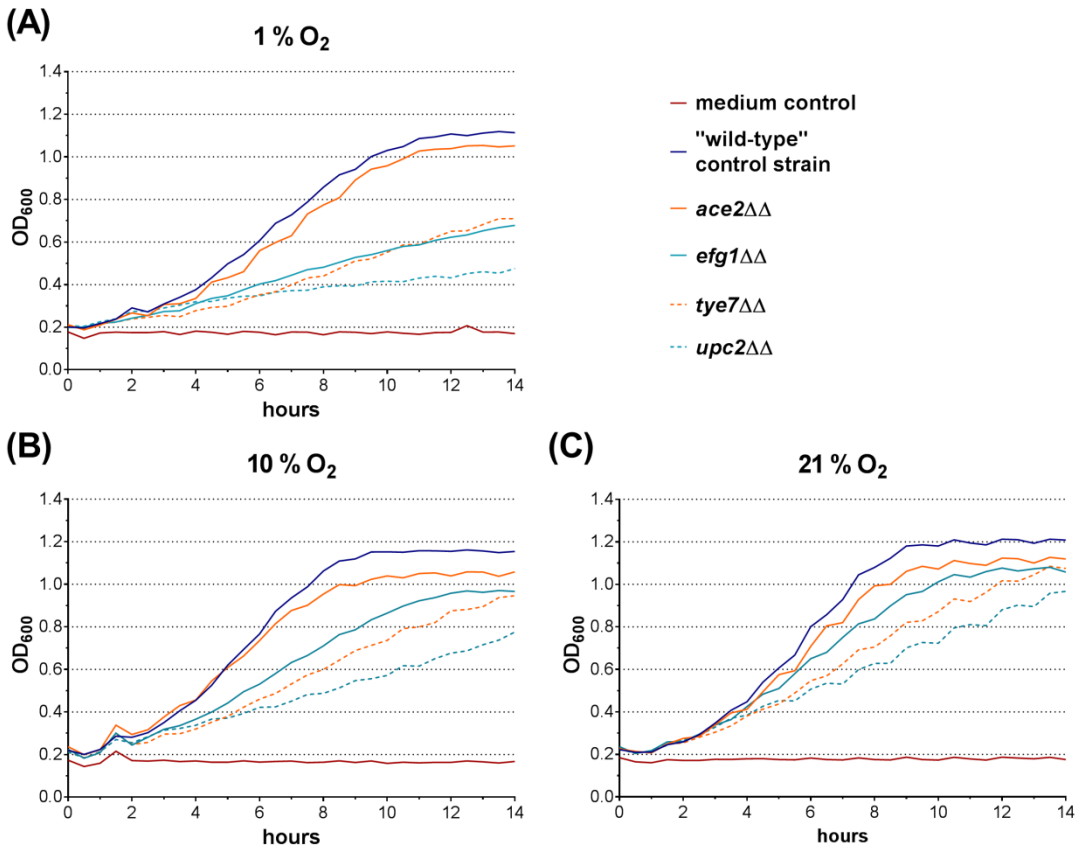

Figure 38: Hypoxia aggravates the impaired growth of *efg1*ΔΔ, *tye7*ΔΔ and *upc2*ΔΔ whereas the growth of *ace2*ΔΔ is comparable with the "wild-type" control strain at hypoxia and normoxia. The *C. albicans* deletion strains *ace2*ΔΔ, *efg1*ΔΔ, *tye7*ΔΔ and *upc2*ΔΔ as well as respective "wild-type" control strain were cultivated at **(A)** 1 %, **(B)** 10 % and **(C)** 21 % O_2 in YPD medium at 37 °C and 5 % CO_2 for 14 h. The OD_{600} was measured manually every 30 min. Data of three biological replicates each performed in triplicates are presented as mean (except for *efg1*ΔΔ, *tye7*ΔΔ and *upc2*ΔΔ at 1 % O_2: two biological replicates).

Consistent with the damage phenotype observed for the *C. albicans* wt strain SC5314 (see 4.3.1.; Figure 17 – Figure 20), the "wild-type" control strain caused increased damage during reoxygenation whereas hypoxic shock reduced fungal-mediated LDH release by enterocytes (Figure 39). However, these oxygen-dependent differences were not as pronounced as observed for SC5314. Almost no LDH levels were detectable for the mutants with deletion of *EFG1* (*efg1*ΔΔ) and *UPC2* (*upc2*ΔΔ), independent of oxygen (Figure 39, B and D) and, hence, independent of fungal growth (see Figure 38). This indicates a general virulence defect of these deletion mutants. The infection of enterocytes with *ace2*ΔΔ also resulted in significantly reduced damage irrespective of oxygen availability, indicating a general virulence defect (Figure 39, A). Interestingly, compared to the "wild-type" control strain the *TYE7* deletion mutant (*tye7*ΔΔ) led to

increased damage at normoxia and during reoxygenation, whereas this mutant was clearly attenuated in infection at hypoxia and during hypoxic shock (Figure 39, C).

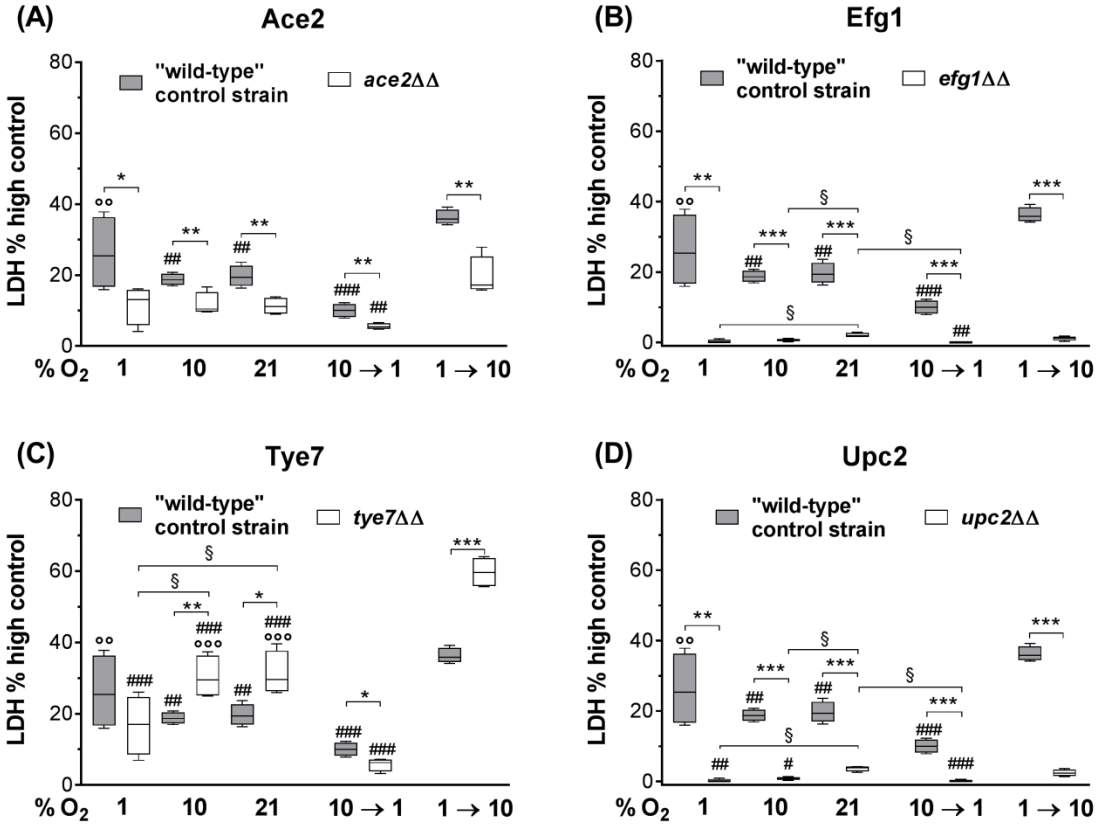

Figure 39: LDH levels for *ace2*ΔΔ, *efg1*ΔΔ, and *upc2*ΔΔ are strongly reduced or almost undetectable but *tye7*ΔΔ leads to increased LDH levels at normoxia and during reoxygenation. C2BBe1 cells were infected with *C. albicans* deletion strains **(A)** *ace2*ΔΔ, **(B)** *efg1*ΔΔ, **(C)** *tye7*ΔΔ and **(D)** *upc2*ΔΔ as well as respective "wild-type" control strain. The LDH level is depicted as percentage LDH release relative to the high control. The LDH release from mock-infected cells was subtracted from all values. Results of four biological replicates each performed in triplicates are shown as Whisker-Box-Plot. Comparison of two strains within each oxygen condition was performed using an unpaired two-tailed *t*-test. * $P < 0.05$, ** $P < 0.01$, *** $P < 0.001$. Differences between the oxygen conditions were analyzed for each fungal strain using a one-way ANOVA with Tukey's multiple comparisons test. § $P < 0.05$ between two conditions indicated by lines. # Significance compared to reoxygenation (1 → 10; ## P < 0.01, ### P < 0.001). ° Significance compared to hypoxic shock (10 → 1; °° P < 0.01, °°° P < 0.001).

These data indicate that fungal adaptation to oxygen specifically affects the interaction with enterocytes. Since Tye7 is the primary regulator of the central carbon metabolism of *C. albicans* [59], these results furthermore suggest that metabolic adaptation plays a key role in oxygen-dependent virulence.

5. Discussion

C. albicans is among the most frequent causes of systemic infections in critically ill patients at intensive care units. Specific risk factors are immunosuppression, vascular catheters and large abdominal surgical procedures [18]. The GIT is thought to be the main source of disseminated *C. albicans* infections [12,28-30], and translocation of *C. albicans* through the gut epithelial barrier into the blood stream appears to be the main route of dissemination leading to systemic *C. albicans* infections [16]. Impairment of the gut barrier function is a prerequisite for fungal translocation from the GIT into the blood stream and internal organs [13,16,21,32]. Besides e.g. cancer therapy, intestinal ischemia-reperfusion (IR) injury occurring during major surgeries or traumatic shock results in intestinal epithelial barrier dysfunction [90,92]. The IR-induced breakdown of intestinal epithelial barrier integrity increases the intestinal permeability and leads to increased bacterial and fungal translocation *in vivo* [92,95,123]. Thus, ischemia and reperfusion represent potential risk factors for the development of systemic *C. albicans* infections. Especially prolonged ischemic periods are crucial for the outcome of the IR injury *in vivo* as the induced barrier dysfunction during ischemia is exacerbated by reperfusion [90,94]. Upon reperfusion, toxic byproducts and metabolites, which accumulate intracellularly during the ischemic period, contribute to the severity of systemic consequences of the IR injury *in vivo*: when the tissue is reperfused the toxic byproducts are flushed into the blood stream and are transported to other organs, thereby leading to tissue dysfunction [94,99,163]. However, to which extend reduced oxygen availability, reperfusion-induced damage, or accumulation of toxic waste products, respectively, contribute to barrier breakdown and fungal translocation is not fully understood. The aim of this study was to focus on the influence of oxygen on the interaction of *C. albicans* with intestinal epithelial cells (IECs), to better understand the impact of fluctuations in oxygen on fungal host cell damage and translocation.

5.1. Reoxygenation-induced enterocyte stress likely contributes to enhanced damage by *C. albicans*

C2BBe1 cells, which were used as an *in vitro* model for IECs and termed as enterocytes throughout this study, represent absorptive enterocytes as they homogeneously express brush borders [133]. They are commonly cultured under atmospheric conditions *in vitro*. However, the oxygen availability in the GIT is significantly lower and, furthermore, steeply decreases along the crypt-to-villus axis and is subject to profound fluctuations due to food intake and fasting periods [84-87]. Thus, the effect of oxygen on these

enterocytes was first investigated in the absence of fungi. C2BBe1 cells were able to maintain their barrier function and proliferation at oxygen concentrations ranging from 1 % to 21 % O_2, including shifts from low to high oxygen (reoxygenation) or *vice versa* (hypoxic shock) within this range. This is consistent with fluctuations of oxygen supply in the intestinal tissue *in vivo* ranging from ~ 15 % to ~ 1 % O_2 [6,86,88,89]. Furthermore, the highest proliferation rate was observed at 10 % O_2, which resembles the physiological oxygen concentration present in the crypts of the GIT where stem cell proliferation occurs *in vivo* [6,71,86]. Thus, the C2BBe1 cell line appears to have preserved the capability of IECs *in vivo* to maintain barrier function across the range of physiologically available oxygen, and thus can be considered to represent an appropriate *in vitro* cell culture model to study the impact of oxygen fluctuation on the interaction of IECs with *C. albicans*. In contrast, pathophysiological hypoxia, namely 0.2 % O_2, was detrimental to enterocyte viability. Previous *in vivo* studies, investigating the effect of intestinal IR on gut barrier function, commonly used arterial clamping to induce ischemia. Since this method generates almost anoxic conditions, comparable to the 0.2 % O_2 used in this study, it is not surprising that these studies observed damaged epithelium, impaired tight junctions and increased permeability of the gut epithelia barrier following IR [93,164-166]. As it appears obvious that ischemia-induced enterocyte cell death leads to barrier breakdown and thereby facilitates translocation of microorganisms through the severely damaged cell layer, this study focused on oxygen conditions that were tolerated by the enterocytes to determine whether non-detrimental alterations in oxygen availability impact the interactions of *C. albicans* and enterocytes.

Indeed, interaction of enterocytes with *C. albicans* was significantly affected by changes in oxygen availability: Reoxygenation of enterocytes shortly before infection significantly increased their susceptibility to *C. albicans* infection enhancing fungal invasion, damage capability and translocation. In contrast, mimicking hypoxic shock conditions was protective, leading to maintained enterocyte barrier function and reduced translocation of *C. albicans*. These observations are consistent with recent *in vivo* studies showing that reperfusion rather than ischemia leads to intestinal barrier breakdown [94,95]. As it was shown that IR injury produces ROS which have destructive effects on cellular membranes [97,98,152], the increased susceptibility of enterocytes to *C. albicans*-mediated damage at reoxygenation could be due to increased ROS production. Surprisingly though, ROS levels of mock-infected enterocytes during reoxygenation were similar to those at normoxia at the onset of infection. At both conditions, ROS levels were higher than after hypoxic shock, which could indicate that the protective effect of hypoxic shock might be in part due to reduced ROS stress, thereby increasing the resilience of

enterocytes to infection. However, reoxygenation in the absence of infection was also associated with increased IL-8 levels. As previous studies showed that oxidative stress correlates with the release of IL-8 in lung and intestinal epithelial cells [167,168], this could indicate that, even though ROS levels were comparable, reoxygenation imposed more stress on enterocytes compared to normoxic conditions, at reducing resilience to additional stressors, and thereby rendering enterocytes more susceptible to *C. albicans* infection. However, this study did not investigate further cellular stress factors. Surprisingly though, the increased ROS levels at reoxygenation, but not normoxia, were diminished in the presence of *C. albicans*. This could be due to differential expression of fungal ROS detoxification systems, especially superoxide dismutases (Sods), located at the surface of *C. albicans* [153,154]. However, the oxygen level for *C. albicans* at reoxygenation and normoxia was the same (10 % and 21 % O_2, respectively), and therefore differential activity/efficacy of Sods could only be explained by influences of enterocytes itself. One factor could be lactate production. Lactate levels were lowest at reoxygenation compared to at all other oxygen regimens, and could result in reduction of pH except for reoxygenation. It was shown that the pH optimum for the Sod activity is 7 [169]. Another study was able to show that pH 8 at 37 °C even increases the transcript levels of *SOD5* [170]. As the cultivation medium exhibits a pH of 7.4 and the presence of increased lactate levels likely reduce this pH, the activity of Sods could be favored at oxygen shifts from low oxygen to normoxia. Thus, the combination of the increased ROS production by enterocytes at the onset of infection, when *C. albicans* was just added, and the ability of *C. albicans* to clear ROS more efficiently in the course of infection to protect itself from oxidative stress during reoxygenation, which likely further enhances hyphal growth and subsequent invasion, could contribute to the severe infection phenotype seen at this condition. However, this hypothesis remains speculative as the expression and activity of Sods was not determined in this study.

5.2. Reoxygenation enhances *C. albicans* invasion

As fungal invasion is an essential initial step for infection and thus influences the subsequent host cell damage, the increased invasion of *C. albicans* observed during reoxygenation likely contributes to the infection phenotype at this condition. One possible explanation for the increased invasion ability is the impairment of tight junctions upon reoxygenation. Even though no significant difference in quantitative expression of junctional proteins was observed for mock-infected enterocytes under the different oxygen regimens, this does not exclude that structural alterations impact barrier function. Furthermore, the expression of junctional proteins was determined 24 h after oxygen

switches took place. Thus, a temporary barrier breakdown, repaired within the 24h time period, appears possible as previous studies showed that damaged epithelial cell layers quickly repair the barrier defect [171,172]. Even a time-limited breakdown of tight junctions could have been sufficient to enhance invasion [121]. A previous study furthermore showed that the tight junctions of enterocytes are impaired during *C. albicans* infection leading to a barrier breakdown [122]. This is accompanied with a decrease in TEER and in turn increases the invasion ability of *C. albicans* [121]. TEER reduction after fungal infection was observed during all oxygen regimes used in this study but the strongest decrease occurred following reoxygenation, accompanied with significantly increased permeability for RITC dextran, indicating impaired tight junctions. Whereas the main route of invasion into intestinal epithelial cells is the transcellular route *via* active penetration mediated by *C. albicans* hyphae [40,115,120], independent of tight junctions [121], it was shown previously that impaired tight junctions induces endocytosis of *C. albicans* by enterocytes contributing to fungal invasion [121]. The impairment of tight junctions would provide access to the underlying adherens junctions, like E-Cadherin which expression was shown to be reduced at late time points of *C. albicans* infection progression [122]. Thus, impaired tight junctions could facilitate the fungal access to the adherens junctions mediating induced endocytosis. Consistent with this hypothesis, a *C. albicans SSA1* deletion mutant showed an invasion and damage defect at reoxygenation only. As Ssa1 mediates induced endocytosis [44], it appears likely that induced endocytosis contributes to fungal invasion during reoxygenation. This further indicates that tight junctions are impaired at this oxygen condition. An increased impairment of tight junctions could be due to a proteolytic degradation by fungal proteases. It is known that Saps, especially Sap5, are able to proteolytically degrade the adherens junction protein E-Cadherin [173]. Thus, it appears likely that tight junction proteins can also be degraded by fungal proteases. But so far, the role of fungal proteases in the tight junction degradation and whether their secretion is oxygen-dependent has not been investigated. Furthermore, it was shown previously that bacterial proteases are able to cleave the tight junction protein Occludin [174]. Another way of action of bacterial proteases to degrade and redistribute Occludin is mediated *via* the action of the host cysteine protease calpain [175]. Additionally, the infection of airway epithelial cells with *Pseudomonas aeruginosa* was shown to induce the cleavage and redistribution of Occludin by calpain *via* TLR2 signaling [176]. Thus, it could be possible that *C. albicans* also activates host-endogenous proteases leading to degradation and redistribution of the tight junction proteins promoting invasion *via* induced endocytosis.

5.3. HIF-1α mediates protection during hypoxic shock

Another factor that likely contributes to the enhanced susceptibility at reoxygenation is the low expression level of HIF-1α. This key regulator of hypoxic adaptation in human cells was already shown to be important for enterocyte barrier function [87], for example during inflammation[84], but also for the protection and defense against microbial pathogens like *Aspergillus fumigatus* [108,110], Gram-positive group A *Streptococcus* [158] and *Mycobacterium marinum* [156]. The induction of HIF-1α by $CoCl_2$ prior to and early during infection significantly decreased the fungal-mediated damage of enterocytes that underwent reoxygenation-like conditions or were constantly cultured under normoxia. This demonstrates a protective effect of HIF-1α. With regard to the effect of HIF-1α on barrier function, the low HIF-1α expression of enterocytes at reoxygenation prior to and early during *C. albicans* infection seems to contribute to the significant increase in fungal-mediated damage. In contrast, HIF-1α levels of enterocytes were elevated at hypoxic shock compared to reoxygenation prior to and early during the infection with *C. albicans*. Since the induction of HIF-1α by $CoCl_2$ at the onset of fungal infection (0 h – 4.5 h) led to decreased enterocyte damage at all oxygen availabilities used in this study, HIF-1α appears to contribute to the protective effect observed at hypoxic shock. Thus, the expression of HIF-1α at early time points of infection rather than at late time points inversely correlates with the enterocyte susceptibility. This would also explain the significantly increased damage after fungal infection at normoxia and reoxygenation for enterocytes treated with the HIF-1α inhibitor BAY 87-2243: HIF-1α expression was strongly decreased at these conditions prior to and 4.5 h after fungal and mock-infection. But whereas the efficacy of BAY 87-2243 was maintained after mock-infection, fungal infection diminished its inhibitory effect. This could be due to a microbe-induced expression or stabilization of HIF-1α, as shown for bacteria and *A. fumigatus* [108,110,157,158], overriding the indirect inhibitory effect of BAY 87-2243 mediated by inhibition of the mitochondrial complex I which prevents the inhibition of prolyl hydroxylases (PHDs) causing degradation of HIF-1α [177].

A previous study showed that *Bacteroides thetaiotamicron*-mediated protection against *C. albicans* involves HIF-1α-dependent production of the cathelicidin LL-37 [109]. In this study, however, no oxygen-dependent differences in LL-37 production were observed and the amount of LL-37 produced was even highest after reoxygenation and infection, the condition associated with the highest enterocyte damage. Thus, the secretion of LL-37 did not protect enterocytes from the fungal-mediated damage and the impaired barrier integrity during reoxygenation. One possible explanation is the low LL-37 concentration

detected in this study (0.3 – 0.6 ng/ml) which was below concentrations previously shown to be effective against *C. albicans* (4.4 µM, equivalent to ~ 20 µg/ml, to 20 µM) [150,151,178]. While this suggests that the protective effect of HIF-1α observed here is independent of LL-37, oxygen availability could affect the sensitivity of *C. albicans* to LL-37, as it was shown for *Escherichia coli* and group A *Streptococcus pyogenes* [179]. In addition, hypoxia supports the efficacy of the human AMP β-defensin 2 against the intracellular pathogen *Mycobacterium tuberculosis* [180]. Thereby, LL-37 might be more effective at low oxygen, even though no quantitative differences were observed. Hypoxia was furthermore found to induce structural changes in the human β-defensin 1 which enhances its antimicrobial activity [181]. Whether oxygen affects structure and efficacy of LL-37 is not known. Finally, it is possible that other AMPs, like human defensins, are produced in higher amounts at low oxygen concentrations and contribute to the protective effect of hypoxic shock.

Another way by which HIF-1α could mediate the protective effect at hypoxic shock is the induction of growth factors that in turn induce mitogen-activated protein kinase (MAPK) and phosphatidylinositide-3-kinase (PI3K) signaling pathways. These have been shown to promote cell survival and proliferation [102,103,105,106]. Furthermore, induction of PI3K/Akt signaling pathway plays a key role in the protection of oral epithelial cells against *C. albicans*-induced damage [182]. A similar pathway could contribute to the protection of enterocytes. Furthermore, the metabolic shift from oxidative phosphorylation toward glycolysis is mediated by HIF-1α [100,103,106,108], ensuring appropriate energy production at hypoxic conditions. This was shown to be the basis for trained immunity of monocytes [183]. It was shown that HIF-1α contributes to the control of bacterial infections by inducing this metabolic shift [183,184]. As HIF-1α is also able to induce cellular resistance to radiation in B-cell lymphocytes [185], and is activated in response to nutrient insufficiency to cope with stress [101], it is likely that several pathways simultaneously contribute to the protective effect of HIF-1α on enterocytes during *C. albicans* infection at hypoxic shock.

5.4. Fungal contribution to oxygen-dependent enterocyte damage

The protective effect observed during hypoxic shock, indicated by reduced damage, retained barrier function and reduced fungal translocation, seems to be also partially mediated by reduced fungal growth and filament elongation during the early stages of infection. This likely contributes to the decreased invasion and subsequent damage, as events early during the *C. albicans*-enterocyte interaction appears to be decisive for the damage outcome at 24 h p.i. The reduced fungal growth and filamentation at low oxygen during early cultivation time points was also observed in the absence of enterocytes. As

growth parameters and filamentation after 24 h were comparable at high and low oxygen, a prolonged adaptation phase rather than a general growth defect appears to be the underlying cause of the differences. In this context it should be noted that *C. albicans* pre-cultures used for experiments were cultivated at normoxic conditions, and thus, the fungus had to adapt to low oxygen at the onset of infection. Although the transcriptional response of *C. albicans* to hypoxia occurs within 30 min [48], the decreased oxygen supply initially also affects energy production which is important for the cell wall biosynthesis and, hence, for fungal growth [45]. Furthermore, hypoxia leads to depletion of ergosterol from fungal membranes as the ergosterol biosynthesis is diminished [47], which likely contributes to the reduced fungal growth. After the fungal metabolism has adapted to the hypoxic condition *via* induction of genes responsible for glycolysis and ergosterol biosynthesis [47,48], growth of *C. albicans* could be restored. This possible explanation is consistent with the fungal growth behavior observed in this study. Thus, hypoxic pre-culture of *C. albicans* might prevent this adaptation phase and possibly prevent the effects of hypoxia on initial fungal growth at infection. This, however, still needs to be tested experimentally.

That the fungal adaptation to hypoxic conditions is crucial for the interaction with host cells was shown in this study by using *C. albicans* mutants deficient for factors involved in hypoxic adaptation. The deletion of *ACE2*, *EFG1* and *UPC2*, which are important for ergosterol synthesis, the filamentous response, and the general response to hypoxia [49,57], led to an oxygen-independent virulence defect. This reveals the general importance of fungal growth and filamentation for host cell damage. In contrast, the deletion of *TYE7*, the central transcriptional regulator of the carbohydrate metabolism and therefore for the glycolytic pathway [59], revealed an oxygen-dependent phenotype as the damage capability of this mutant was attenuated only at hypoxia and hypoxic shock. Importantly, a previous study showed that a *TYE7* deletion mutant is largely impaired in GIT colonization of mice but is not attenuated during systemic infections [60]. In the context of the work presented here, this suggests that the adaptation of *C. albicans* to low oxygen availability as performed here *in vitro* is also relevant for fungal survival in the gut *in vivo*, and that the *in vitro* model recapitulates important aspects of *in vivo Candida*-enterocyte interactions.

In addition to the fungal adaptation to hypoxia, *C. albicans* seems to be influenced by the enterocytes, as hyphae were significantly shorter on enterocytes subjected to hypoxic shock compared to those grown at constant hypoxia. As the oxygen availability for *C. albicans* was the same at both oxygen regimes, this difference in filamentation seems to be host-dependent. Lactate production, reduction of glucose, and the oxygen-

dependent release of soluble factors could be excluded as factors influencing fungal filamentation. Thus, the influence of the host seems to be mediated by direct cell-cell-contact which is supported by the differences in fungal adhesion. As in the clinical setting ischemic hypoxia occurs prior to reoxygenation, it is likely that the increased number of adhered fungal cells at hypoxic shock in combination with the subsequent increased invasion at reoxygenation contributes to increased tissue damage and translocation. The raised fungal adhesion ability could be mediated *via* an increased expression of fungal adhesins and/or their binding targets on the surface of enterocytes at hypoxic shock. For endothelial cells it was already shown that a reduced oxygen supply increased the expression of cell adhesion molecules like cadherins which enhances the neutrophil adherence [2,99]. Thus, it is likely that an oxygen-dependent expression of host surface molecules influences fungal adherence.

This raised the question which surface molecules of enterocytes influences the interaction with *C. albicans*. It is known that *C. albicans* is recognized by pattern recognition receptors (PRRs) from host cells of the innate immunity *via* the interaction with pathogen-associated molecular patterns (PAMPs) [114,186]. Human mucosal epithelial cells are known to express a wide range of PRRs like the Toll-like receptors (TLRs) TLR2 and TLR4, and the C-type lectin receptor (CLR) Dectin-1 [186-188]. However, which PRRs mediate the recognition of *C. albicans* by epithelial cells, and especially IECs, is unknown [22,114]. Additionally, the discrimination between *C. albicans* yeast and hyphal cells by epithelial cells seems to be independent of known PRRs [188]. A recent study demonstrated that the recognition of *C. albicans* by human IECs is at least in part mediated by CEACAMs [159]. Binding of *C. albicans* leads to an increased expression of membrane-bound CEACAM1 and soluble CEACAM6 and is associated with an immunomodulatory response [159]. The findings presented here clearly showed that the infection with *C. albicans* induces the expression of both membrane-bound and soluble CEACAM1 and CEACAM6 in enterocytes especially at reoxygenation. This indicates an increased host response at these conditions which is consistent with the increased IL-8 levels at reoxygenation, since it was shown that the CEACAM1 expression induces IL-8 production [159], and thus correlates with the extend of fungal damage. However, it is unlikely that the inhibitory effect soluble CEACAM6 exerts to membrane-bound CEACAM1, shown by Klaile *et al.* 2017 [159], is responsible for the protective effect seen at hypoxic shock conditions as the protein level of both CEACAMs were comparable at this condition. The exact mechanisms mediating this oxygen-dependent expression difference remain to be determined. Furthermore, as this study did not perform a detailed

analysis of host receptors involved in the fungal recognition, PRRs cannot be excluded to contribute to the oxygen-dependent host response.

5.5. Conclusion

This study revealed a significant impact of oxygen on the *C. albicans*-enterocyte interaction: not ischemia but rather reoxygenation enhances enterocyte damage, *C. albicans* invasion, and translocation. These findings are consistent with recent *in vivo* studies [94,95]. Whereas reoxygenation renders the enterocytes highly susceptible to the fungal infection, the reduced oxygen supply during hypoxic shock led to protective effects regarding the barrier integrity of enterocytes and the reduced fungal translocation. These different infection outcomes are mediated by several factors from both the fungal and the host side. The increased ROS production, the low expression of HIF-1α, an enhanced fungal response *via* CEACAMs and the subsequent cytokine release, as well as the increased fungal growth and, thus, the increased invasion of *C. albicans* partly mediated by induced endocytosis contribute to the higher susceptibility of enterocytes at reoxygenation. HIF-1α does contribute to the protective effect seen at hypoxic shock independent of LL-37 production. The delayed fungal growth on enterocytes at low oxygen availabilities accounts for the reduced damage and translocation. This effect, however, is influenced by the host cell adaptation to oxygen *via* direct cell-cell-contact. Furthermore, the adaptation of *C. albicans* to hypoxia is essential for the host-fungus interaction. Although the detailed mechanisms remain to be elucidated, this study provides furthermore evidence that the early stages of the infection progression are crucial for the oxygen-dependent fate of enterocytes.

More general, the results obtained in this study furthermore emphasize that cultivation conditions can have a significant impact on host-pathogen interactions *in vitro*; mimicking physiological conditions, including oxygen supply, is an important factor in increasing translatability of *in vitro* results to the *in vivo* situation.

6. References

1. Bleuven C, Landry CR. Molecular and cellular bases of adaptation to a changing environment in microorganisms. *Proc Biol Sci* 2016; **283**(1841).

2. Carreau A, El Hafny-Rahbi B, Matejuk A, Grillon C, Kieda C. Why is the partial oxygen pressure of human tissues a crucial parameter? Small molecules and hypoxia. *J Cell Mol Med* 2011; **15**(6): 1239-53.

3. Grant MM, Kolamunne RT, Lock FE, Matthews JB, Chapple IL, Griffiths HR. Oxygen tension modulates the cytokine response of oral epithelium to periodontal bacteria. *J Clin Periodontol* 2010; **37**(12): 1039-48.

4. Shreiner AB, Kao JY, Young VB. The gut microbiome in health and in disease. *Curr Opin Gastroenterol* 2015; **31**(1): 69-75.

5. Lozupone CA, Stombaugh JI, Gordon JI, Jansson JK, Knight R. Diversity, stability and resilience of the human gut microbiota. *Nature* 2012; **489**(7415): 220-30.

6. Espey MG. Role of oxygen gradients in shaping redox relationships between the human intestine and its microbiota. *Free Radic Biol Med* 2013; **55**: 130-40.

7. Hoffmann C, Dollive S, Grunberg S, et al. Archaea and fungi of the human gut microbiome: correlations with diet and bacterial residents. *PLoS One* 2013; **8**(6): e66019.

8. Sam QH, Chang MW, Chai LY. The Fungal Mycobiome and Its Interaction with Gut Bacteria in the Host. *Int J Mol Sci* 2017; **18**(2).

9. Chabé M, Lokmer A, Ségurel L. Gut Protozoa: Friends or Foes of the Human Gut Microbiota? *Trends Parasitol* 2017; **33**(12): 925-34.

10. Dobell C. The Discovery of the Intestinal Protozoa of Man. *Proc R Soc Med* 1920; **13**(Sect Hist Med): 1-15.

11. Hallen-Adams HE, Suhr MJ. Fungi in the healthy human gastrointestinal tract. *Virulence* 2017; **8**(3): 352-8.

12. Cohen R, Roth FJ, Delgado E, Ahearn DG, Kalser MH. Fungal flora of the normal human small and large intestine. *N Engl J Med* 1969; **280**(12): 638-41.

13. Eggimann P, Garbino J, Pittet D. Epidemiology of *Candida* species infections in critically ill non-immunosuppressed patients. *Lancet Infect Dis* 2003; **3**(11): 685-702.

14. Polke M, Hube B, Jacobsen ID. *Candida* survival strategies. *Adv Appl Microbiol* 2015; **91**: 139-235.

15. Köhler JR, Hube B, Puccia R, Casadevall A, Perfect JR. Fungi that Infect Humans. *Microbiol Spectr* 2017; **5**(3).

16. Mavor AL, Thewes S, Hube B. Systemic fungal infections caused by *Candida* species: epidemiology, infection process and virulence attributes. *Curr Drug Targets* 2005; **6**(8): 863-74.

17. Odds FC. *Candida* infections: an overview. *Crit Rev Microbiol* 1987; **15**(1): 1-5.

18. Brown GD, Denning DW, Gow NA, Levitz SM, Netea MG, White TC. Hidden killers: human fungal infections. *Sci Transl Med* 2012; **4**(165): 165rv13.

19. Felix TC, de Brito Röder DVD, Dos Santos Pedroso R. Alternative and complementary therapies for vulvovaginal candidiasis. *Folia Microbiol (Praha)* 2018.

20. Akpan A, Morgan R. Oral candidiasis. *Postgrad Med J* 2002; **78**(922): 455-9.

21. Pasqualotto AC, Nedel WL, Machado TS, Severo LC. Risk factors and outcome for nosocomial breakthrough candidaemia. *J Infect* 2006; **52**(3): 216-22.

22. Williams DW, Jordan RP, Wei XQ, et al. Interactions of *Candida albicans* with host epithelial surfaces. *J Oral Microbiol* 2013; **5**.

23. Flevari A, Theodorakopoulou M, Velegraki A, Armaganidis A, Dimopoulos G. Treatment of invasive candidiasis in the elderly: a review. *Clin Interv Aging* 2013; **8**: 1199-208.

24. Pfaller MA, Diekema DJ. Epidemiology of invasive candidiasis: a persistent public health problem. *Clin Microbiol Rev* 2007; **20**(1): 133-63.

25. Soll DR, Galask R, Schmid J, Hanna C, Mac K, Morrow B. Genetic dissimilarity of commensal strains of *Candida* spp. carried in different anatomical locations of the same healthy women. *J Clin Microbiol* 1991; **29**(8): 1702-10.

26. Ghannoum MA, Jurevic RJ, Mukherjee PK, et al. Characterization of the oral fungal microbiome (mycobiome) in healthy individuals. *PLoS Pathog* 2010; **6**(1): e1000713.

27. Drell T, Lillsaar T, Tummeleht L, et al. Characterization of the vaginal micro- and mycobiome in asymptomatic reproductive-age Estonian women. *PLoS One* 2013; **8**(1): e54379.

28. Miranda LN, van der Heijden IM, Costa SF, et al. *Candida* colonisation as a source for candidaemia. *J Hosp Infect* 2009; **72**(1): 9-16.

29. Nucci M, Anaissie E. Revisiting the source of candidemia: skin or gut? *Clin Infect Dis* 2001; **33**(12): 1959-67.

30. Gouba N, Drancourt M. Digestive tract mycobiota: a source of infection. *Med Mal Infect* 2015; **45**(1-2): 9-16.

31. Koh AY, Köhler JR, Coggshall KT, Van Rooijen N, Pier GB. Mucosal damage and neutropenia are required for *Candida albicans* dissemination. *PLoS Pathog* 2008; **4**(2): e35.

32. Yan L, Yang C, Tang J. Disruption of the intestinal mucosal barrier in *Candida albicans* infections. *Microbiol Res* 2013; **168**(7): 389-95.

33. Pande K, Chen C, Noble SM. Passage through the mammalian gut triggers a phenotypic switch that promotes *Candida albicans* commensalism. *Nat Genet* 2013; **45**(9): 1088-91.

34. Miller MG, Johnson AD. White-opaque switching in *Candida albicans* is controlled by mating-type locus homeodomain proteins and allows efficient mating. *Cell* 2002; **110**(3): 293-302.

35. Sudbery P, Gow N, Berman J. The distinct morphogenic states of *Candida albicans*. *Trends Microbiol* 2004; **12**(7): 317-24.

36. Noble SM, Gianetti BA, Witchley JN. *Candida albicans* cell-type switching and functional plasticity in the mammalian host. *Nat Rev Microbiol* 2017; **15**(2): 96-108.

37. Tao L, Du H, Guan G, et al. Discovery of a "white-gray-opaque" tristable phenotypic switching system in *Candida albicans*: roles of non-genetic diversity in host adaptation. *PLoS Biol* 2014; **12**(4): e1001830.

38. Mayer FL, Wilson D, Hube B. *Candida albicans* pathogenicity mechanisms. *Virulence* 2013; **4**(2): 119-28.

39. Moyes DL, Wilson D, Richardson JP, et al. Candidalysin is a fungal peptide toxin critical for mucosal infection. *Nature* 2016; **532**(7597): 64-8.

40. Naglik JR, Moyes DL, Wächtler B, Hube B. *Candida albicans* interactions with epithelial cells and mucosal immunity. *Microbes Infect* 2011; **13**(12-13): 963-76.

41. Hall RA, Bates S, Lenardon MD, et al. The Mnn2 mannosyltransferase family modulates mannoprotein fibril length, immune recognition and virulence of *Candida albicans*. *PLoS Pathog* 2013; **9**(4): e1003276.

42. Buurman ET, Westwater C, Hube B, Brown AJ, Odds FC, Gow NA. Molecular analysis of CaMnt1p, a mannosyl transferase important for adhesion and virulence of *Candida albicans*. *Proc Natl Acad Sci U S A* 1998; **95**(13): 7670-5.

43. Bates S, Hall RA, Cheetham J, et al. Role of the *Candida albicans MNN1* gene family in cell wall structure and virulence. *BMC Res Notes* 2013; **6**: 294.

44. Sun JN, Solis NV, Phan QT, et al. Host cell invasion and virulence mediated by *Candida albicans* Ssa1. *PLoS Pathog* 2010; **6**(11): e1001181.

45. Brown AJ, Brown GD, Netea MG, Gow NA. Metabolism impacts upon *Candida* immunogenicity and pathogenicity at multiple levels. *Trends Microbiol* 2014; **22**(11): 614-22.

46. Lu Y, Su C, Solis NV, Filler SG, Liu H. Synergistic regulation of hyphal elongation by hypoxia, CO_2, and nutrient conditions controls the virulence of *Candida albicans*. *Cell Host Microbe* 2013; **14**(5): 499-509.

47. Grahl N, Shepardson KM, Chung D, Cramer RA. Hypoxia and fungal pathogenesis: to air or not to air? *Eukaryot Cell* 2012; **11**(5): 560-70.

48. Sellam A, van het Hoog M, Tebbji F, Beaurepaire C, Whiteway M, Nantel A. Modeling the transcriptional regulatory network that controls the early hypoxic response in *Candida albicans*. *Eukaryot Cell* 2014; **13**(5): 675-90.

49. Ernst JF, Tielker D. Responses to hypoxia in fungal pathogens. *Cell Microbiol* 2009; **11**(2): 183-90.

50. Chung D, Haas H, Cramer RA. Coordination of hypoxia adaptation and iron homeostasis in human pathogenic fungi. *Front Microbiol* 2012; **3**: 381.

51. Stoldt VR, Sonneborn A, Leuker CE, Ernst JF. Efg1p, an essential regulator of morphogenesis of the human pathogen *Candida albicans*, is a member of a conserved class of bHLH proteins regulating morphogenetic processes in fungi. *EMBO J* 1997; **16**(8): 1982-91.

52. Stichternoth C, Ernst JF. Hypoxic adaptation by Efg1 regulates biofilm formation by *Candida albicans*. *Appl Environ Microbiol* 2009; **75**(11): 3663-72.

53. Setiadi ER, Doedt T, Cottier F, Noffz C, Ernst JF. Transcriptional response of *Candida albicans* to hypoxia: linkage of oxygen sensing and Efg1p-regulatory networks. *J Mol Biol* 2006; **361**(3): 399-411.

54. Desai PR, van Wijlick L, Kurtz D, Juchimiuk M, Ernst JF. Hypoxia and Temperature Regulated Morphogenesis in *Candida albicans*. *PLoS Genet* 2015; **11**(8): e1005447.

55. Mulhern SM, Logue ME, Butler G. *Candida albicans* transcription factor Ace2 regulates metabolism and is required for filamentation in hypoxic conditions. *Eukaryot Cell* 2006; **5**(12): 2001-13.

56. Yang H, Tong J, Lee CW, Ha S, Eom SH, Im YJ. Structural mechanism of ergosterol regulation by fungal sterol transcription factor Upc2. *Nat Commun* 2015; **6**: 6129.

57. Synnott JM, Guida A, Mulhern-Haughey S, Higgins DG, Butler G. Regulation of the hypoxic response in *Candida albicans*. *Eukaryot Cell* 2010; **9**(11): 1734-46.

58. Bonhomme J, Chauvel M, Goyard S, Roux P, Rossignol T, d'Enfert C. Contribution of the glycolytic flux and hypoxia adaptation to efficient biofilm formation by *Candida albicans*. *Mol Microbiol* 2011; **80**(4): 995-1013.

59. Askew C, Sellam A, Epp E, et al. Transcriptional regulation of carbohydrate metabolism in the human pathogen *Candida albicans*. *PLoS Pathog* 2009; **5**(10): e1000612.

60. Pérez JC, Kumamoto CA, Johnson AD. *Candida albicans* commensalism and pathogenicity are intertwined traits directed by a tightly knit transcriptional regulatory circuit. *PLoS Biol* 2013; **11**(3): e1001510.

61. Thursby E, Juge N. Introduction to the human gut microbiota. *Biochem J* 2017; **474**(11): 1823-36.

62. Peterson LW, Artis D. Intestinal epithelial cells: regulators of barrier function and immune homeostasis. *Nat Rev Immunol* 2014; **14**(3): 141-53.

63. Wang B, Yao M, Lv L, Ling Z, Li L. The Human Microbiota in Health and Disease. *Engineering* 2017; **3**: 71-82.

64. PubMedHealth. Lower Gastrointestinal Tract. May 17 2018. https://www.ncbi.nlm.nih.gov/pubmedhealth/PMHT0022856/.

65. Rao JN, Wang JY. Regulation of Gastrointestinal Mucosal Growth. San Rafael (CA); 2010.

66. Vaupel P, Schaible H-G, Mutschler E. Anatomie, Physiologie und Pathophysiologie des Menschen: wissenschaftliche Verlagsgesellschaft Stuttgart; 2007.

67. Eastwood GL. Gastrointestinal epithelial renewal. *Gastroenterology* 1977; **72**(5 Pt 1): 962-75.

68. Van Leeuwen PA, Boermeester MA, Houdijk AP, et al. Clinical significance of translocation. *Gut* 1994; **35**(1 Suppl): S28-34.

69. AJCC AJCoC-. Colon and Rectum Cancer Staging 7th Edition. 2009. https://cancerstaging.org/references-tools/quickreferences/Documents/ ColonMedium.pdf.

70. Umar S. Intestinal stem cells. *Curr Gastroenterol Rep* 2010; **12**(5): 340-8.

71. van der Flier LG, Clevers H. Stem cells, self-renewal, and differentiation in the intestinal epithelium. *Annu Rev Physiol* 2009; **71**: 241-60.

72. Yeung TM, Chia LA, Kosinski CM, Kuo CJ. Regulation of self-renewal and differentiation by the intestinal stem cell niche. *Cell Mol Life Sci* 2011; **68**(15): 2513-23.

73. Clevers H. The intestinal crypt, a prototype stem cell compartment. *Cell* 2013; **154**(2): 274-84.

74. Muniz LR, Knosp C, Yeretssian G. Intestinal antimicrobial peptides during homeostasis, infection, and disease. *Front Immunol* 2012; **3**: 310.

75. Ostaff MJ, Stange EF, Wehkamp J. Antimicrobial peptides and gut microbiota in homeostasis and pathology. *EMBO Mol Med* 2013; **5**(10): 1465-83.

76. Okumura R, Takeda K. Roles of intestinal epithelial cells in the maintenance of gut homeostasis. *Exp Mol Med* 2017; **49**(5): e338.

77. Mitic LL, Van Itallie CM, Anderson JM. Molecular physiology and pathophysiology of tight junctions I. Tight junction structure and function: lessons from mutant animals and proteins. *Am J Physiol Gastrointest Liver Physiol* 2000; **279**(2): G250-4.

78. Capaldo CT, Powell DN, Kalman D. Layered defense: how mucus and tight junctions seal the intestinal barrier. *J Mol Med (Berl)* 2017; **95**(9): 927-34.

79. Niessen CM. Tight junctions/adherens junctions: basic structure and function. *J Invest Dermatol* 2007; **127**(11): 2525-32.

80. Chiba H, Osanai M, Murata M, Kojima T, Sawada N. Transmembrane proteins of tight junctions. *Biochim Biophys Acta* 2008; **1778**(3): 588-600.

81. Mowat AM, Viney JL. The anatomical basis of intestinal immunity. *Immunol Rev* 1997; **156**: 145-66.

82. Thompson CG, Gay CL, Kashuba ADM. HIV Persistence in Gut-Associated Lymphoid Tissues: Pharmacological Challenges and Opportunities. *AIDS Res Hum Retroviruses* 2017; **33**(6): 513-23.

83. Nakamura Y, Kimura S, Hase K. M cell-dependent antigen uptake on follicle-associated epithelium for mucosal immune surveillance. *Inflamm Regen* 2018; **38**: 15.

84. Colgan SP, Taylor CT. Hypoxia: an alarm signal during intestinal inflammation. *Nat Rev Gastroenterol Hepatol* 2010; **7**(5): 281-7.

85. Zeitouni NE, Chotikatum S, von Köckritz-Blickwede M, Naim HY. The impact of hypoxia on intestinal epithelial cell functions: consequences for invasion by bacterial pathogens. *Mol Cell Pediatr* 2016; **3**(1): 14.

86. Zheng L, Kelly CJ, Colgan SP. Physiologic hypoxia and oxygen homeostasis in the healthy intestine. A Review in the Theme: Cellular Responses to Hypoxia. *Am J Physiol Cell Physiol* 2015; **309**(6): C350-60.

87. Glover LE, Lee JS, Colgan SP. Oxygen metabolism and barrier regulation in the intestinal mucosa. *J Clin Invest* 2016; **126**(10): 3680-8.

88. Ward JB, Keely SJ, Keely SJ. Oxygen in the regulation of intestinal epithelial transport. *J Physiol* 2014; **592**(12): 2473-89.

89. Colgan SP, Campbell EL, Kominsky DJ. Hypoxia and Mucosal Inflammation. *Annu Rev Pathol* 2016; **11**: 77-100.

90. Grootjans J, Lenaerts K, Buurman WA, Dejong CH, Derikx JP. Life and death at the mucosal-luminal interface: New perspectives on human intestinal ischemia-reperfusion. *World J Gastroenterol* 2016; **22**(9): 2760-70.

91. Valparaiso AP, Vicente DA, Bograd BA, Elster EA, Davis TA. Modeling acute traumatic injury. *J Surg Res* 2015; **194**(1): 220-32.

92. Collard CD, Gelman S. Pathophysiology, clinical manifestations, and prevention of ischemia-reperfusion injury. *Anesthesiology* 2001; **94**(6): 1133-8.

93. Grootjans J, Lenaerts K, Derikx JP, et al. Human intestinal ischemia-reperfusion-induced inflammation characterized: experiences from a new translational model. *Am J Pathol* 2010; **176**(5): 2283-91.

94. Kalogeris T, Baines CP, Krenz M, Korthuis RJ. Ischemia/Reperfusion. *Compr Physiol* 2016; **7**(1): 113-70.

95. Tassopoulos A, Chalkias A, Papalois A, Iacovidou N, Xanthos T. The effect of antioxidant supplementation on bacterial translocation after intestinal ischemia and reperfusion. *Redox Rep* 2017; **22**(1): 1-9.

96. Cuzzocrea S, Riley DP, Caputi AP, Salvemini D. Antioxidant therapy: a new pharmacological approach in shock, inflammation, and ischemia/reperfusion injury. *Pharmacol Rev* 2001; **53**(1): 135-59.

97. Nilsson UA, Lundgren O, Haglind E, Bylund-Fellenius AC. Radical production during *in vivo* intestinal ischemia and reperfusion in the cat. *Am J Physiol* 1989; **257**(3 Pt 1): G409-14.

98. Sasaki M, Joh T. Oxidative stress and ischemia-reperfusion injury in gastrointestinal tract and antioxidant, protective agents. *J Clin Biochem Nutr* 2007; **40**(1): 1-12.

99. Riedemann NC, Ward PA. Complement in ischemia reperfusion injury. *Am J Pathol* 2003; **162**(2): 363-7.

100. Ziello JE, Jovin IS, Huang Y. Hypoxia-Inducible Factor (HIF)-1 regulatory pathway and its potential for therapeutic intervention in malignancy and ischemia. *Yale J Biol Med* 2007; **80**(2): 51-60.

101. Chen S, Sang N. Hypoxia-Inducible Factor-1: A Critical Player in the Survival Strategy of Stressed Cells. *J Cell Biochem* 2016; **117**(2): 267-78.

102. Semenza GL. Targeting HIF-1 for cancer therapy. *Nat Rev Cancer* 2003; **3**(10): 721-32.

103. Masoud GN, Li W. HIF-1alpha pathway: role, regulation and intervention for cancer therapy. *Acta Pharm Sin B* 2015; **5**(5): 378-89.

104. Nizet V, Johnson RS. Interdependence of hypoxic and innate immune responses. *Nat Rev Immunol* 2009; **9**(9): 609-17.

105. Semenza G. Signal transduction to hypoxia-inducible factor 1. *Biochem Pharmacol* 2002; **64**(5-6): 993-8.

106. Ke Q, Costa M. Hypoxia-inducible factor-1 (HIF-1). *Mol Pharmacol* 2006; **70**(5): 1469-80.

107. Friedrich D, Fecher RA, Rupp J, Deepe GS, Jr. Impact of HIF-1alpha and hypoxia on fungal growth characteristics and fungal immunity. *Microbes Infect* 2017; **19**(3): 204-9.

108. Fliesser M, Morton CO, Bonin M, et al. Hypoxia-inducible factor 1alpha modulates metabolic activity and cytokine release in anti-*Aspergillus fumigatus* immune responses initiated by human dendritic cells. *Int J Med Microbiol* 2015; **305**(8): 865-73.

109. Fan D, Coughlin LA, Neubauer MM, et al. Activation of HIF-1alpha and LL-37 by commensal bacteria inhibits *Candida albicans* colonization. *Nat Med* 2015; **21**(7): 808-14.

110. Shepardson KM, Jhingran A, Caffrey A, et al. Myeloid derived hypoxia inducible factor 1-alpha is required for protection against pulmonary *Aspergillus fumigatus* infection. *PLoS Pathog* 2014; **10**(9): e1004378.

111. Böhm L, Torsin S, Tint SH, Eckstein MT, Ludwig T, Pérez JC. The yeast form of the fungus *Candida albicans* promotes persistence in the gut of gnotobiotic mice. *PLoS Pathog* 2017; **13**(10): e1006699.

112. Hiller E, Zavrel M, Hauser N, et al. Adaptation, adhesion and invasion during interaction of *Candida albicans* with the host - Focus on the function of cell wall proteins. *Int J Med Microbiol* 2011; **301**(5): 384-9.

113. Moyes DL, Richardson JP, Naglik JR. *Candida albicans*-epithelial interactions and pathogenicity mechanisms: scratching the surface. *Virulence* 2015; **6**(4): 338-46.

114. Naglik JR, Moyes D. Epithelial cell innate response to *Candida albicans*. *Adv Dent Res* 2011; **23**(1): 50-5.

115. Dalle F, Wächtler B, L'Ollivier C, et al. Cellular interactions of *Candida albicans* with human oral epithelial cells and enterocytes. *Cell Microbiol* 2010; **12**(2): 248-71.

116. Phan QT, Myers CL, Fu Y, et al. Als3 is a *Candida albicans* invasin that binds to cadherins and induces endocytosis by host cells. *PLoS Biol* 2007; **5**(3): e64.

117. Tong Y, Tang J. *Candida albicans* infection and intestinal immunity. *Microbiol Res* 2017; **198**: 27-35.

118. Yang W, Yan L, Wu C, Zhao X, Tang J. Fungal invasion of epithelial cells. *Microbiol Res* 2014; **169**(11): 803-10.

119. da Silva Dantas A, Lee KK, Raziunaite I, et al. Cell biology of *Candida albicans*-host interactions. *Curr Opin Microbiol* 2016; **34**: 111-8.

120. Allert S, Förster TM, Svensson CM, et al. *Candida albicans*-Induced Epithelial Damage Mediates Translocation through Intestinal Barriers. *MBio* 2018; **9**(3).

121. Goyer M, Loiselet A, Bon F, et al. Intestinal Cell Tight Junctions Limit Invasion of *Candida albicans* through Active Penetration and Endocytosis in the Early Stages of the Interaction of the Fungus with the Intestinal Barrier. *PLoS One* 2016; **11**(3): e0149159.

122. Böhringer M, Pohlers S, Schulze S, et al. *Candida albicans* infection leads to barrier breakdown and a MAPK/NF-kappaB mediated stress response in the intestinal epithelial cell line C2BBe1. *Cell Microbiol* 2016; **18**(7): 889-904.

123. Yan L, Wu CR, Wang C, Yang CH, Tong GZ, Tang JG. Effect of *Candida albicans* on Intestinal Ischemia-reperfusion Injury in Rats. *Chin Med J (Engl)* 2016; **129**(14): 1711-8.

124. Gillum AM, Tsay EY, Kirsch DR. Isolation of the *Candida albicans* gene for orotidine-5'-phosphate decarboxylase by complementation of *S. cerevisiae* ura3 and *E. coli* pyrF mutations. *Mol Gen Genet* 1984; **198**(2): 179-82.

125. Fonzi WA, Irwin MY. Isogenic strain construction and gene mapping in *Candida albicans*. *Genetics* 1993; **134**(3): 717-28.

126. Homann OR, Dea J, Noble SM, Johnson AD. A phenotypic profile of the *Candida albicans* regulatory network. *PLoS Genet* 2009; **5**(12): e1000783.

127. Noble SM, Johnson AD. Strains and strategies for large-scale gene deletion studies of the diploid human fungal pathogen *Candida albicans*. *Eukaryot Cell* 2005; **4**(2): 298-309.

128. Li XS, Sun JN, Okamoto-Shibayama K, Edgerton M. *Candida albicans* cell wall ssa proteins bind and facilitate import of salivary histatin 5 required for toxicity. *J Biol Chem* 2006; **281**(32): 22453-63.

129. Inc. TFS. Technical resources - Media Formulations 41965 - DMEM, high glucose. 2018. http://www.thermofisher.com/de/de/home/technical-resources/media-formulation.170.html.

130. Inc. TFS. Technical resources - Media Formulations 31053 - DMEM, high glucose, no glutamine, no phenol red. 2018. http://www.thermofisher.com/de/de/home/technical-resources/media-formulation.42.html.

131. Rousset M. The human colon carcinoma cell lines HT-29 and Caco-2: two *in vitro* models for the study of intestinal differentiation. *Biochimie* 1986; **68**(9): 1035-40.

132. Pinto M, Robin-Leon, S., Appay, M.D., Kedinger, M., Triadou, N., Dussaulx, E., Lacroix, B., Simon-Assman, P., Haffen, K., Fogh, J., Zweibaum, A. Enterocyte-like differentiation and polarization of the human-colon carcinoma cell-line Caco-2 in culture. *Biology of the Cell* 1983; **47**: 323 - 30.

133. Peterson MD, Mooseker MS. Characterization of the enterocyte-like brush border cytoskeleton of the C2BBe clones of the human intestinal cell line, Caco-2. *J Cell Sci* 1992; **102 (Pt 3)**: 581-600.

134. Sambuy Y, De Angelis I, Ranaldi G, Scarino ML, Stammati A, Zucco F. The Caco-2 cell line as a model of the intestinal barrier: influence of cell and culture-related factors on Caco-2 cell functional characteristics. *Cell Biol Toxicol* 2005; **21**(1): 1-26.

135. Pegg DE. Principles of cryopreservation. *Methods Mol Biol* 2007; **368**: 39-57.

136. Valvona CJ, Fillmore HL, Nunn PB, Pilkington GJ. The Regulation and Function of Lactate Dehydrogenase A: Therapeutic Potential in Brain Tumor. *Brain Pathol* 2016; **26**(1): 3-17.

137. Jacobs E, Hissin PJ, Propper W, Mayer L, Sarkozi L. Stability of lactate dehydrogenase at different storage temperatures. *Clin Biochem* 1986; **19**(3): 183-8.

138. Decker T, Lohmann-Matthes ML. A quick and simple method for the quantitation of lactate dehydrogenase release in measurements of cellular cytotoxicity and tumor necrosis factor (TNF) activity. *J Immunol Methods* 1988; **115**(1): 61-9.

139. Martin A, Clynes M. Comparison of 5 microplate colorimetric assays for in vitro cytotoxicity testing and cell proliferation assays. *Cytotechnology* 1993; **11**(1): 49-58.

140. Cooper JA. Effects of cytochalasin and phalloidin on actin. *J Cell Biol* 1987; **105**(4): 1473-8.

141. Bradski G. The OpenCV Library. *Dr Dobb's Journal: Software Tools for the Professional Programmer* 2000; **25**(11): 4.

142. Jones E, Oliphant, E., Peterson, P. SciPy: Open Source Scientific Tools for Python. 2001. http://www.scipy.org/

143. Farhan M, Yli-Harja, O., Niemistö, A. A novel method for splitting clumps of convex objects incorporating image intensity and using rectangular window-based concavity point-pair search. *Pattern Recognition* 2013; **46**(3): 11.

144. Brandes S, Dietrich S, Hünniger K, Kurzai O, Figge MT. Migration and interaction tracking for quantitative analysis of phagocyte-pathogen confrontation assays. *Med Image Anal* 2017; **36**: 172-83.

145. Kitamura K, Kaneko T, Yamamoto Y. Lysis of viable yeast cells by enzymes of *Arthrobacter luteus*. *Arch Biochem Biophys* 1971; **145**(1): 402-4.

146. Jung HC, Eckmann L, Yang SK, et al. A distinct array of proinflammatory cytokines is expressed in human colon epithelial cells in response to bacterial invasion. *J Clin Invest* 1995; **95**(1): 55-65.

147. Angrisano T, Pero R, Peluso S, et al. LPS-induced IL-8 activation in human intestinal epithelial cells is accompanied by specific histone H3 acetylation and methylation changes. *BMC Microbiol* 2010; **10**: 172.

148. Rodríguez-Cerdeira C, Lopez-Bárcenas A, Sánchez-Blanco B, Arenas R. The role of IL-33 in host response to *Candida albicans*. *ScientificWorldJournal* 2014; **2014**: 340690.

149. Shirota K, LeDuy L, Yuan SY, Jothy S. Interleukin-6 and its receptor are expressed in human intestinal epithelial cells. *Virchows Arch B Cell Pathol Incl Mol Pathol* 1990; **58**(4): 303-8.

150. Tsai PW, Cheng YL, Hsieh WP, Lan CY. Responses of *Candida albicans* to the human antimicrobial peptide LL-37. *J Microbiol* 2014; **52**(7): 581-9.

151. Tsai PW, Yang CY, Chang HT, Lan CY. Human antimicrobial peptide LL-37 inhibits adhesion of *Candida albicans* by interacting with yeast cell-wall carbohydrates. *PLoS One* 2011; **6**(3): e17755.

152. Zweier JL, Flaherty JT, Weisfeldt ML. Direct measurement of free radical generation following reperfusion of ischemic myocardium. *Proc Natl Acad Sci U S A* 1987; **84**(5): 1404-7.

153. Frohner IE, Bourgeois C, Yatsyk K, Majer O, Kuchler K. *Candida albicans* cell surface superoxide dismutases degrade host-derived reactive oxygen species to escape innate immune surveillance. *Mol Microbiol* 2009; **71**(1): 240-52.

154. Fradin C, De Groot P, MacCallum D, et al. Granulocytes govern the transcriptional response, morphology and proliferation of *Candida albicans* in human blood. *Mol Microbiol* 2005; **56**(2): 397-415.

155. Richard ML, Plaine A. Comprehensive analysis of glycosylphosphatidylinositol-anchored proteins in *Candida albicans*. *Eukaryot Cell* 2007; **6**(2): 119-33.

156. Elks PM, Brizee S, van der Vaart M, et al. Hypoxia inducible factor signaling modulates susceptibility to mycobacterial infection *via* a nitric oxide dependent mechanism. *PLoS Pathog* 2013; **9**(12): e1003789.

157. Koury J, Deitch EA, Homma H, et al. Persistent HIF-1alpha activation in gut ischemia/reperfusion injury: potential role of bacteria and lipopolysaccharide. *Shock* 2004; **22**(3): 270-7.

158. Peyssonnaux C, Datta V, Cramer T, et al. HIF-1alpha expression regulates the bactericidal capacity of phagocytes. *J Clin Invest* 2005; **115**(7): 1806-15.

159. Klaile E, Müller MM, Schäfer MR, et al. Binding of *Candida albicans* to Human CEACAM1 and CEACAM6 Modulates the Inflammatory Response of Intestinal Epithelial Cells. *MBio* 2017; **8**(2).

160. Kasper L, Miramón P, Jablonowski N, et al. Antifungal activity of clotrimazole against *Candida albicans* depends on carbon sources, growth phase and morphology. *J Med Microbiol* 2015; **64**(7): 714-23.

161. Noverr MC, Huffnagle GB. Regulation of *Candida albicans* morphogenesis by fatty acid metabolites. *Infect Immun* 2004; **72**(11): 6206-10.

162. Sabina J, Brown V. Glucose sensing network in *Candida albicans*: a sweet spot for fungal morphogenesis. *Eukaryot Cell* 2009; **8**(9): 1314-20.

163. Collange O, Charles AL, Lavaux T, et al. Compartmentalization of Inflammatory Response Following Gut Ischemia Reperfusion. *Eur J Vasc Endovasc Surg* 2015; **49**(1): 60-5.

164. Li Y, Xu B, Xu M, et al. 6-Gingerol protects intestinal barrier from ischemia/reperfusion-induced damage *via* inhibition of p38 MAPK to NF-kappaB signalling. *Pharmacol Res* 2017; **119**: 137-48.

165. Hsiao JK, Huang CY, Lu YZ, Yang CY, Yu LC. Magnetic resonance imaging detects intestinal barrier dysfunction in a rat model of acute mesenteric ischemia/reperfusion injury. *Invest Radiol* 2009; **44**(6): 329-35.

166. Huang CY, Hsiao JK, Lu YZ, Lee TC, Yu LC. Anti-apoptotic PI3K/Akt signaling by sodium/glucose transporter 1 reduces epithelial barrier damage and bacterial translocation in intestinal ischemia. *Lab Invest* 2011; **91**(2): 294-309.

167. He D, Sougioultzis S, Hagen S, et al. *Clostridium difficile* toxin A triggers human colonocyte IL-8 release *via* mitochondrial oxygen radical generation. *Gastroenterology* 2002; **122**(4): 1048-57.

168. Lakshminarayanan V, Beno DW, Costa RH, Roebuck KA. Differential regulation of interleukin-8 and intercellular adhesion molecule-1 by H_2O_2 and tumor necrosis factor-alpha in endothelial and epithelial cells. *J Biol Chem* 1997; **272**(52): 32910-8.

169. Gunasekaran U, Yang R, Gunasekaran M. Regulation of superoxide dismutase synthesis in *Candida albicans*. *Mycopathologia* 1998; **141**(2): 59-63.

170. Martchenko M, Alarco AM, Harcus D, Whiteway M. Superoxide dismutases in *Candida albicans*: transcriptional regulation and functional characterization of the hyphal-induced SOD5 gene. *Mol Biol Cell* 2004; **15**(2): 456-67.

171. Blikslager AT, Moeser AJ, Gookin JL, Jones SL, Odle J. Restoration of barrier function in injured intestinal mucosa. *Physiol Rev* 2007; **87**(2): 545-64.

172. Derikx JP, Matthijsen RA, de Bruïne AP, et al. Rapid reversal of human intestinal ischemia-reperfusion induced damage by shedding of injured enterocytes and reepithelialisation. *PLoS One* 2008; **3**(10): e3428.

173. Villar CC, Kashleva H, Nobile CJ, Mitchell AP, Dongari-Bagtzoglou A. Mucosal tissue invasion by *Candida albicans* is associated with E-cadherin degradation, mediated by transcription factor Rim101p and protease Sap5p. *Infect Immun* 2007; **75**(5): 2126-35.

174. Bücker R, Krug SM, Rosenthal R, et al. Aerolysin from *Aeromonas hydrophila* perturbs tight junction integrity and cell lesion repair in intestinal epithelial HT-29/B6 cells. *J Infect Dis* 2011; **204**(8): 1283-92.

175. Sumitomo T, Nakata M, Higashino M, et al. Streptolysin S contributes to group A streptococcal translocation across an epithelial barrier. *J Biol Chem* 2011; **286**(4): 2750-61.

176. Chun J, Prince A. TLR2-induced calpain cleavage of epithelial junctional proteins facilitates leukocyte transmigration. *Cell Host Microbe* 2009; **5**(1): 47-58.

177. Ellinghaus P, Heisler I, Unterschemmann K, et al. BAY 87-2243, a highly potent and selective inhibitor of hypoxia-induced gene activation has antitumor activities by inhibition of mitochondrial complex I. *Cancer Med* 2013; **2**(5): 611-24.

178. Lopez-Garcia B, Lee PH, Yamasaki K, Gallo RL. Anti-fungal activity of cathelicidins and their potential role in *Candida albicans* skin infection. *J Invest Dermatol* 2005; **125**(1): 108-15.

179. Eini A, Sol A, Coppenhagen-Glazer S, Skvirsky Y, Zini A, Bachrach G. Oxygen deprivation affects the antimicrobial action of LL-37 as determined by microplate real-time kinetic measurements under anaerobic conditions. *Anaerobe* 2013; **22**: 20-4.

180. Nickel D, Busch M, Mayer D, Hagemann B, Knoll V, Stenger S. Hypoxia triggers the expression of human beta defensin 2 and antimicrobial activity against *Mycobacterium tuberculosis* in human macrophages. *J Immunol* 2012; **188**(8): 4001-7.

181. Schroeder BO, Wu Z, Nuding S, et al. Reduction of disulphide bonds unmasks potent antimicrobial activity of human beta-defensin 1. *Nature* 2011; **469**(7330): 419-23.

182. Moyes DL, Shen C, Murciano C, et al. Protection against epithelial damage during *Candida albicans* infection is mediated by PI3K/Akt and mammalian target of rapamycin signaling. *J Infect Dis* 2014; **209**(11): 1816-26.

183. Cheng SC, Quintin J, Cramer RA, et al. mTOR- and HIF-1alpha-mediated aerobic glycolysis as metabolic basis for trained immunity. *Science* 2014; **345**(6204): 1250684.

184. Braverman J, Sogi KM, Benjamin D, Nomura DK, Stanley SA. HIF-1alpha Is an Essential Mediator of IFN-gamma-Dependent Immunity to *Mycobacterium tuberculosis*. *J Immunol* 2016; **197**(4): 1287-97.

185. Lall R, Ganapathy S, Yang M, et al. Low-dose radiation exposure induces a HIF-1-mediated adaptive and protective metabolic response. *Cell Death Differ* 2014; **21**(5): 836-44.

186. Gauglitz GG, Callenberg H, Weindl G, Korting HC. Host defence against *Candida albicans* and the role of pattern-recognition receptors. *Acta Derm Venereol* 2012; **92**(3): 291-8.

187. Zheng NX, Wang Y, Hu DD, Yan L, Jiang YY. The role of pattern recognition receptors in the innate recognition of *Candida albicans*. *Virulence* 2015; **6**(4): 347-61.

188. Moyes DL, Runglall M, Murciano C, et al. A biphasic innate immune MAPK response discriminates between the yeast and hyphal forms of *Candida albicans* in epithelial cells. *Cell Host Microbe* 2010; **8**(3): 225-35.

7. List of Abbreviations

A.	*Aspergillus*
AB 30 %	acrylamide/bisacrylamide 30 %
Als	agglutinin-like sequence protein
AMP	antimicrobial peptide
ANOVA	analysis of variance
APS	ammonium persulfate
ATCC	American Type Culture Collection
BCA	bicinchoninic acid
BSA	bovine serum albumin
C.	*Candida*
CEACAM	carcinoembryonic antigen-related cell adhesion molecule
CFUs	colony forming units
CGB	collection gel buffer
CLR	C-type lectin receptor
$CoCl_2$	Cobalt(II) chloride
DCF	2'7'-dichlorofluorescein
DCFDA	2'7'-dichlorofluorescein diacetate
ddH_2O	bis-distilled water
DMEM	Dulbeccos Modified Eagle's Medium
DMSO	dimethyl sulfoxide
DSMZ	Deutsche Sammlung von Mikroorganismen und Zellkulturen
ELISA	enzyme-linked immunosorbent assay
FCS	fetal calf serum
GALT	gut associated lymphoid tissue
GIT	gastrointestinal tract
GM-CSF	granulocyte-macrophage colony-stimulating factor
GSH	glutathione
HIF	hypoxia-inducible factor
HRE	hypoxic responsible elements

HRP	horseradish peroxidase
Hsp70	heat shock protein 70
Hwp1	hyphal wall protein 1
IEC	intestinal epithelial cell
IESC	intestinal epithelial stem cell
IL	interleukin
INT	iodotetrazolium chloride
IR	ischemia-reperfusion
kDa	kilodalton
LDH	lactate dehydrogenase
LPS	lipopolysaccharide
M	molar
MCP-1	monocyte chemoattractant protein-1
mM	millimolar
µm	micrometer
M cells	microfold cells
MAPK	mitogen-activated protein kinase
nm	nanometer
nM	nanomolar
OD	optical density
PAMP	pathogen-associated molecular pattern
PBS	phosphate buffered saline
PBST	PBS supplemented with 0.01 % Tween20
p.i.	post infection
PI3K	phospatidylinositide-3-kinase
PHD	prolyl hydroxylase
PRR	pattern recognition receptor
PVDF	polyvinylidenfluorid
RITC	Rhodamine B isothiocyanate
ROS	reactive oxygen species
rpm	revolutions per minute
RT	room temperature

Sap	secreted aspartyl protease
SD	standard deviation
SDS	sodium dodecyl sulfate
SDS-PAGE	sodium dodecyl sulfate polyacrylamide gel electrophoresis
SGB	separation gel buffer
sIgA	secreted Immunoglobulin A
SLB	sample lysis buffer
Sod	superoxide dismutase
SREBP	sterol regulatory element-binding protein
Suppl.	Supplementary
TBHP	tert-butyl hydrogen peroxide
TBST	Tris-buffered saline supplemented with Tween20
TEER	transepithelial electrical resistance
TEMED	N,N,N',N'-tetramethylethylendiamine
TLR	Toll-like receptor
TNFα	tumor necrosis factor α
VHL	von Hippel Lindau protein
v/v	volume per volume
VVC	vulvovaginal candidiasis
WR	Working Reagent
wt	wild-type
w/w	weight per weight
YPD	yeast peptone dextrose

8. Appendix

8.1. Supplementary Figures

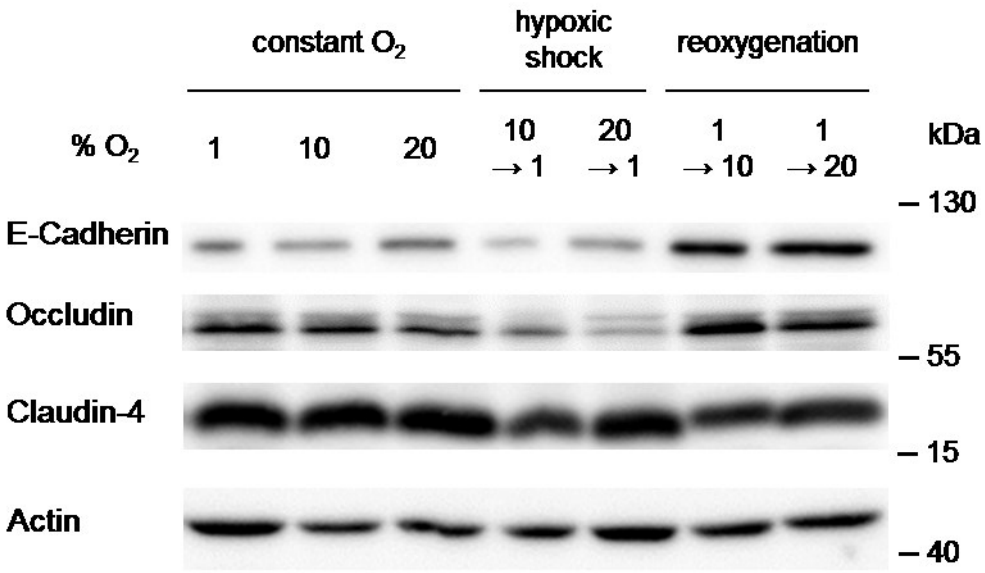

Suppl. Figure 1: Western Blot analysis of the expression of cell junction proteins. The protein expression of the tight junction (Claudin-4, Occludin) and the adherens junction (E-Cadherin) proteins was determined from seven days old C2BBe1 cells *via* Western Blot using whole cell lysates in RIPA lysis buffer. 12.5 % acrylamide separation gels were used for the detection of Occludin and Claudin-4 and 10 % acrylamide separation gels were used to detect E-Cadherin. 15 µg protein per sample were used. Western Blots shown are representative for three individual experiments.

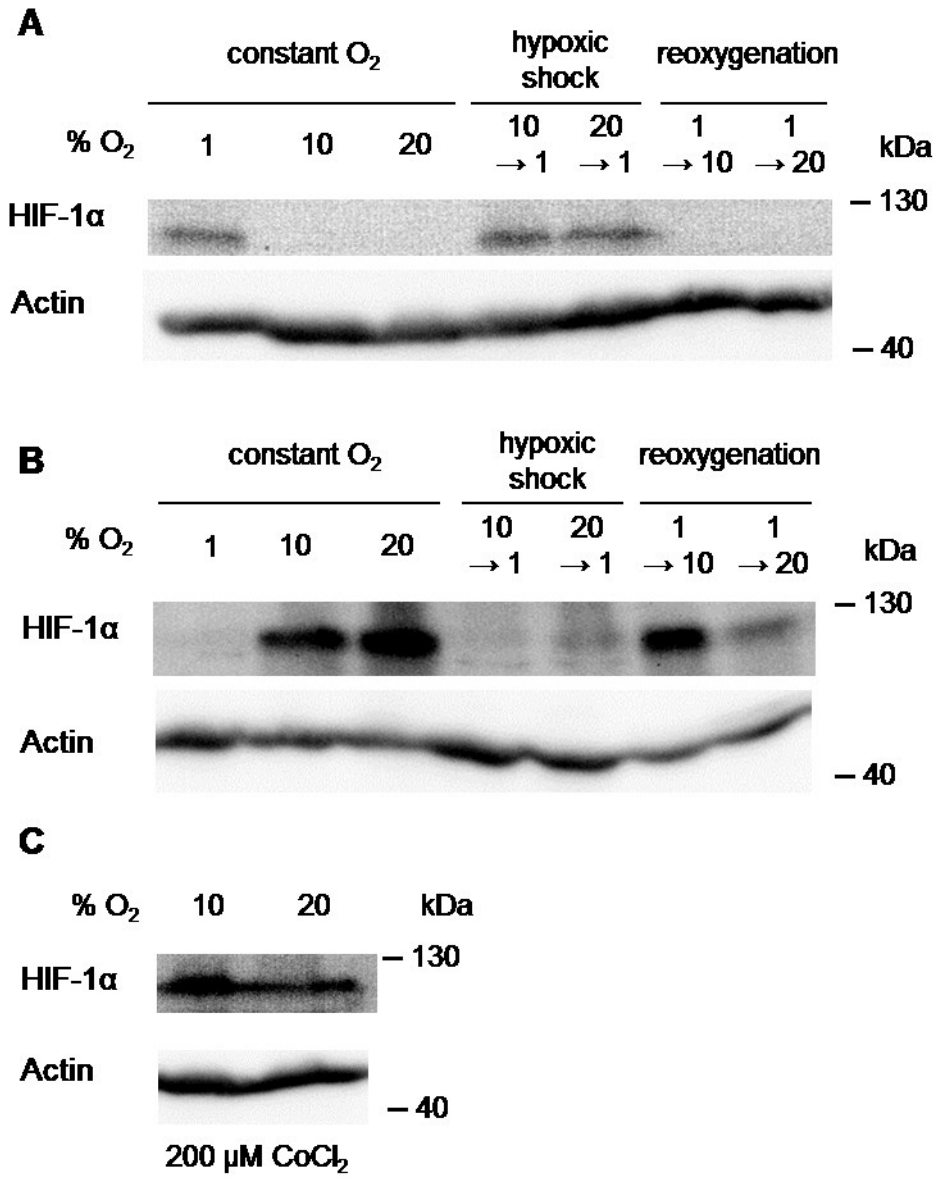

Suppl. Figure 2: Western Blot analysis of the HIF-1α expression. The protein expression of HIF-1α was determined from seven days old **(A)** mock-infected, **(B)** *C. albicans*-infected and **(C)** mock-infected enterocytes treated with 200 µM $CoCl_2$ (positive control). 15 µl of whole cell lysates in 1x SLB and 7.5 % acrylamide separation gels were used for the detection of HIF-1α protein bands *via* Western Blot. Western Blots shown are representative for three individual experiments.

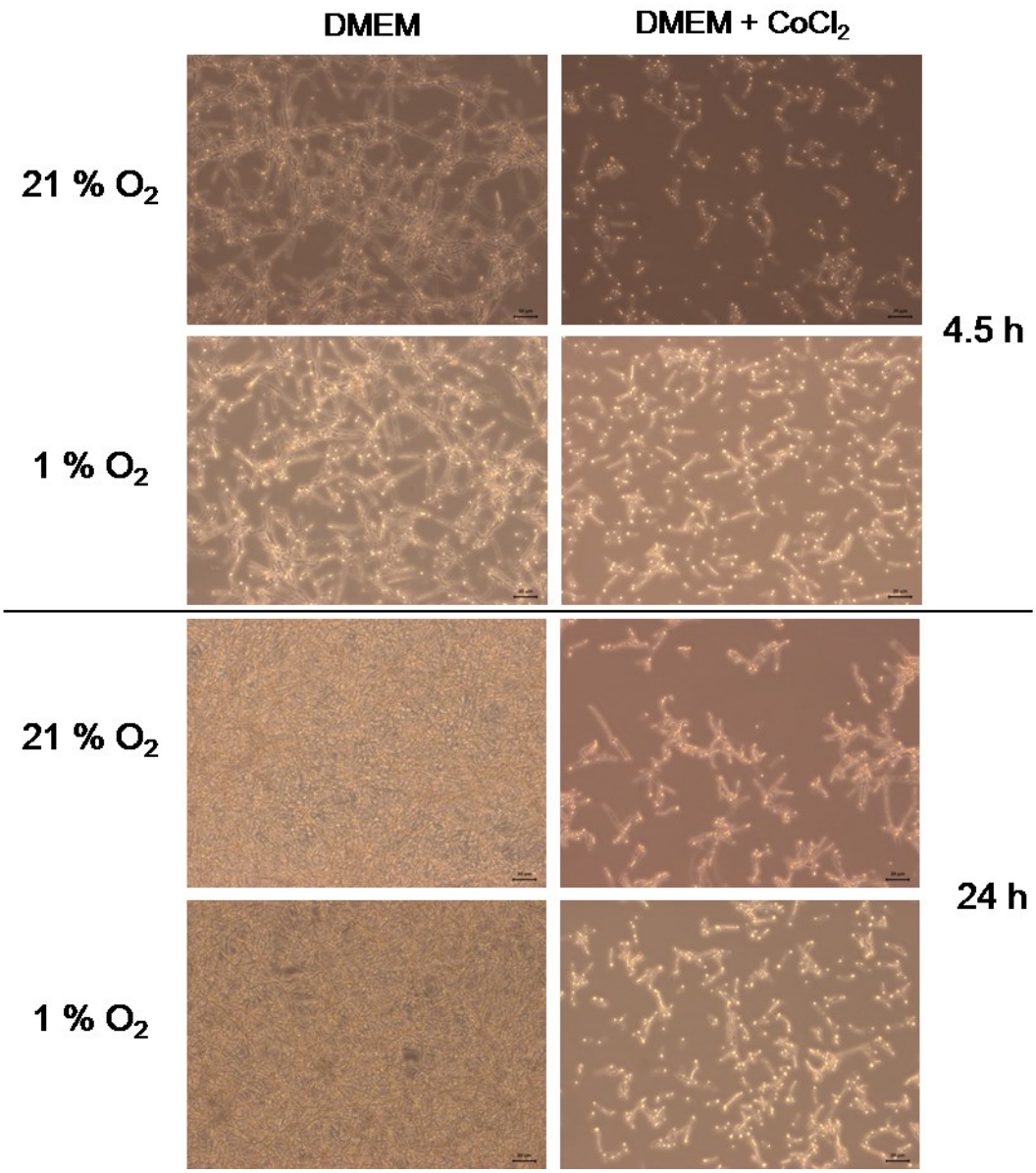

Suppl. Figure 3: The treatment of *C. albicans* with $CoCl_2$ inhibits filamentation. *C. albicans* cells were seeded on collagen I-coated wells without enterocytes in DMEM for 4.5 h and 24 h at both 1 % and 21 % O_2, 37 °C and 5 % CO_2. Respective fungal cells were treated with 200 µM $CoCl_2$. Filamentation was documented using an inverse light microscope with the software ZEN 2 (Carl Zeiss Microscopy GmbH). Representative pictures are shown.

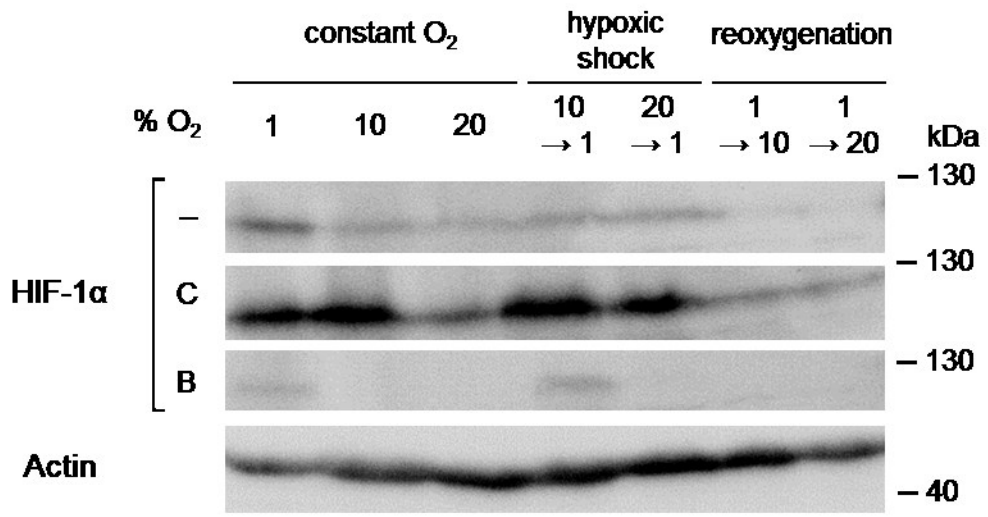

Suppl. Figure 4: Western Blot analysis of HIF-1α expression in $CoCl_2$- and BAY 87-2243-treated enterocytes prior to mock-/infection. The protein expression of HIF-1α was determined from seven days old enterocytes immediately before mock- or fungal infection but 1.5 h after respective oxygen shifts. C2BBe1 cells were treated with 200 µM $CoCl_2$ (24 h; abbreviation C), 100 nM BAY 87-2243 (5 h; abbreviation B) or left untreated (–). 15 µl of whole cell lysates in 1x SLB and 7.5 % acrylamide separation gels were used for the detection of HIF-1α protein bands *via* Western Blot. Western Blots shown are representative for three individual experiments.

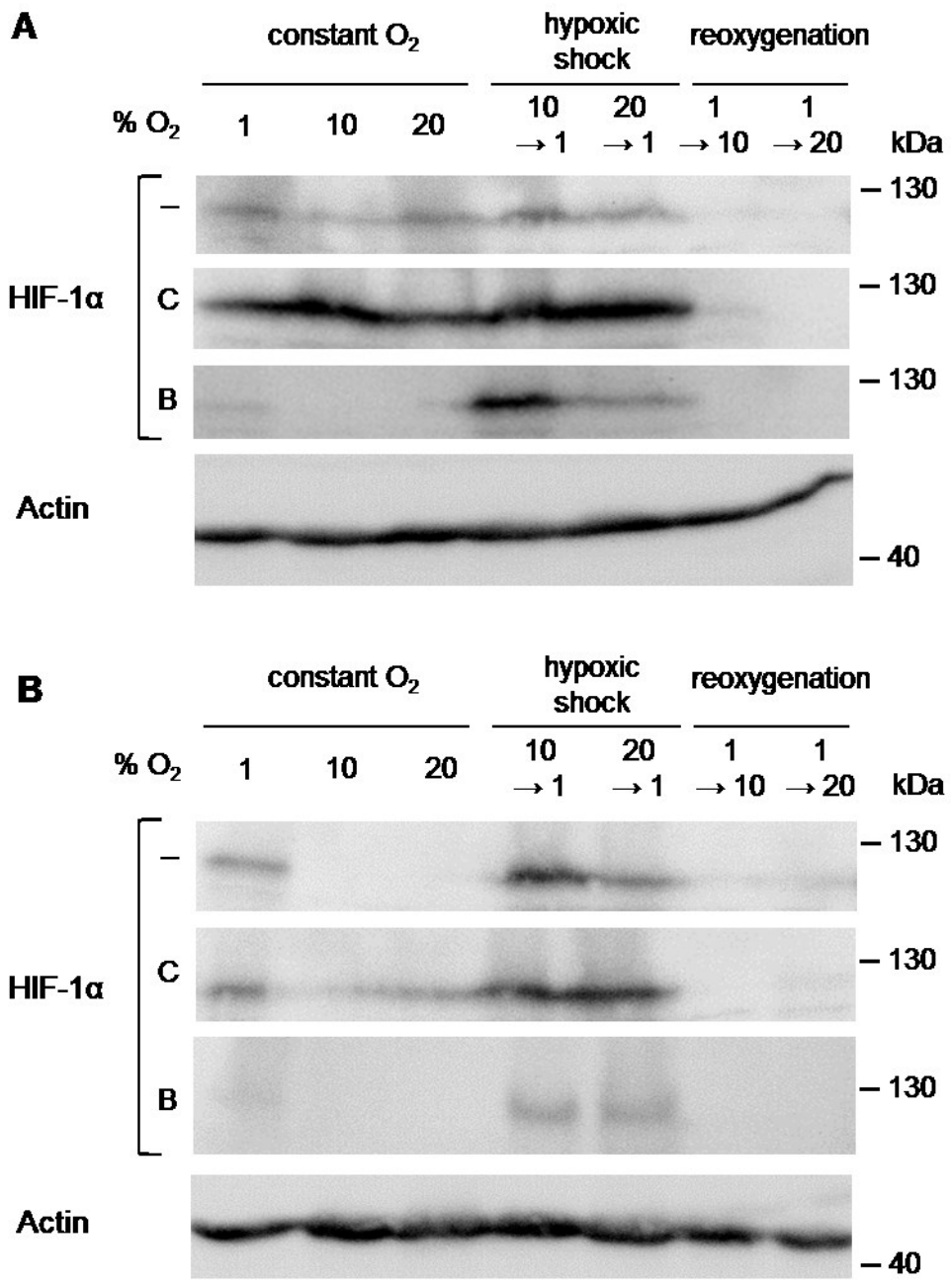

Suppl. Figure 5: Western Blot analysis of HIF-1α expression in $CoCl_2$- and BAY 87-2243-treated enterocytes after mock-infection. The protein expression of HIF-1α was determined from seven days old enterocytes **(A)** 4.5 h and **(B)** 24 h after mock-infection. Prior to mock-infection, C2BBe1 cultures were treated with 200 µM $CoCl_2$ (24 h; abbreviation C), 100 nM BAY 87-2243 (5 h; abbreviation B) or left untreated (–). In parallel to mock-infection, the respective enterocyte cultures were treated with 100 nM BAY 87-2243. 15 µl of whole cell lysates in 1x SLB and 7.5 % acrylamide separation gels were used for the detection of HIF-1α protein bands *via* Western Blot. Western Blots shown are representative for three individual experiments.

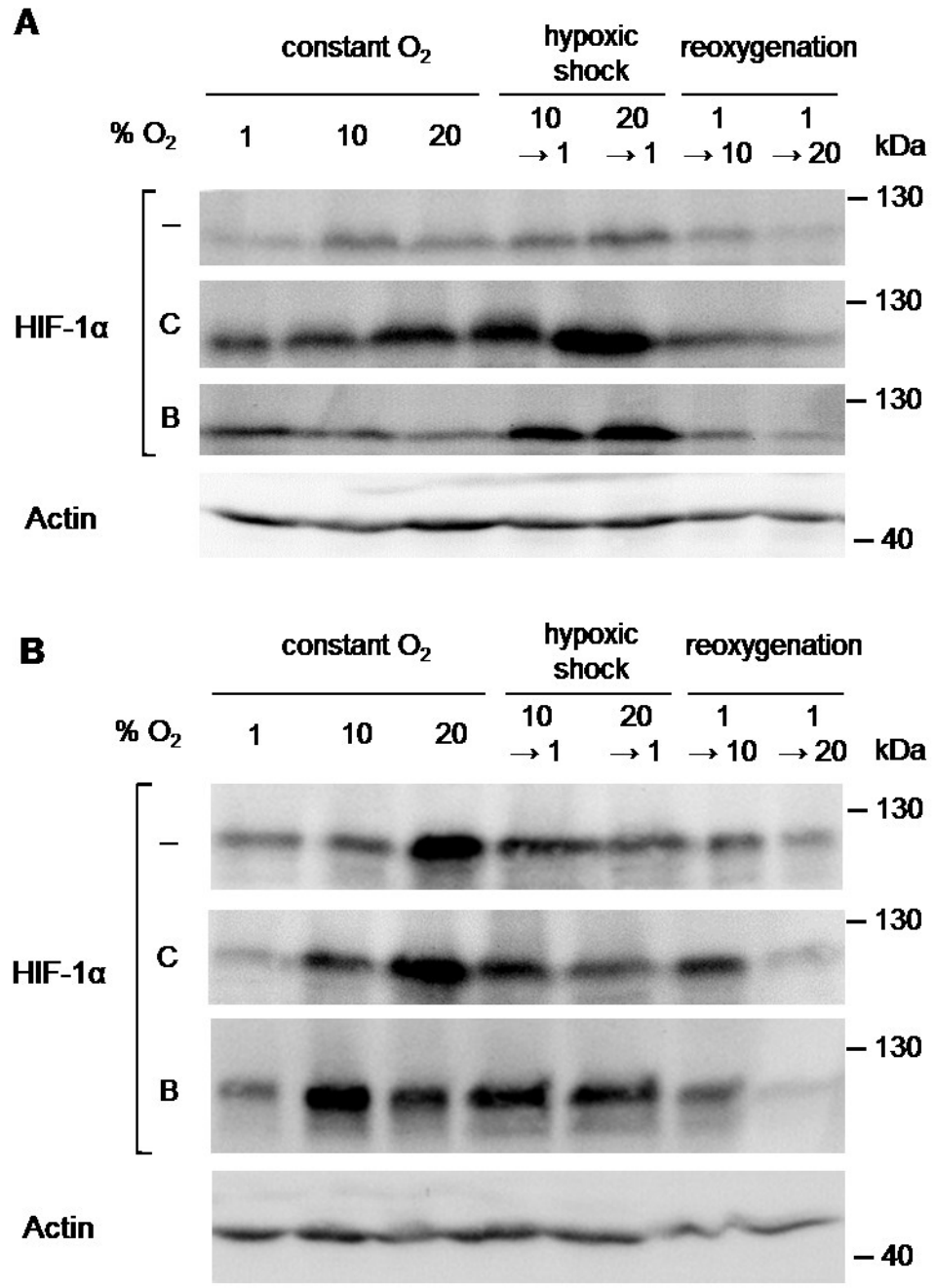

Suppl. Figure 6: Western Blot analysis of HIF-1α expression in $CoCl_2$- and BAY 87-2243-treated enterocytes after infection with *C. albicans*. The protein expression of HIF-1α was determined from seven days old enterocytes **(A)** 4.5 h and **(B)** 24 h after fungal infection. Prior to infection with *C. albicans*, C2BBe1 cultures were treated with 200 µM $CoCl_2$ (24 h; abbreviation C), 100 nM BAY 87-2243 (5 h; abbreviation B) or left untreated (–). In parallel to fungal infection, the respective enterocyte cultures were treated with 100 nM BAY 87-2243. 15 µl of whole cell lysates in 1x SLB and 7.5 % acrylamide separation gels were used for the detection of HIF-1α protein bands *via* Western Blot. Western Blots shown are representative for three individual experiments.

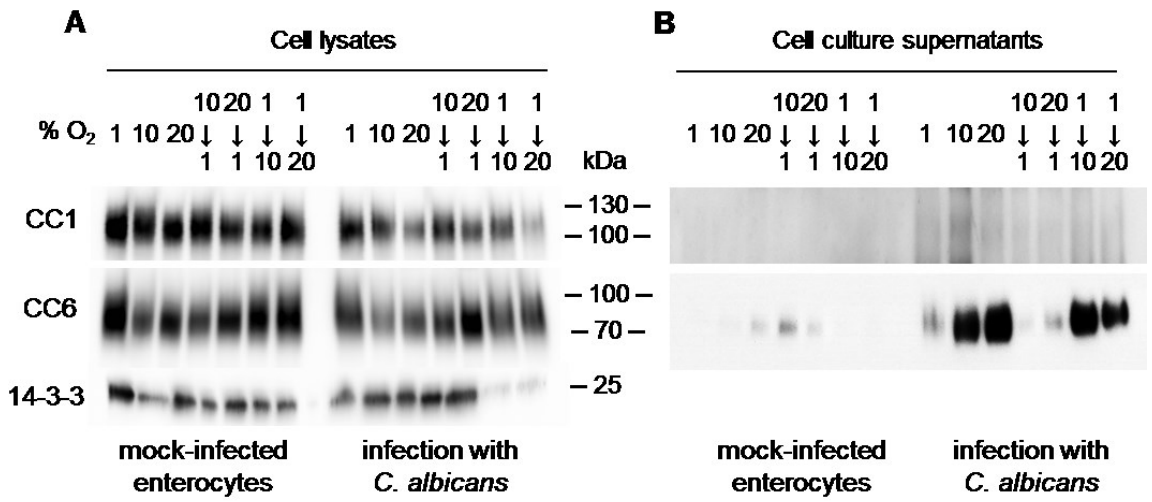

Suppl. Figure 7: Western Blot analysis of CEACAM1 and CEACAM6 protein expression. The protein expression of CEACAM1 (CC1) and CEACAM6 (CC6) was determined from seven days old mock- and *C. albicans*-infected enterocytes using (A) cell lysates from whole cell extracts in RIPA lysis buffer and (B) cell culture supernatants. 10 µg of protein per cell lysate (1 µg for reoxygenation samples of *C. albicans*-infected C2BBe1 cultures) and corresponding volumes of cell culture supernatants were used for the detection of the CEACAM protein bands *via* Western Blot. Western Blots shown are representative for three individual experiments.

8.2. Publication

Engert-Ellenberger, N., Mikolajczyk, R., Gressler, E., Dietrich, S., Klaile, E., Förster, T.M., Bauer, M., Jungnickel, B., Figge, M.T., Slevogt, H., Hube, B., Jacobsen, I.D.: "Oxygen availability influences the interaction of *Candida albicans* with enterocytes." in preparation for submission to PLOS Pathogens

8.3. Talks and poster presentations

Talks

06/2018 5th Joint Meeting of "Invasive Mycoses in Haematological Malignancies" (IMIHM) XII and the Collaborative Research Center/Transregio 124 "Pathogenic fungi and their human host: Networks of Interaction – FungiNet", Würzburg. *Hypoxia influences the Candida albicans-enterocyte interaction*

03/2017 6th International Conference on Microbial Communication for Young Scientists. Jena. *Hypoxia influences the Candida albicans-enterocyte interaction*

03/2017 Joint Symposium "Infection and Immunity" of the Working Group Infection Immunology of the "German Society for Immunology" (DGfI) and the "German Society for Hygiene and Microbiology" (DGHM) and the Working Group Eukaryotic Pathogens of the DGHM, Burg Rothenfels. *Hypoxia influences the Candida albicans-enterocyte interaction*

12/2016 Symposium of the "Jena School for Microbial Communication" (JSMC), Jena. *Hypoxia influences the Candida albicans-enterocyte interaction*

03/2016 3rd Joint Meeting of "Invasive Mycoses in Haematological Malignancies" (IMIHM) X and the Collaborative Research Center/Transregio 124 "Pathogenic fungi and their human host: Networks of Interaction – FungiNet", Würzburg. *Hypoxia influences the Candida albicans-enterocyte interaction*

01/2016 Status Workshop of the DGHM Working Group Eukaryotic Pathogens, Aachen. *Hypoxia influences the Candida albicans-enterocyte interaction*

03/2015 2nd Joint Meeting of "Invasive Mycoses in Haematological Malignancies" (IMIHM) IX and the Collaborative Research Center/Transregio 124 "Pathogenic fungi and their human host: Networks of Interaction – FungiNet", Würzburg. *Influence of hypoxia on the interaction of Candida albicans with*

intestinal epithelial cells

Poster presentations

03/2017 5th joint conference of the DGHM and the "Association for General and Applied Microbiology" (VAAM): Microbiology and Infection 2017, Würzburg. *Hypoxia influences the Candida albicans-enterocyte interaction*

09/2016 50th Scientific Conference of the "German speaking Mycological Society" (DMykG) e.V., Essen. *Hypoxia influences the Candida albicans-enterocyte interaction*

03/2016 3rd Joint Meeting of "Invasive Mycoses in Haematological Malignancies" (IMIHM) X and the Collaborative Research Center/Transregio 124 "Pathogenic fungi and their human host: Networks of Interaction – FungiNet", Würzburg. *Hypoxia influences the Candida albicans-enterocyte interaction*

11/2015 JSMC Retreat, Bad Sulza. *Influence of hypoxia on the interaction of Candida albicans with intestinal epithelial cells*

09/2015 49th Scientific Conference of the DMykG e.V. and 1st International Symposium of the Collaborative Research Centre/Transregio FungiNet, Jena. *Influence of hypoxia on interaction of Candida albicans with intestinal epithelial cells*

05/2015 6th FEBS Advanced Lecture Course: Human Fungal Pathogens – Molecular Mechanisms of Host-Pathogen Interactions and Virulence, La Colle-sur-Loup, France. *Influence of hypoxia on interaction of Candida albicans with intestinal epithelial cells*

04/2015 5th International Student Conference on Microbial Communication, Jena. *Influence of hypoxia on interaction of Candida albicans with intestinal epithelial cells*

05/2015 2nd Joint Meeting of "Invasive Mycoses in Haematological Malignancies" (IMIHM) IX and the Collaborative Research Center/Transregio 124 "Pathogenic fungi and their human host: Networks of Interaction – FungiNet", Würzburg. *Influence of hypoxia on the interaction of Candida albicans with intestinal epithelial cells*

11/2014 Annual Meeting of the Collaborative Research Center/Transregio 124

"Pathogenic fungi and their human host: Networks of Interaction – FungiNet", Kloster Banz. *Influence of hypoxia on interaction of Candida albicans with intestinal epithelial cells*

10/2014 4th joint conference of the DGHM and the VAAM: Microbiology and Infection 2014, Dresden. *Influence of hypoxia on interaction of Candida albicans with intestinal epithelial cells*

09/2014 JSMC Symposium, Jena. *Influence of hypoxia on interaction of Candida albicans with intestinal epithelial cells*

8.4. Courses

09/2016 Workshop "Scientific Presentations" organized by the Graduate Academy of the Friedrich-Schiller-University Jena

06/2016 Workshop "Academic Writing Skills" organized by the Graduate Academy of the Friedrich-Schiller-University Jena

11/2015 Workshop "Finding a job in Germany – applying and working outside academia" organized by the Graduate Academy of the Friedrich-Schiller University Jena

10/2015 Workshop "Überzeugen im Vorstellungsgespräch" organized by the Graduate Academy of the Friedrich-Schiller-University Jena

09/2015 Workshop "Scientific Writing and Publishing – Basics" organized by the Graduate Academy of the Friedrich-Schiller-University Jena

01/2015 Workshop "English Conversation" organized by the Graduate Academy of the Friedrich-Schiller-University Jena

01/2015 Workshop "Speech and Vocal Training" organized by the Graduate Academy of the Friedrich-Schiller-University Jena

12/2014 Workshop "English Grammar and Pronunciation" organized by the Graduate Academy of the Friedrich-Schiller-University Jena

11/2014 Workshop "wissenschaftliches Publizieren im digitalen Zeitalter" organized by the Graduate Academy of the Friedrich-Schiller-University Jena

09/2014 2nd International Workshop on "Image-based Systems Biology – IbSB 2014" organized by the Research Group Applied Systems Biology from

the Hans Knöll Institute Jena

8.5. Additional affiliations

01/2014 – present	Member of the Excellence Graduate School “Jena School for Microbial Communication” (JSMC)
01/2014 – present	Associated member of the Collaborative Research Center/Transregio 124 – FungiNet, Pathogenic fungi and their human hosts: Networks of Interaction, Project C5

8.6. Travel grant

01/2017	DGHM travel grant for attending the Status Workshop of the “German Society for Hygiene and Microbiology” (DGHM), Working Group Eukaryotic Pathogens, Aachen

8.7. Supervision

10/2016 – 03/2018	Master Thesis Rebecca Mikolajczyk
03/2016 – 10/2016	Master Thesis Elisabeth Gressler: supervision of the *in vitro* Translocation Assays
03/2015 – 09/2015	Bachelor Thesis Rebecca Mikolajczyk

8.8. Acknowledgments

First and foremost, I am grateful to Prof. Ilse Jacobsen for selecting me during the JSMC Recruitment in December 2013 to work on this great project. I thank Ilse for all of her support, advices, ideas, the proofreading of this thesis and, especially, her faith in me. I appreciate this a lot because I was able to learn so much from her experience and knowledge to improve my own skills. And whenever feasible, she took the time to sit together and to talk and discuss about the latest results, problems, further experimental steps or organizational stuff despite her often overcrowded to-do-list and time schedule. This really is applaudable!

I especially thank Rebecca Mikolajczyk for her great experimental help and spending hours and hours at the microscope. She contributed a lot to the data of the Damage, Adhesion and Invasion Assays done with the C2BBe1 cells and did a lot of hyphal length measurements. In addition, I want to thank Elisabeth Gressler helping me to establish the Translocation Assay at hypoxic and oxygen shift conditions. Supervising both Rebecca and Lise was a great pleasure and I really appreciate the friendly contact which developed.

Furthermore, I thank our former student assistants Julia Fiedler, Romy Rietschel and Astha Jain for spending so many hours at the microscope taking pictures and measuring hyphal length.

I am indebted to Stefanie Dietrich from the Research Group of Applied Systems Biology for the great job she did with the automated image analysis of all the microscopy pictures from the Adhesion Assays thereby quantifying the fungal adhesion to the enterocytes. As she knows best what she did for the quantification of the *C. albicans* adherence, she kindly wrote down this method and provided it for this thesis.

I thank Esther Klaile from Host Septomics for performing SDS-PAGEs and Western Blots for the CEACAM protein detection and for providing me with the Blot pictures and the normalized expression data. I further want to thank Toni Förster from the Department of Microbial Pathogenicity Mechanisms for executing the Zymolyase®-treatment and the plating of all the CFUs for the Translocation Assay. He also supported Lise and me with the respective SOP and hints to establish the Translocation Assay in our lab.

Furthermore I am thankful to PD Alexander S. Mosig, Marco Gröger (Institute for Biochemistry II, Jena University Hospital; Center for Sepsis Control and Care [CSCC], Jena University Hospital) and Cora Richert (Institute for Clinical Chemistry and

Laboratory Diagnostic, Jena University Hospital) for the suggestion, organization and performance of lactate and glucose measurements and for providing me with these data. Special thanks also go to Dorinja Zapf from the Clinics for Infectious Diseases and Microbiology at the University Lübeck for our fruitful discussion about HIF-1α at the Joint Symposium of “Infection and Immunity”. She provided me with key information to optimize the protein isolation and Western Blot procedure for the HIF-1α detection. Her priceless help enabled me to finally detect this protein.

I want to thank Prof. Berit Jungnickel for her constructive ideas and advices, especially for the suggestion to further investigate on the role of HIF-1α for this host-fungus interaction.

I really appreciated the excellent atmosphere in our team and therefore I want to thank all current and former members of the Research Group Microbial Immunology and the Department of Microbial Pathogenicity Mechanisms. I especially thank Tony, Katja S, Christine, Silke, Hanna, Isabel, Sindy Sravya, Orsolya, Melanie, Hannah, Stefanie, Theresa, Birgit, Daniel, Stefanie, Stephie, Daniela, Franzi, Sarah, Annemarie, Karolin, Osama and Ann-Kristin for making me laugh every day, for scientific discussions and stimulating conversations, for enjoyable coffee breaks, for making me feel so comfortable and for creating such a great, cooperative and cheerful working atmosphere in the lab. I want to thank the “Erfurt-gang” Annika, Marcel and Wibke for making the commuting between Erfurt and Jena so delightful and enjoyable.

I especially want to thank one of my best friends, Matthias, for proofreading some parts of this thesis while he was fully working, partly ill and organizing his move within Berlin.

My most sincere gratitude goes to all of my friends and to my family, especially to my mum Kerstin and my husband Martin for their unconditional support and love, for their faith in me, for encouraging words on hard days and for just being there when I needed someone to talk to. You are the greatest gifts I can imagine!

8.9. Selbstständigkeitserklärung

Hiermit erkläre ich, dass ich die vorliegende Arbeit selbst verfasst habe und keine anderen als die angegebenen Quellen und Hilfsmittel verwendet habe.

Mir ist die geltende Promotionsordnung der Fakultät für Biowissenschaften der Friedrich-Schiller-Universität Jena bekannt.

Personen, die mich bei den Experimenten, der Datenanalyse, der Auswertung und der Verfassung der Dissertation unterstützt haben, sind in der Danksagung der Dissertation vermerkt.

Die Hilfe eines Promotionsberaters wurde nicht in Anspruch genommen. Es haben Dritte weder unmittelbar noch mittelbar geldwerte Leistungen für Arbeiten erhalten, die im Zusammenhang mit dem Inhalt der vorgelegten Dissertation stehen.

Die vorliegende Arbeit wurde in gleicher oder ähnlicher Form noch bei keiner anderen Hochschule als Dissertation eingereicht und auch nicht als Prüfungsarbeit für eine staatliche oder andere wissenschaftliche Prüfung verwendet.

Jena, den 13.05.2019 _____

Nicole Engert-Ellenberger